ULTIMATE LOAD CAPACITY OF CONTINUOUS COMPOSITE PLATE GIRDERS

APPROVED BY SUPERVISORY COMMITTEE:

Karl H. Frank

[signature]

[signature]

[signature]

John L. Tassoulas

to my wife Jae Yong

ULTIMATE LOAD CAPACITY OF CONTINUOUS
COMPOSITE PLATE GIRDERS

by

CHONG-ONE BAK, B.S.,M.S.

DISSERTATION

Presented to the Faculty of the Graduate School of

The University of Texas at Austin

in Partial Fulfillment

of the Requirements

for the Degree of

DOCTOR OF PHILOSOPHY

THE UNIVERSITY OF TEXAS AT AUSTIN

May, 1992

ACKNOWLEDGMENTS

I wish to express my indebtedness and gratitude to Prof. Karl H. Frank for his guidance, inspiration and kindness throughout the course of this study. I am especially thankful to Prof. Joseph A. Yura for his support and encouragement. Sincere appreciations are extended to the other members of my committee, Prof. James O. Jirsa, Prof. John L. Tassoulas and Prof. Stelios Kyriakides for their reviewing the dissertation and offering helpful suggestions.

I would like to express my sincere gratitude to my family for their love and encouragement during my study.

ULTIMATE LOAD CAPACITY OF CONTINUOUS COMPOSITE PLATE GIRDERS

Publication No. _____

Chong-One Bak, Ph.D.
The University of Texas at Austin, 1992
Supervisor: Karl H. Frank

A composite plate girder consists of a concrete slab attached to a steel plate girder through shear connectors. An evaluation of the ultimate load capacity of continuous composite plate girders is very important in providing adequate design criteria. The ultimate capacity of a continuous beam can be determined by the simple plastic mechanism method if the interior support section has a sufficient rotation capacity for a mechanism to form. However, most plate girders have slenderness sections whose slenderness ratios generally exceed the limiting values required for plastic design. Moreover, the ultimate bending strengths of these slender sections are affected by local instabilities of compression flange and/or web, which cause premature failure. In the LFD method of the AASHTO Specifications, continuous composite plate girder bridges are designed based on elastic analyses and the elastic Maximum Load moment at any section is limited to the yield moment. Test results have shown that typical composite plate girders in positive bending can reach their plastic moment capacities due to the small web depth in compression. Nevertheless, the use of the plastic moment capacity of positive bending sections is limited to simple span bridge design because the moment-rotation behaviors of negative bending sections are not well known.

The objective of this study is to evaluate the ultimate load capacity of continuous composite plate girders. The ultimate capacity of a continuous composite girder depends on the moment-rotation characteristics of the positive and negative bending sections. Moment-curvature relationship of a positive

v

bending section is quite different from that of a negative bending section. In this study, moment-rotation characteristics of the positive and negative bending sections are investigated using analytical and experimental data respectively. To evaluate the moment-rotation characteristics of a composite plate girder in negative bending, an ultimate load test was performed on a 1/2 scale component specimen.

A nonlinear computer program was developed to calculate the ultimate capacity of a continuous composite girder with varying moment-curvature relationships for the positive and negative bending sections. Based on the results of a parametric study of the ultimate load capacity, a new design method was proposed. Currently used design methods are investigated and the ultimate capacity calculated by these methods are compared with that by the new design method.

The parametric study indicated that the load at which the elastic maximum positive moment reached the plastic moment or the elastic maximum negative moment reached the maximum bending capacity of the pier section (whichever was smaller) provided a lower bound estimate of the ultimate load capacity of continuous composite plate girders. In the new design method of continuous composite plate girder bridges, the maximum positive and negative moments by an elastic analysis are limited to the plastic moment of the positive section and the maximum bending strength of the pier section respectively. This procedure improves the limit state criteria and provides a more economical design than the LFD method.

TABLE OF CONTENTS

LIST OF TABLES

LIST OF FIGURES

xiii

CHAPTER ONE

INTRODUCTION

A composite plate girder consists of a concrete slab attached to a steel plate girder through shear connectors. In the positive bending region where the concrete slab is in compression, this composite system increases the stiffness and ultimate strength of the section greatly reducing the weight of steel and allowing longer span length for a given steel section. In the negative bending region, the concrete slab which is in tension is assumed to be ineffective after cracking and the reinforcing steel bars are considered to act compositely with the steel section. Therefore, the benefits of composite action are reduced in the negative moment region. Nevertheless, continuous composite plate girders are the most common type of superstructure for long span steel bridges due to the advantages in the positive bending region.

In the Load Factor Design (LFD) method of the American Association of State Highway and Transportation Officials (AASHTO) Specifications[6], steel bridges are designed based on elastic analyses. In the AASHTO Guide Specifications for Alternate Load-Factor Design Procedures[5], the ultimate load capacity of a continuous steel beam bridge is determined by the plastic-mechanism method. However, this method applies only to compact sections. This research is an analytical study of the ultimate load carrying capacity of continuous composite plate girders with noncompact sections. Based on a parametric study of the ultimate load capacity, a new design method is proposed. The scope of this study is limited to laterally braced fully composite plate girders. Therefore, incomplete interaction between the concrete slab and the steel plate girder and the limit state of lateral torsional buckling are not considered in this study.

1.1 Ultimate Strength

An evaluation of the ultimate load carrying capacity of continuous composite plate girders is very important in providing adequate design criteria. Elastic analysis can be used to evaluate the ultimate strength of continuous beams with compact sections. In this procedure, the elastic moment diagram is adjusted to indirectly account for moment redistribution beyond the elastic limit. In the Allowable Stress Design of AISC Specifications[1] and Load Factor Design of AASHTO Specifications[6], the maximum negative moment is reduced by 10% with a corresponding increase of positive moment before the sections are designed. But this procedure may not reflect the true inelastic behavior and ultimate strength. The ultimate capacity of a continuous beam bridge can be determined by the simple plastic-mechanism method if the negative moment section has sufficient rotation capacity at its plastic moment for a mechanism to form. Fig.1.1 shows the collapse mechanism for a two span continuous beam with an elastic-perfectly plastic moment-rotation relationship.

However, most plate girders have slender sections whose flange and web slenderness ratios generally exceed the limiting values required for plastic design. The ultimate bending strength and the rotation capacity of these slender sections are affected by local instabilities such as compression flange and/or web buckling, which may cause premature failure. The ultimate load carrying capacity of a continuous composite girder depends on the moment-curvature characteristics of the positive and negative bending sections. Moment-curvature relationship of a positive bending section is quite different from that of a negative bending section. The main features which affect the moment-curvature characteristics of the positive bending section are steel section yielding and concrete crushing. Concrete cracking, steel section yielding, and local buckling are the major events determining the behavior in negative bending.

In this study, moment-curvature characteristics of positive and negative bending sections of continuous composite plate girders were investigated using

(a) Loading condition

(b) Collapse Mechanism

(c) Moment diagram at
collapse mechanism
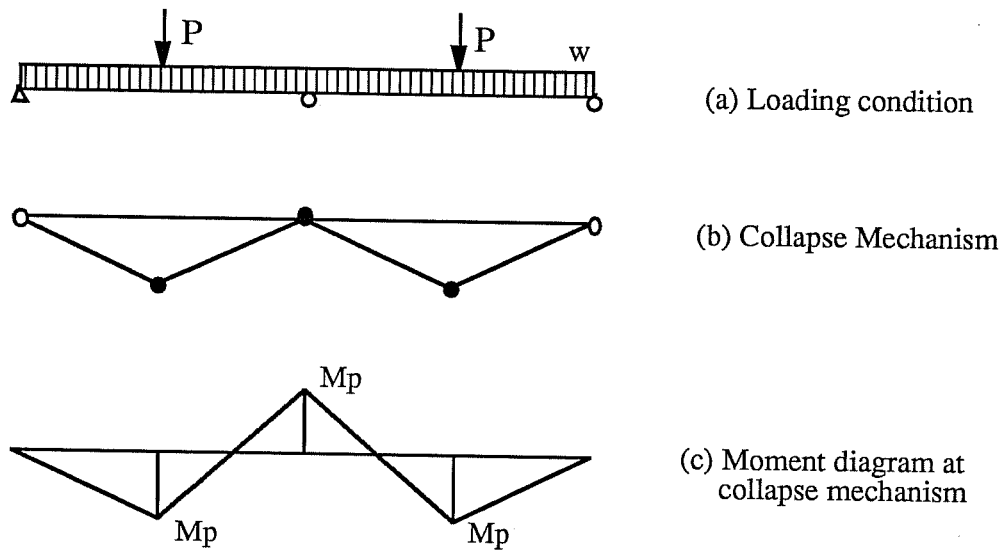
Figure 1.1 Plastic analysis of a continuous beam

experimental and analytical data. A nonlinear computer program was developed and used to calculate the ultimate load carrying capacity of continuous composite plate girders with varying moment-curvature relationships for positive and negative bending sections.

1.2 Experimental Program

A composite plate girder with slender web was tested under negative bending moment. To improve the rotation capacity, the slenderness ratio of the compression flange was reduced below the compact section limit. The prototype was a two-span continuous $(200' - 200')$ composite plate girder bridge with $13' - 0''$ transverse girder spacing. A linear scale factor of $1/2$ was used for the cross sectional dimensions and the model length. The model was made of the

same materials as the prototype. To simulate a composite section in negative bending, the model was supported at the ends and loaded upward at the center. Most composite beam bridges are built without shorings and the dead weight of concrete is supported by the steel section only. To investigate the behavior of an unshored composite girder, the steel plate girder was loaded up to a simulated dead load. With the steel girder held at that load, concrete was placed. After the concrete slab cured, the composite girder was loaded to failure.

1.3 Development of Nonlinear Computer Program

To evaluate the ultimate loading capacity of a continuous composite plate girder, redistribution of moments must be considered. Since the moment-rotation curve of a negative bending section has a descending branch beyond its maximum moment, moment redistrbution occurs through the interaction of the descending curve of the negative section and the rising curve of the positive section. To investigate the ultimate load capacity of continuous composite plate girders, one-dimensional nonlinear program, NACB, was developed. To consider the descending curve of the negative bending section and produce faster convergence, the initial stiffness method, which is unconditionally convergent, is combined with the tangential stiffness method at selective iterative intervals. An incremental equilibrium approach is used in the numerical solution procedure. For each increment of the applied load, the displacement is successively corrected until the equilibrium position is obtained. The load at which the solution does not converge is the ultimate load of the continuous composite plate girder.

This report is composed of nine chapters. In chapter 2, moment-curvature characteristics of composite girders in positive bending are evaluated numerically. In chapter 3, the nominal moment strength of noncomposite and com-

posite plate girders is discussed. Currently used design methods are presented in chapter 4. Experimental results are summarized in chapter 5. The nonlinear computer program, NACB, is developed in chapter 6. In chapter 7, the ultimate load carrying capacity of continuous composite girders is investigated varying the moment-curvature characteristics of the positive and negative bending sections. The proposed design method is discussed and conclusions are presented in chapter 8 and 9 respectively.

CHAPTER TWO

BEHAVIOR AND STRENGTH OF THE POSITIVE BENDING SECTION

The moment-curvature relationships of composite plate girders in positive bending are investigated using a numerical analysis method. The elements of a composite plate girder section are the concrete slab, the reinforcing bars, the structural steel and the shear connectors. In positive bending, the concrete slab is in compression. A composite plate girder in positive bending may be idealized as a steel plate girder to which a concrete cover plate is attached. Most composite plate girders in positive bending have an unsymmetrical steel section with a large bottom flange and a small top flange for better efficiency. The concrete cover plate shifts the elastic neutral axis close to the concrete slab reducing the web depth in compression. Therefore, a composite plate girder with a slender web can reach its ultimate bending moment without web instability problems.

Reinforcing bars are not considered in the analyses because the effect on the cross sectional behavior and ultimate strength is insignificant in positive bending. No shear deformation between the concrete slab and the steel girder is considered in this study.

2.1. Materials

2.1.1 Stress-strain relationship of concrete

Hognestad's stress-strain curve for concrete in compression[7] is used for the concrete slab. This curve is composed of a parabolic ascending part and a straight descending part as shown in Fig.2.1. The tensile strength of concrete is

6

relatively small compared with the compressive strength and the tensile stress-strain relationship is represented as a straight line up to the modulus of rupture, fr. After cracking, concrete is assumed to have no tensile strength. The initial modulus of elasticity, E_c, is taken as 1,800,000 + 500f_c'' psi.

2.1.2 Stress-strain relationship of structural steel

A typical tensile stress-strain curve of structural steel is illustrated in Fig.2.2. The main features characterizing this stress-strain curve are as follows:

a) linear elastic region up to the yield strain, ε_y;

b) yield plateau region up to the strain hardening strain, ε_{st} ;

c) strain hardening region up to the ultimate strain, ε_{ul} ;

d) ultimate plateau region up to the failure strain, ε_f ;

2.2 Plastic Bending Moment

The plastic bending moment of a composite plate girder can be easily calculated by assuming a fully plastic state of stress for both concrete and steel. Two different stress distributions are possible corresponding to the different position of the plastic neutral axis as shown in Fig. 2.3. The plastic bending moment is not affected by the construction methods.

The 1983 AASHTO specification[6] limits the bending capacity of a composite girder to its first yield moment, M_y, when the web slenderness ratio exceeded the compact section limit. But test results show that composite plate girders with very slender webs can develop the plastic bending moment, M_p, in positive bending because the concrete slab shifts the neutral axis upward reducing the web area in compression.
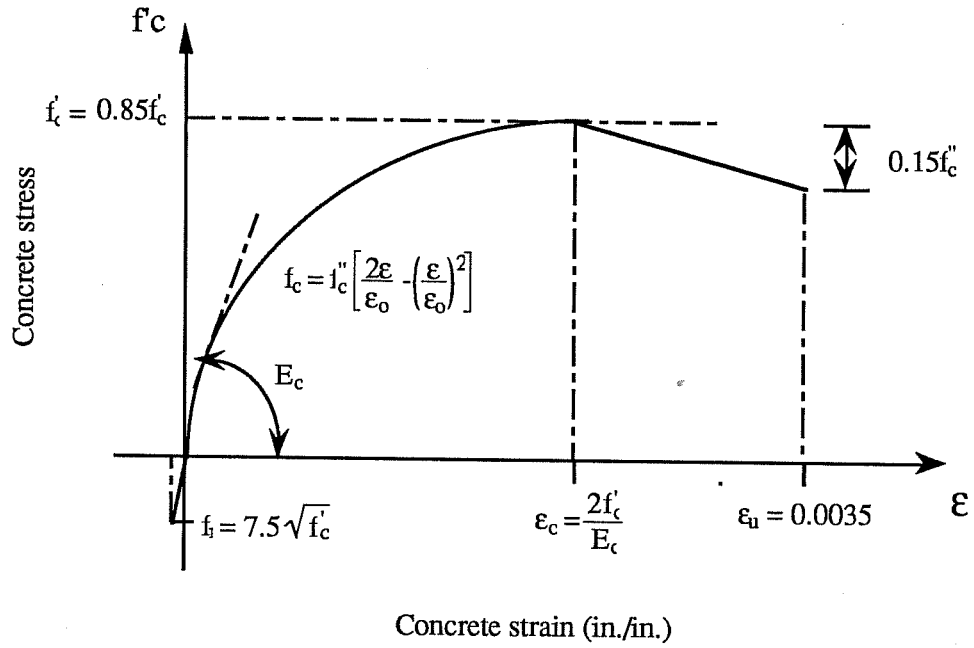
Figure 2.1 Stress-strain curve for concrete

The figure shows concrete stress ($f'c$) on the vertical axis versus concrete strain (ε) on the horizontal axis. Key labeled values:

$f'_c = 0.85 f'_c$

$f_c = f''_c \left[\dfrac{2\varepsilon}{\varepsilon_o} - \left(\dfrac{\varepsilon}{\varepsilon_o}\right)^2 \right]$

E_c

$0.15 f''_c$

$f_t = 7.5 \sqrt{f'_c}$

$\varepsilon_c = \dfrac{2 f'_c}{E_c}$

$\varepsilon_u = 0.0035$

Concrete strain (in./in.)
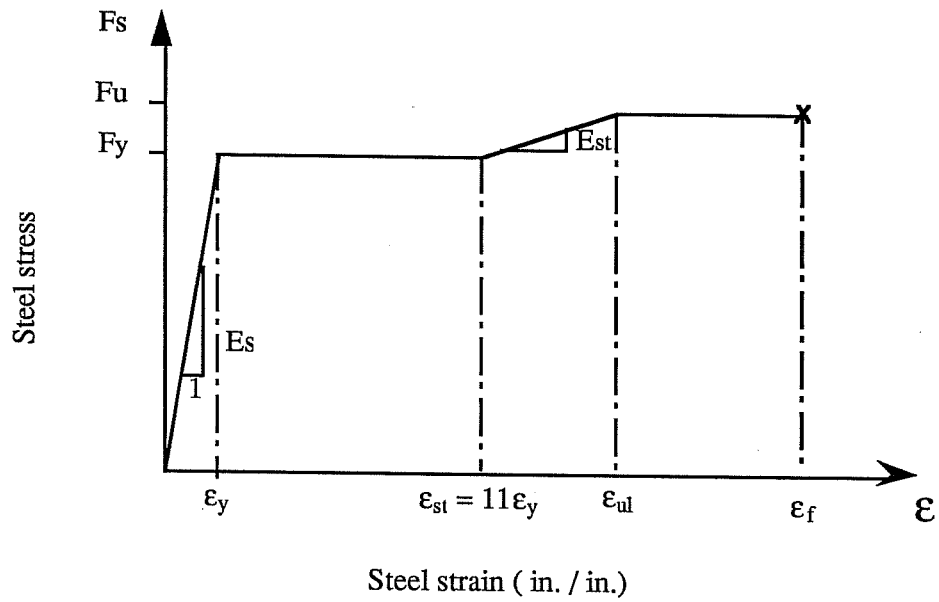
Figure 2.2 Stress-strain curve for structural steel

Steel stress (F_s) versus steel strain (ε). Labeled values: F_u, F_y, E_{st}, E_s, 1, ε_y, $\varepsilon_{st} = 11\varepsilon_y$, ε_{ul}, ε_f.

Steel strain (in. / in.)
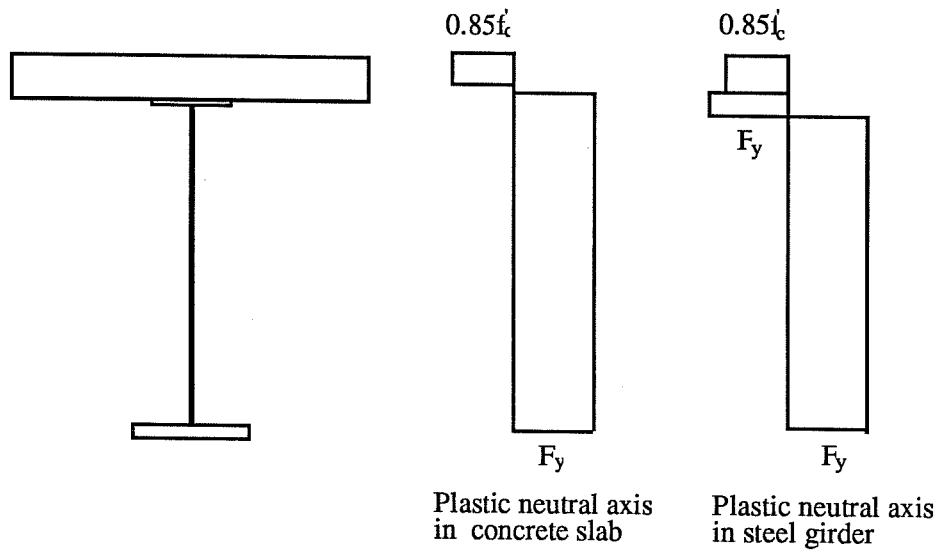
Figure 2.3 Plastic stress distribution for positive bending

2.3 Moment-Curvature Analysis

The moment-curvature curve of a cross section can be obtained using an iteration process. The cross section is idealized as a set of uniform layers as shown in Fig.2.4. The flange layers are further subdivided into a number of segments in order to model the variation in residual stresses along the width of the flange. For a given strain at the top extreme fiber, the stress of each layer is determined from the stress-strain curves for the concrete and structural steel. A linear strain distribution across the cross section is used assuming that a plane section remains plane during bending. Several iterations are made until the horizontal equilibrium of internal forces is obtained by varying the location of the neutral axis. The curvature is obtained as the strain at the top fiber divided by the distance between the top fiber and the neutral axis. The corresponding moment is obtained by summing the contributions of all the layers of the cross section.
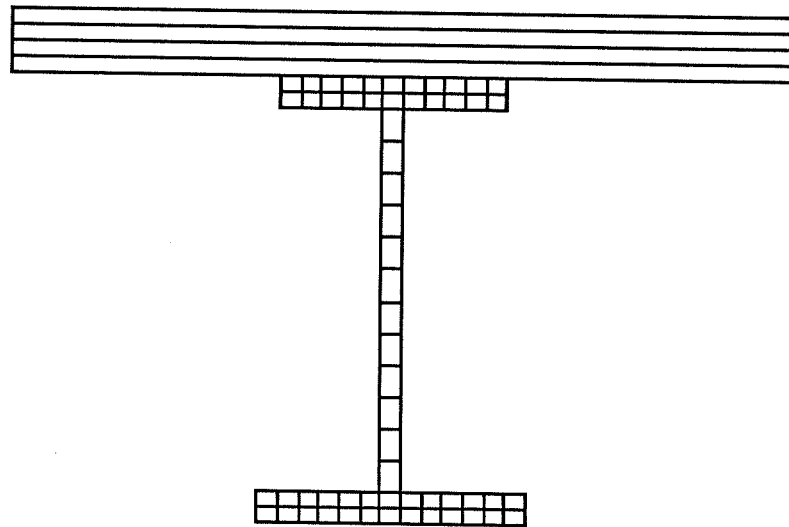
Figure 2.4 Idealization of cross section

2.3.1 Moment-curvature relationship

The behavior of a composite plate girder in positive bending is linear-elastic until the bottom flange starts to yield. As the yielding progresses, the neutral axis moves upward and the bending stiffness of the cross section is gradually reduced. The ultimate bending capacity is determined either by the concrete crushing or by the fracture of the structural steel. In most composite plate girders, concrete crushing occurs first. When the strain at the top surface of the concrete slab reaches an assumed limiting value of 0.0035, the composite plate girder is considered to fail by crushing of the concrete slab. The moment-curvature characteristics of a composite plate girder depend on many parameters such as material strength, cross sectional dimension, residual stresses, and the construction method. The effects of these parameters on the moment-curvature relationship were investigated in the analysis. Fig. 2.5 shows the cross section and material properties of the basic model used in the analysis. The variations in the above-mentioned parameters are summarized in Table
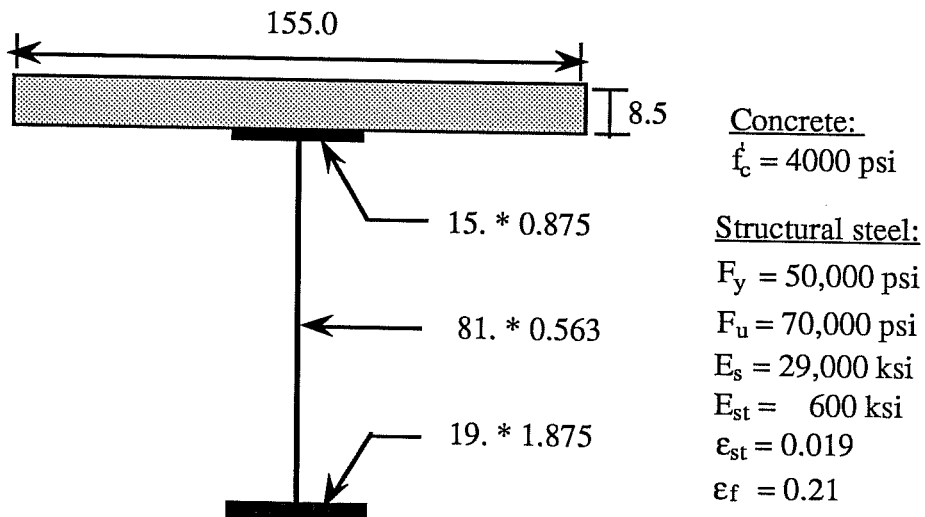
**Figure 2.5 Girder dimensions and material properties
of analytical model**

2.1. In this table, M_y, M_p, and D_p were calculated using the cross sectional properties and M_u, ϕ_u, and D_c were obtained in the analysis.

2.3.2 Concrete strength and crushing strain

High strength concrete did not increase the plastic moment greatly because the compressive force in the concrete slab could not exceed the full yield strength of the steel plate girder. High strength concrete shifted the plastic neutral axis upwards producing larger strain in steel section. Therefore, the ductility was increased in the strain hardening range with a consequent increase in the ultimate moment as shown in Fig. 2.6. To see the effect of conctete crushing strain, ε_u, three different values of ε_u were used with the same concrete strength of 4000 psi. As can be seen in Fig. 2.7, an increase in

Table 2.1 Summary of various parameters and analysis results

Section	f_c' (psi)	F_y (ksi)	Slab (B*T)	ε_u	$\frac{M_{dl}}{M_p}$	M_p (k-ft)	$\frac{M_y}{M_p}$	D_p	D_c	$\frac{M_u}{M_p}$	Φ_u ($\times 10^{-3}$)	Comments
T	4000	50	155 x 8.5	.0035	0.0	21800	0.80	83.5	82.0	1.06	34.08	basic model
A-1	3000	50	155 x 8.5	.0035	0.0	21440	0.81	82.9	77.9	0.98	24.35	conc. strength
A-2	5000	50	155 x 8.5	.0035	0.0	22100	0.80	84.8	83.5	1.11	39.76	
B-1	4000	50	155 x 8.5	.0030	0.0	21800	0.80	85.6	82.1	1.03	29.50	concrete ultimate strain
B-2	4000	50	155 x 8.5	.0040	0.0	21800	0.80	83.0	81.9	1.09	38.68	
C-1	4000	36	155 x 8.5	.0035	0.0	15980	0.79	83.5	83.6	1.24	40.60	steel yield stress
C-2	4000	65	155 x 8.5	.0035	0.0	27900	0.82	83.5	77.6	0.98	23.87	
D-1	4000	50	133 x 8.5	.0035	0.0	21600	0.81	83.2	80.2	1.02	29.15	slab width
D-2	4000	50	177 x 8.5	.0035	0.0	21990	0.80	84.1	83.0	1.09	37.93	
E-1	4000	50	155 x 7.0	.0035	0.0	21320	0.80	83.1	79.6	1.03	31.50	slab thickness
E-2	4000	50	155 x 10.0	.0035	0.0	22360	0.80	84.5	83.4	1.06	33.82	
F	4000	50	155 x 8.5	.0035	0.0	21800	0.08	83.5	82.0	1.06	34.08	residual stress
G-1	4000	50	155 x 8.5	.0035	0.2	21800	0.74	83.5	83.7	1.08	35.73	construction method
G-2	4000	50	155 x 8.5	.0035	0.3	21800	0.70	83.5	84.1	1.10	37.39	

Dp = depth of the composite girder in compression at the plastic moment, Mp

Dc = depth of the composite girder in compression at concrete crushing

Mu = ultimate moment at concrete crushing

Φ_u = ultimate curvature at concrete crushing
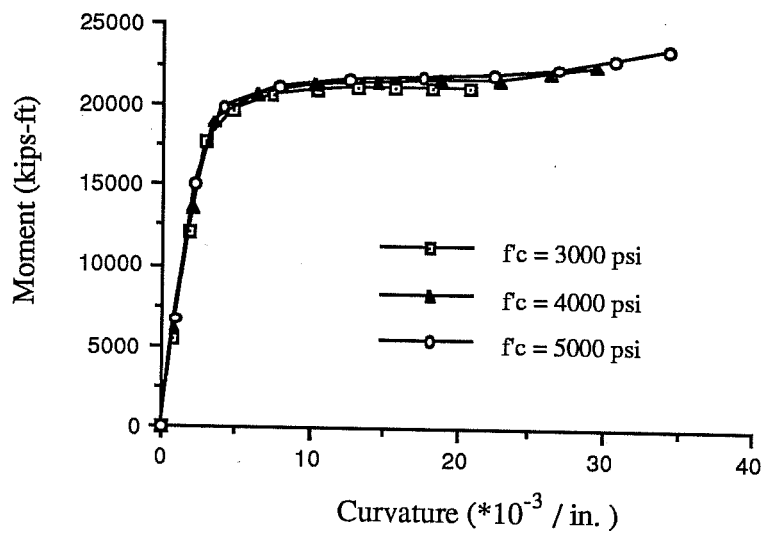
Figure 2.6 Effect of concrete strength
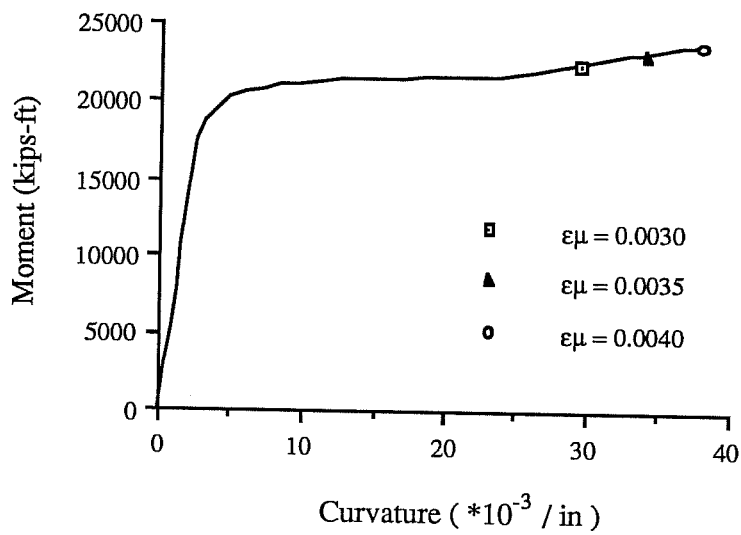
Figure 2.7 Effect of ultimate concrete strain

the concrete crushing strain allowed larger curvature increasing the ductility
and the ultimate moment capacity, but the difference was insignificant.

2.3.3 Steel yield stress

While high yield stress increased the plastic moment greatly, the ductil-
ity was reduced as shown in Fig. 2.8. To see the effect of steel yield stress
on the moment-curvature characteristics, the moment-curvature curves were
nondimensionalized by the plastic moment and the plastic curvature as shown
in Fig. 2.9. This figure shows that yield stress had little effect on the moment-
curvature characteristics. Lower yield stress increased the ductility due to the
upward shift of the plastic neutral axis. The higher neutral axis produced larger
curvature at failure. The ultimate stress, F_u, of 58, 65, and 80 ksi was used for
material with the yield stress of 36, 50, and 65 ksi respectively. Same E_s, E_{st},
and ε_f values were used.
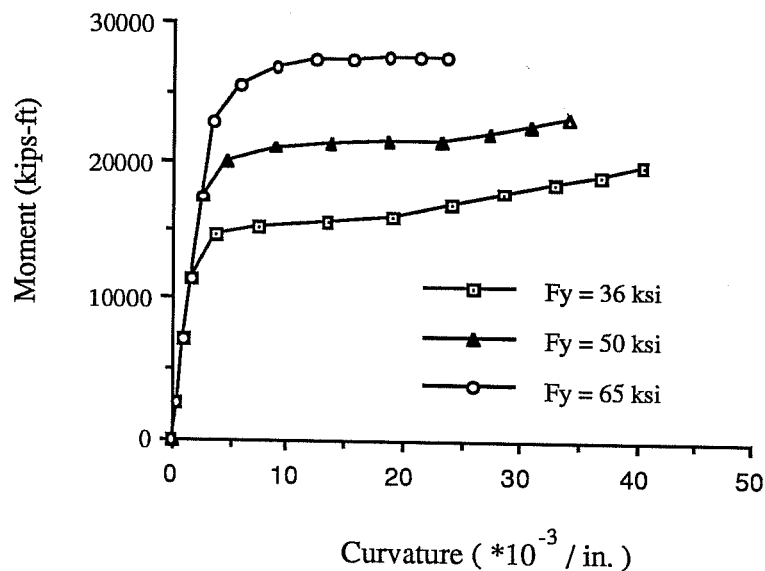
Figure 2.8 Effect of steel yield stress
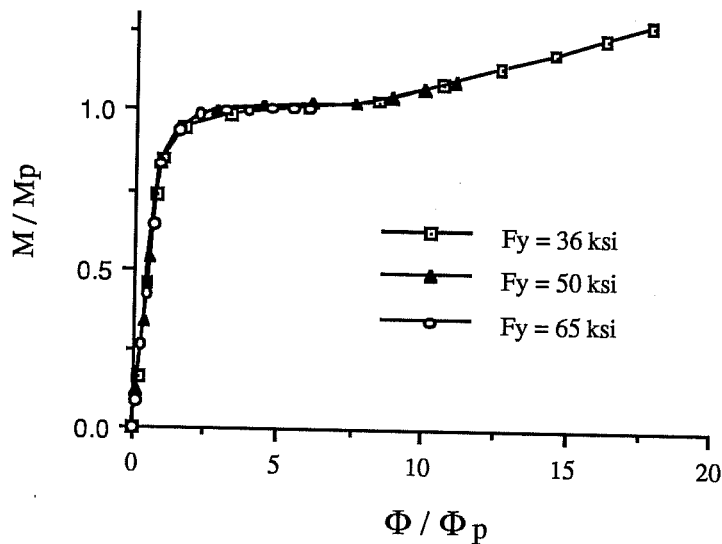
Figure 2.9 Effect of steel yield stress in a nondimensional form

2.3.4 Slab dimension

An increase in slab width had little effect on the plastic moment but increases the ductility with a consequent increase in the ultimate moment as can be seen in Fig. 2.10. An increase in slab thickness increased the plastic moment a little, but the difference was insignificant as shown in Fig. 2.11. The ductility was affected little by the slab thickness. The ratio of the yield moment to the plastic moment ranged from 0.80 to 0.81.

2.3.5 Residual Stresses

Most welded plate girders are fabricated from flame-cut plates. The magnitude and distribution of residual stresses in a welded shape are quite different from those in a rolled shape. The residual stress distribution in a welded shape [8] was idealized in the analysis as shown in Fig. 2.12. As shown in Fig. 2.13,
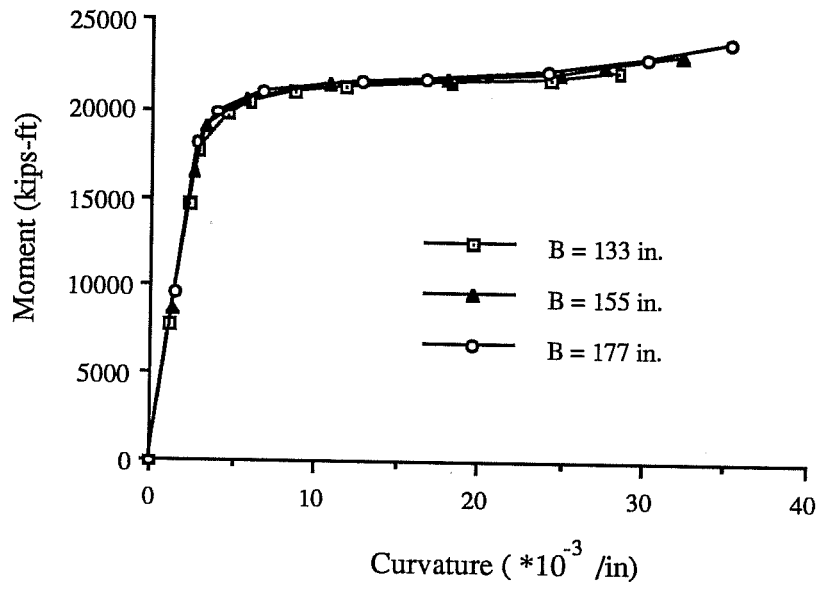
Figure 2.10 Effect of slab width
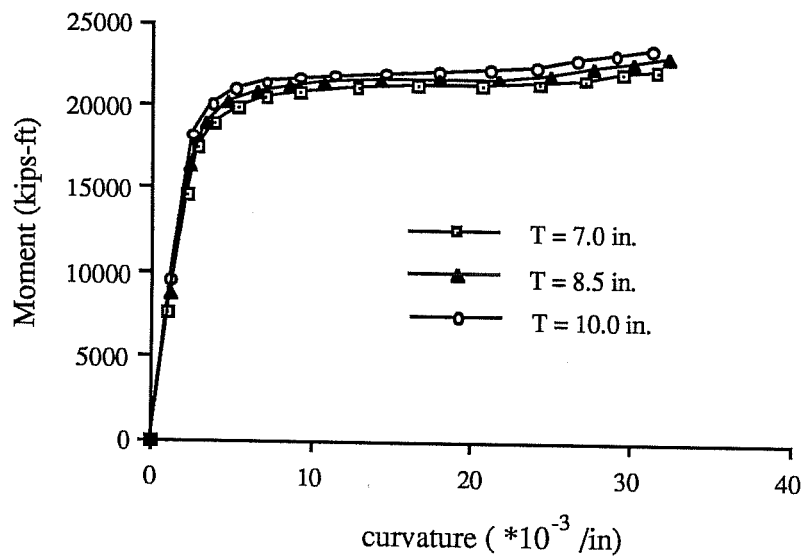
Figure 2.11 Effect of slab thickness

a) Typical pattern   b) Idealized pattern
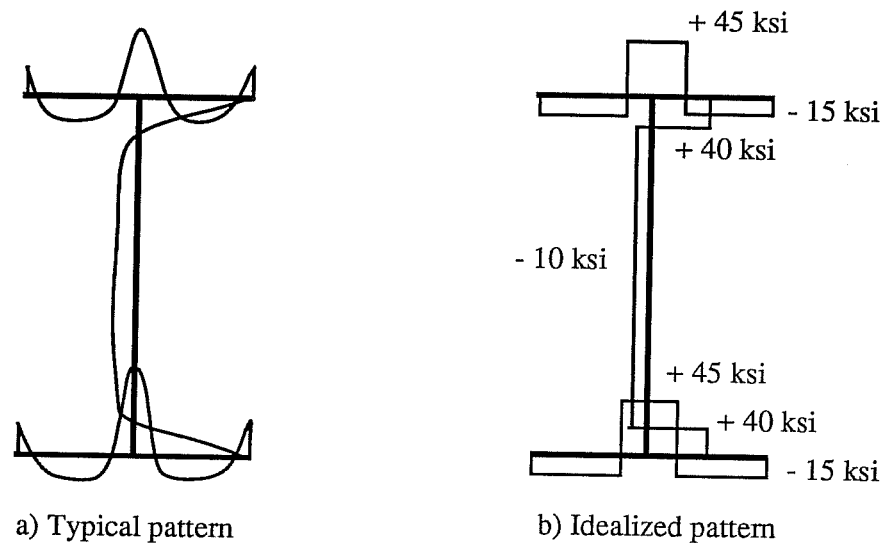
Figure 2.12 Typical and idealized residual stress patterns

a cross section starts to yield at an early stage of loading due to the high tensile residual stress in the tension flange. But the effect of residual stress on the moment-curvature characteristics is minor because the high tensile residual stress is confined to a small area.

2.3.6 Construction method

If a bridge is not shored during construction, the dead weight of concrete is supported by the steel section only, and any additional dead load plus live load are supported by the composite section once the concrete has cured. Significant stresses exist in the steel section before the bridge acts compositely. Therefore,
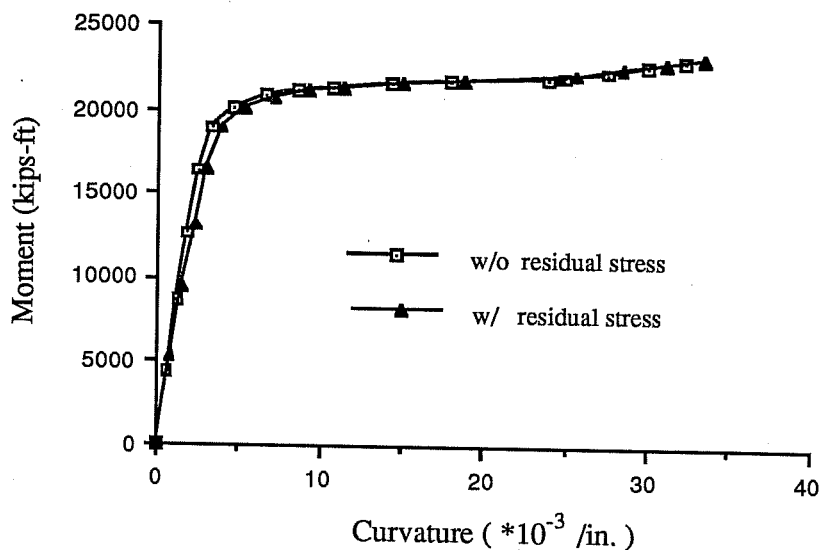
Figure 2.13 Effect of residual stress

an unshored composite section suffers earlier yielding than a shored composite section. The moment-curvature curves with three different ratios of dead load moment to plastic moment, M_{dl}/M_p, are shown in Fig. 2.14. When the ratio was increased from 0.0 to 0.3, the yield moment, M_y, was reduced from $0.80M_p$ to $0.7M_p$.

To see the effect of unshored construction, the curves for the unshored sections were shifted horizontally to meet the curve for the shored section at the dead load moments as shown in Fig. 2.15. In this figure, moment-curvature curves for the noncomposite steel sections were not shown. Larger dead load moment causes earlier yielding of the bottom flange and earlier departure from the linear elastic portion of the moment-curvature curve. The difference between the curves is reduced as the moment approaches the plastic moment, which is not affected by the construction method. Ductility is increased as the
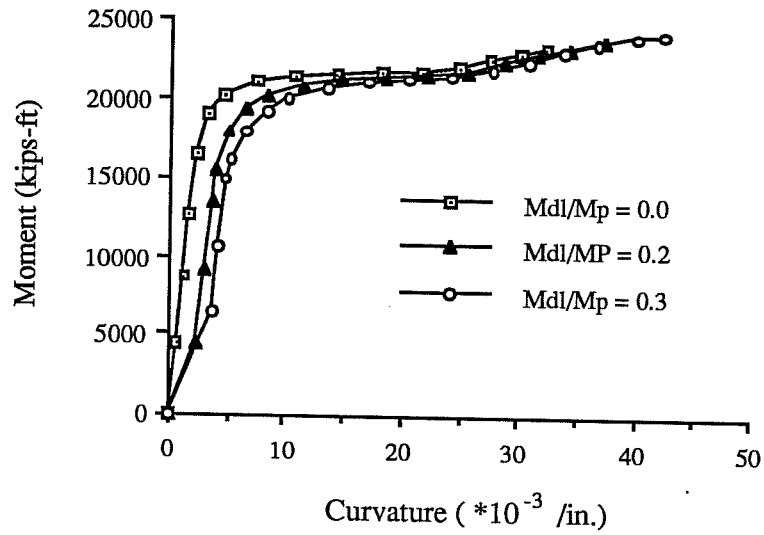
Figure 2.14 Effect of construction method
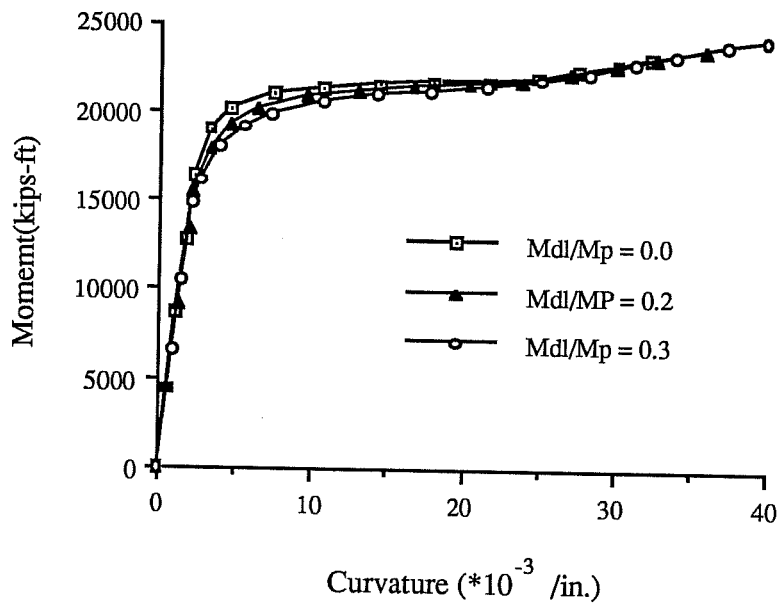
Figure 2.15 Comparison of composite actions

dead load moment ratio is increased because the earlier yielding of the bottom flange due to the higher dead load shifts the neutral axis further upwards.

2.3.7 Comparison with test results

Analytical moment-curvature curves were compared with experimental curves for composite plate girders tested by Vasseghi and Frank[9] in Fig. 2.16. The cross sections and material properties of Girder 1 and 2 are described in Table 2.2. In the test, Girder 1 was a shored composite girder. For Girder 2 which was tested as an unshored composite girder, a comparison was done for the composite loading. The noncomposite dead load moment of Girder 2 was about 20% of the plastic moment of the composite section. As can be seen in this figure, analytical and experimental results were in good agreement.

Table 2.2 Dimensions and material properties of G1 and G2

Specimens	Slab	Top Flange	Web	Bottom Flange
G1	$4.5 * 42.5$ $f' = 6200psi$	$0.50 * 10.0$ $f_y = 46.0ksi$	$0.257 * 40.0$ $f_y = 49.0ksi$	$1.010 * 16.0$ $f_y = 48.0ksi$
G2	$7.5 * 47.0$ $f' = 5700psi$	$0.50 * 10.0$ $f_y = 46.0ksi$	$0.3195 * 40.0$ $f_y = 42.0ksi$	$1.005 * 16.0$ $f_y = 48.8ksi$

2.4 Summary of Results

1. Concrete strength had little effect on the moment-curvature characteristics. An increase in steel yield stress increased the plastic moment greatly, but the effect on the moment-curvature characteristics is insignificant.
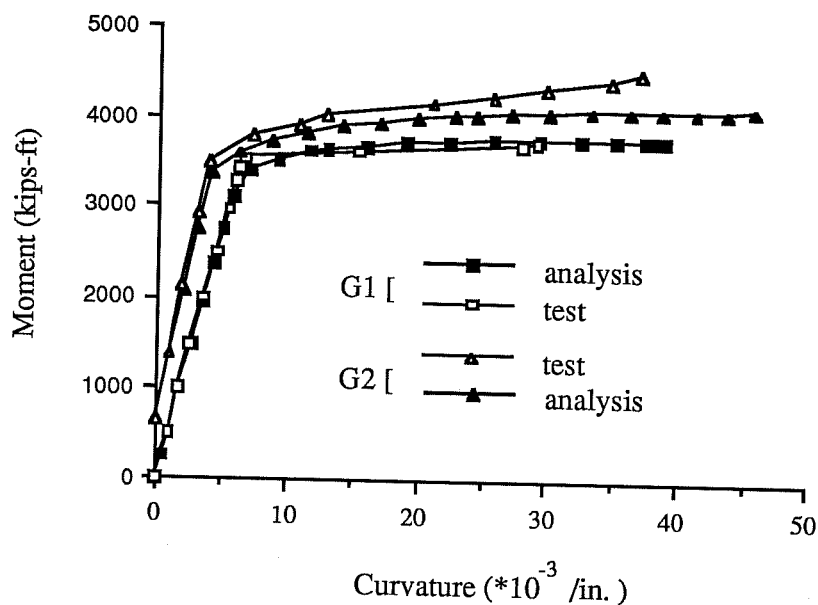
Figure 2.16 Comparison with test results

2. The change in slab dimension had little effect on the moment-curvature characteristics. The ratio of the yield moment to the plastic moment ranged from 0.8 to 0.82.

3. In composite sections with unshored construction, the noncomposite dead load caused early yielding and increased the curvature considerably thereafter. When the noncomposite dead load moment was increased from 0 to $0.3M_p$, the yield moment was reduced from $0.81M_p$ to $0.7M_p$.

4. High tensile residual stress in the tension flange caused yielding right after the load was applied, but the departure from elastic behavior was insignificant.

5. All the curves obtained in this analysis are nondimensionalized and shown in Fig. 2.17. The dotted curve is the elastic-perfectly plastic moment-curvature curve which provides the upper bound. The yield moment of the
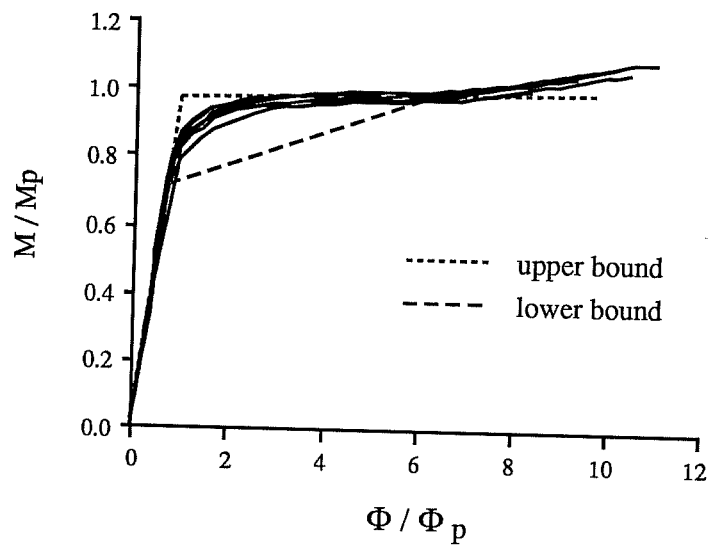
Figure 2.17 Upper and lower bounds

dashed curve is $0.7M_p$ and the inelastic stiffness is 1/20 of the elastic stiffness. These values are selected arbitrarily to provide a conservative lower bound. These upper and lower bound curves are used in the ultimate strength analysis of continuous composite plate girders in chapter 7.

CHAPTER THREE

BEHAVIOR AND STRENGTH OF THE NEGATIVE BENDING SECTION

The concrete slab of a composite plate girder in negative bending is subjected to tensile stress. When the applied moment exceeds the cracking moment, the concrete slab cracks and the stiffness of the cross section is reduced considerably. Therefore, negative bending sections of continuous composite plate girders have been traditionally designed as noncomposite sections ignoring the effects of the concrete slab and the reinforcing bars. Actually, however, the cracked concrete slab can transfer the longitudinal force in the reinforcing bars to the plate girder through the shear studs and the composite action between the reinforcing bars and the plate girder exists in the negative bending section.

3.1 Ultimate Bending Capacity

The concrete slab is assumed to carry no tensile stress after cracking. Thus, the plastic moment of a composite plate girder in negative bending is computed from the resultant moment of the fully yielded stress distribution of the steel section including the reinforcing steel bars as shown in Fig. 3.1.

The ultimate bending strength of an unbraced composite plate girder in negative bending is determined by the lateral torsional buckling and/or local buckling. Since this study is limited to the laterally braced girders, the limit state of lateral torsional buckling is not considered. Most plate girders have very slender webs and the reinforcing steel bars shift the neutral axis increasing the web area in compression. Therefore, the ultimate bending strength is affected

23
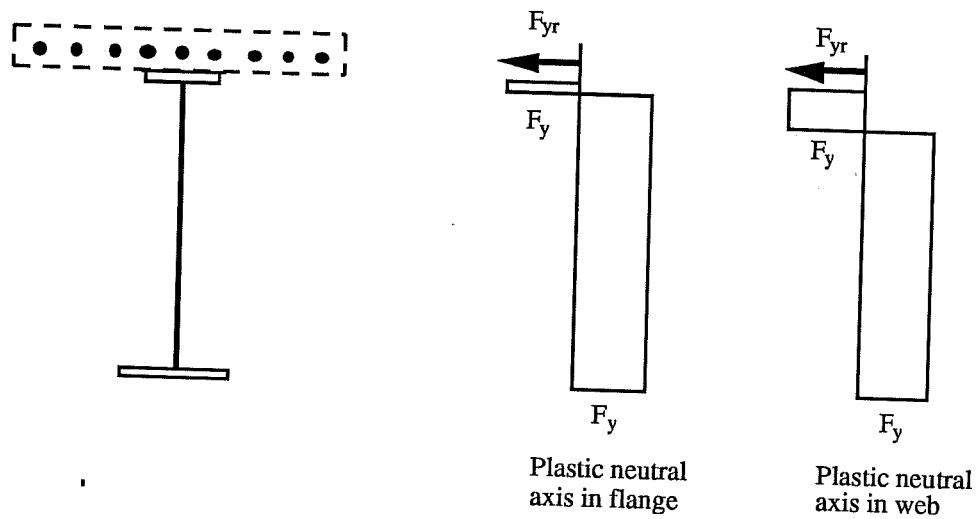
Figure 3.1 Plastic stress distribution for negative bending

by local instabilities such as web and/or compression flange buckling, which may cause premature failure before the section reaches its plastic moment.

3.2 Moment-Rotation Relationship

Typical moment-rotation curves of laterally braced beams are shown in Fig.3.2. In this figure, R represents the rotation capacity. Rotation capacity of 3.0 is sufficient for a mechanism to develop in practical structures. The cross sections can be classified into three ranges by their moment rotation characteristics[10].

1) A compact section has the ability to exceed the plastic moment and provide sufficient rotation capacity at that moment for a plastic mechanism to form ($R \geq 3$).

2) A noncompact section can reach the yield moment.
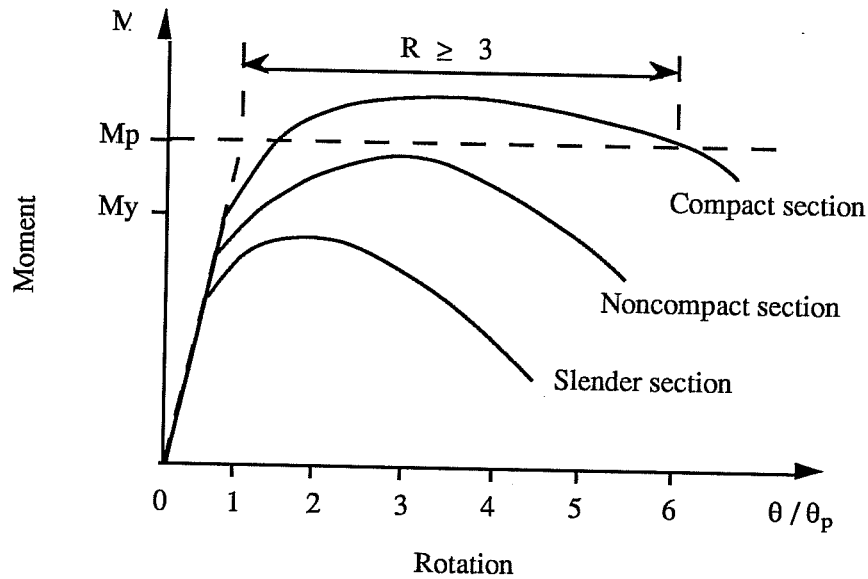
Figure 3.2 Generalized beam behavior

3) A slender section can not reach the yield moment because local buckling of the web and/or the compression flange occurs before the extreme fiber reaches the yield strain.

The ability of a cross section to reach these levels depends mainly on its compression flange and web slenderness ratios. The web slenderness ratio of an unsymmetrical section is defined as twice the depth of the web in compression divided by the web thickness.

3.3 Plate Buckling Strength

Beams and plate girders are composed of plate elements. The theoretical elastic buckling stress for a rectangular plate is represented by the following formula:

$$F_{cr} = \frac{k\pi^2 E}{12(1-\mu^2)(b/t)^2} \tag{3.1}$$

where k is a buckling coefficient depending on type of edge stress and boundary conditions; E is the modulus of elasticity, μ is Poisson's ratio, and b/t is the width-to-thickness ratio. The values of k which can be used to develop the slenderness ratio limits are listed in Table 3.1[11].

3.3.1 Width/thickness ratio for compression flanges

The buckling strength of a plate element in edge compression may be represented in a dimensionless form as shown in Fig. 3.3[12]. For a compression element to reach its yield stress without local buckling, the value of Eq. 3.1 must be equal to the yield stress, F_y. This is the intersection of the elastic buckling curve and the yield stress line, which is represented by point A at λ_c = 1.0 in Fig. 3.3. Using $\lambda_c = 1.0$ gives for b/t
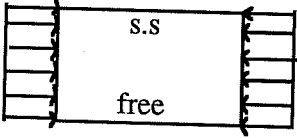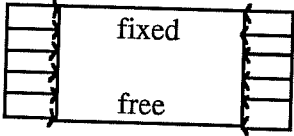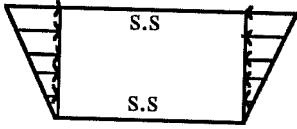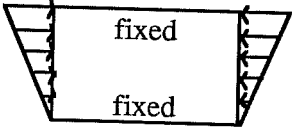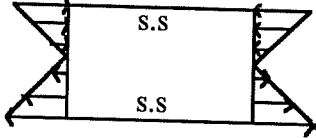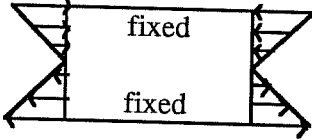
$$\frac{b}{t} = \frac{162}{\sqrt{F_y/k}} \tag{3.2}$$

where F_y is in ksi. Since plate elements have residual stress and imperfections, the actual strength is represented by a transition curve which deviates from the elastic buckling curve at λ_e which is greater than 1.0.

In the 1986 AISC LRFD Specification[2], the compressive residual stress in the compression flange, F_r, is deducted from F_y under the root sign to consider the effect of residual stresses. To account for the restraint provided by the web, k = 0.76 (about halfway between case (a) and (b) in Table 3.1) is selected as a buckling coefficient for rolled sections. Using this k value and $F_r = 10$ ksi gives the width/thickness limit for noncompact rolled sections as

$$\frac{b}{t} = \frac{141}{\sqrt{F_y - 10}} \tag{3.3}$$

Table 3.1 Plate buckling coefficient k

CASE	BOUNDARY CONDITION*	STRESS TYPE	k
(a)	s.s / free	compression	0.425
(b)	fixed / free	compression	1.277
(c)	s.s / s.s	compression + bending	7.8
(d)	fixed / fixed	compression + bending	13.6
(e)	s.s / s.s	bending	23.9
(f)	fixed / fixed	bending	39.6

* Loaded edges are simply supported

$$\lambda_c = \sqrt{\frac{F_y}{F_{cr}}} = \frac{b}{t}\sqrt{\frac{F_y}{E}\frac{12\,(1\text{-}\mu^2)}{\pi^2 k}}$$
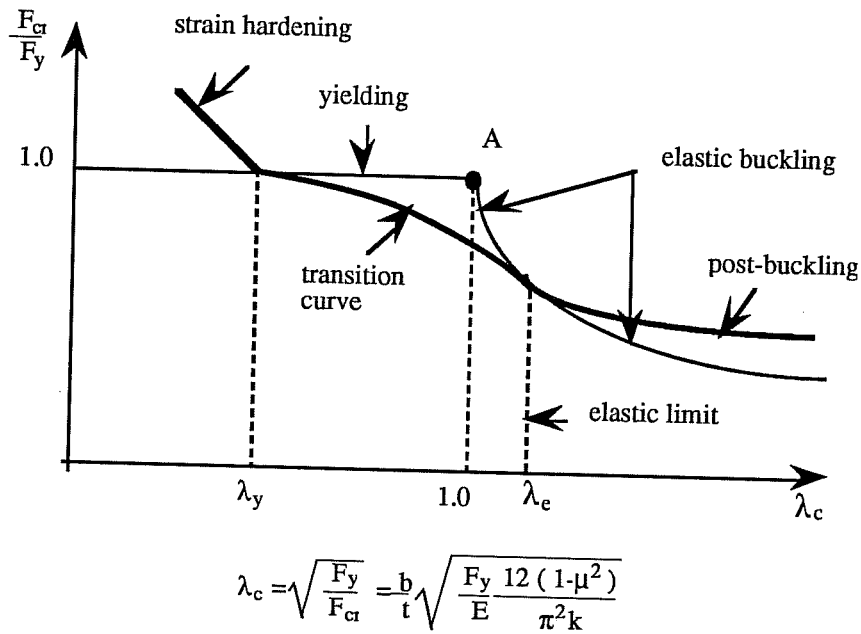
Figure 3.3 Plate buckling strength in edge compression

where b is half the full nominal flange width.

For welded sections, k = 0.43 which is the limiting case (a) in Table 3.1 for no web restraint is used based on Johnson's test[13]. Thus, the slenderness ratio limit for noncompact welded sections is

$$\frac{b}{t} = \frac{106}{\sqrt{F_y - 16.5}} \tag{3.4}$$

where compressive residual stress for welded sections of 16.5 ksi was deducted from F_y. Eq. 3.3 and Eq. 3.4 are used as the slenderness ratio limits for noncompact sections in the AISC LRFD Specification (Table A-F1.1).

In the AISC LRFD Specification, a section whose slenderness ratio is equal to the noncompact section limit can reach its maximum elastic moment, $M_r = S_x(F_{yf} - F_r)$, where F_{yf} is the yield stress of the compression flange and S_x is the section modulus. In the 1990 AASHTO Interim Specifications[4], a noncompact

section is defined as a section which can reach its yield moment, $M_y = S_x F_{yf}$. For a section to reach its yield moment, a reduced value of b/t should be used as can be seen in Fig. 3.3. The following equation is used as the limit for noncompact sections in the 1990 AASHTO Interim Specifications (formula 10-98).

$$\frac{b}{t} \leq \frac{69.5}{\sqrt{F_y}} \tag{3.5}$$

For $F_y = 36$ ksi, Eq. 3.4 and Eq. 3.5 give b/t = 24.0 and 11.6 respectively. For $F_y = 50$ ksi, Eq. 3.4 gives b/t = 18.3 and Eq. 3.5 gives b/t = 9.8.

For plastic design, the compression flange must achieve sufficient deformation at yield stress without local buckling. The 1978 AISC Specification[3] used a very severe restriction reducing λ_c to λ_y (= 0.46 for unstiffened compression elements) for plastic design. A buckling coefficient of k = 0.42, case (a) in Table 3.1, was used because a yielded web was assumed to provide no restraint. From these values, the width/thickness ratio is obtained as

$$\frac{b}{t} \leq \frac{48.5}{\sqrt{F_y}} \tag{3.6}$$

This equation was used as the slenderness ratio limit for plastic design sections in Part 2 of the 1978 AISC Specification (Section 2.7) and for compact sections in the 1983 AASHTO Specifications[6] (formula 10-92). The term "ultracompact section" was introduced in the literature[27] and used to name the compression flange sections which satisfy the requirement of Eq. 3.6.

Lukey and Adams performed experiments to investigate the relationship between the flange slenderness ratio and the rotation capacity of wide-flange beams under a moment gradient[15]. The rotation capacity R (as shown in Fig. 3.2) becomes greater than 3 which is considered to be a sufficient value for plastic design, when

$$\frac{b}{t} \leq \frac{65}{\sqrt{F_y}} \tag{3.7}$$

This equation is used as the slenderness ratio limit for compact sections in the AISC LRFD Specification (Table A-F1.1) and the 1990 AASHTO Interim Specifications (formula 10-92).

3.3.2 Width/thickness ratio for webs

To make the cross section of a beam more efficient, the flange area is increased and the web thickness is minimized. As a result, the web becomes very slender and may buckle elastically before the yield strength is reached. The elastic bend buckling strength of a web can be calculated using Eq. 3.1. To avoid elastic local buckling, Eq. 3.1 must be equal to the yield stress, F_y. Selecting 36.2 as a k value arbitrarily between case (e) and (f), 80% of the difference toward the fully fixed case (f), gives

$$\frac{h_c}{t_w} \leq \frac{970}{\sqrt{F_{yf}}} \tag{3.8}$$

where h_c is the clear distance between flanges for a symmetrical section and twice the web depth in compression for an unsymmetrical section. Eq. 3.8 is used as the web slenderness ratio limit for noncompact sections in the AISC LRFD Specification (Table A-F1.1) and the 1990 AASHTO Interim Specifications (formula 10-99).

When the web slenderness ratio exceeds the limit of Eq. 3.8, some of the web area in compression is not fully effective after buckling. But the web still has some post-buckling strength and the stress is redistributed across the cross section increasing the stress in the compression flange as shown in Fig. 3.4. To allow for the strength reduction of the cross section due to the web buckling, the AISC LRFD Specification (A-G2-3) and the 1990 AASHTO Interim Specifications (formula 10-102b) use a strength reduction factor proposed by Basler and Thurlimann[16],
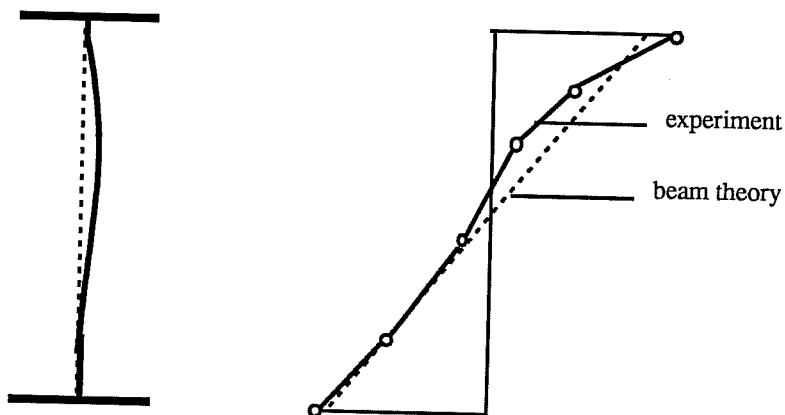
Figure 3.4 Stress distribution for a plate girder with a slender web

$$R = 1 - 0.0005a_r(\frac{h_c}{t_w} - \frac{970}{\sqrt{F_{cr}}}) \leq 1.0 \qquad (3.9)$$

where a_r is the ratio of the web area to the compression flange area in the AISC LRFD Specification and the ratio of twice the web area in compression to the compression flange area in the AASHTO Specifications. F_{cr} is the critical compression flange stress. In Eq. 3.9, $0.0005a_r$ is a simplified form for plate girders with $a_r \leq 2.0$. Yura recommended to replace $0.0005a_r$ with a more general equation by Basler and Thurlimann[16], a_r / (1200 + 300a_r), for plate girders with $a_r \leq 10.0$.

Della Croce conducted tests on eight continuous welded girders with unstiffened webs[15]. Based on the test data, the ASIC LRFD Specification (Table A-F1.1) adopted the web slenderness ratio limit for compact sections as

$$\frac{h_c}{t_w} = \frac{640}{\sqrt{F_{yf}}} \qquad (3.10)$$

Th web slenderness ratio limit for compact sections in the 1990 AASHTO Interim Specifications (formula 10-93) is also based on this equation.

Grubb and Carskaddan suggested the following interaction equation to re-define the allowable limits when both the flange and web slenderness ratios exceed 75% of the limits for compact sections[16].

$$\frac{h_c}{t_w} + 9.35(\frac{b}{t}) \leq \frac{33650}{\sqrt{F_{yf}}} \tag{3.11}$$

where F_{yf} is in psi. This interaction equation is used in the 1990 AASHTO Interim Specifications (formula 10-94). However, some sections in the tests by Holtz and Kulak reached their plastic moments without any interaction effect[19].

3.4 Nominal Flexural Strength

Based on the slenderness ratio limits developed in the previous sections, the ASIC LRFD Specification determines the nominal flexural strength. The variation in the nominal flexural strength with the flange or web slenderness ratio is shown in Fig. 3.5 for beams. For beams, two separate equations (Eq.3.3 and Eq.3.4) are used to define the flange slenderness ratio limit for noncompact sections, λ_r, depending on the type of construction. The two equations were derived using two different k values in Eq. 3.2. For rolled sections, a buckling coefficient k = 0.76 was arbitrarily selected to be about halfway between k = 0.425 (no web restraint) and k = 1.277 (fixed restraint). For welded sections, k = 0.43 was used. When the flange slenderness ratio exceeds the noncompact section limit, the nominal flexural strength is obtained from the elastic buckling equation (Eq. 3.1) with k = 0.76 for rolled sections and k = 0.43 for welded sections.

However, the theoretical plate buckling analysis does not consider the type of construction and Johnson's tests show that the restraining effect of the web varies with the slenderness ratio h/t[13]. Thus, using k = 0.43 for a welded

section with a stocky web would reduce the resistance unjustifiably and using k = 0.76 for a rolled section with a slender web would give unconservative results by the current AISC LRFD approach. Therefore, Yura recommended an approach that accounts directly for the restraining effect of the web based on Johnson's tests[14]. In his recommendation, λ_r is calculated as follows,

$$\lambda_r = \frac{162}{\sqrt{(F_y - F_r)/k}} \tag{3.12}$$

$$k = \frac{4}{\sqrt{h/t}} \leq 0.763 \quad \text{and} \quad h/t \leq \frac{970}{\sqrt{F_y}} \tag{3.13}$$

In the AISC LRFD Specification, plate girders are distinguished from beams based on the web slenderness ratio. For plate girders, whose web slenderness ratio is greater than the noncompact section limit of Eq. 3.8, different provisions shall apply for design flexural strength. Fig. 3.6 shows the variation in the critical stress with the flange slenderness ratio for plate girders. The maximum flange stress of a plate girder is limited to the yield stress, F_y, because web buckling occurs before the yield stress in the flange is reached. When the flange slenderness ratio exceeds the noncompact section limit, the critical stress is obtained using the elastic buckling equation (Eq. 3.1) with k = 0.43. The flexural strength obtained from the relationship in Fig. 3.6 is reduced by the reduction factor of Eq. 3.9 to get the nominal flexural strength.

In the 1990 AASHTO Interim Specifications, the variation in the nominal flexural strength with the flange or web slenderness ratio is determined as shown in Fig. 3.7. The lower value controls. The AASHTO Specifications do not have any provisions to apply for design flexural strength when the compression flange slenderness ratio, b/t, exceeds the noncompact section limit. If the maximum moment a beam is subjected to, M, is less than the yield moment, M_y, b/t may be increased by the ratio $\sqrt{M_y/M}$. When the slenderness ratio of a web
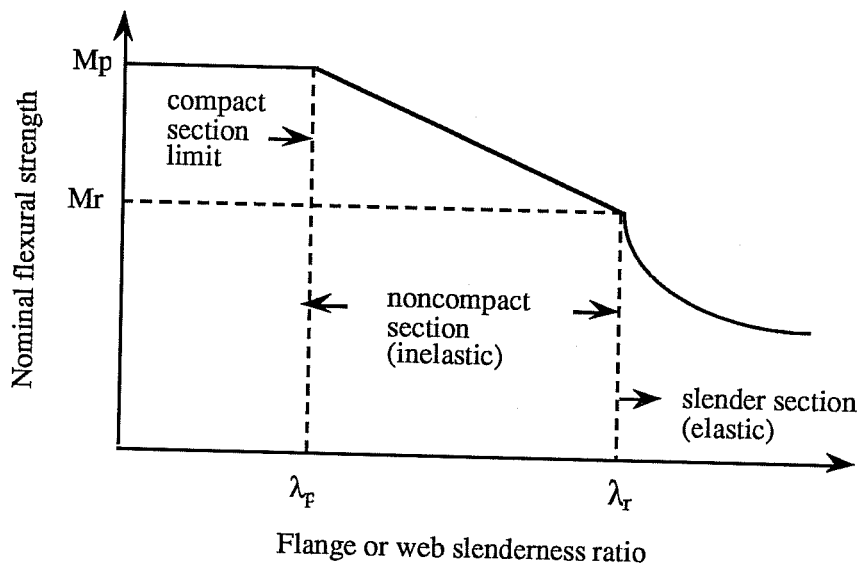
Figure 3.5 Nominal flexural strength vs generalized slenderness ratio for beams
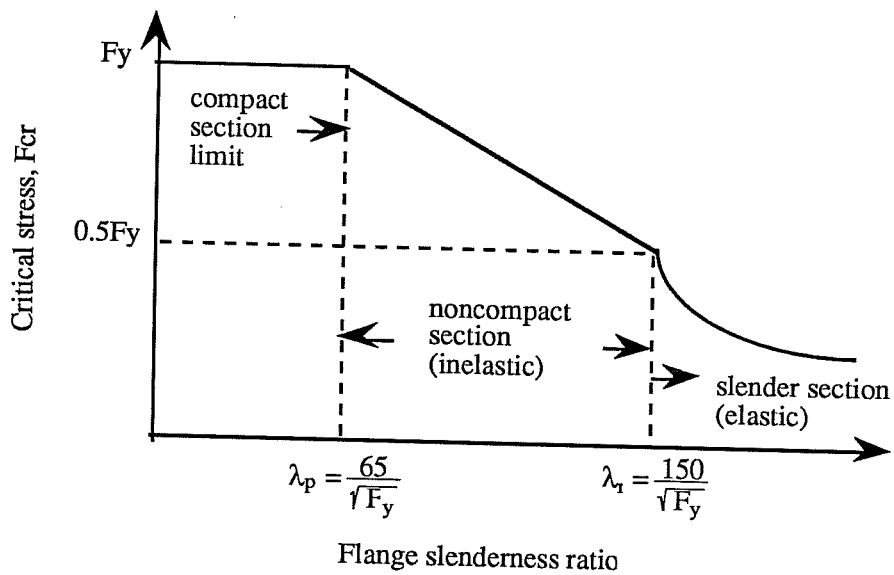
Figure 3.6 Critical stress vs flange slenderness ratio for plate girders
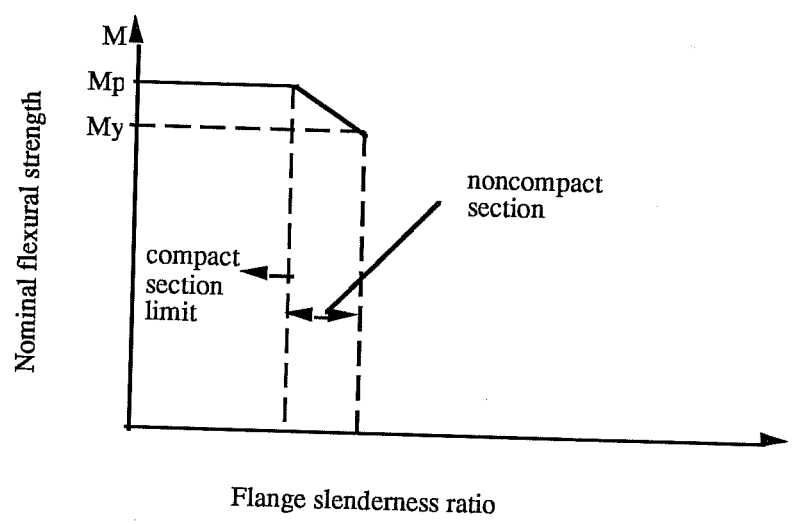
(a) Nominal flexural strength vs flange slenderness ratio
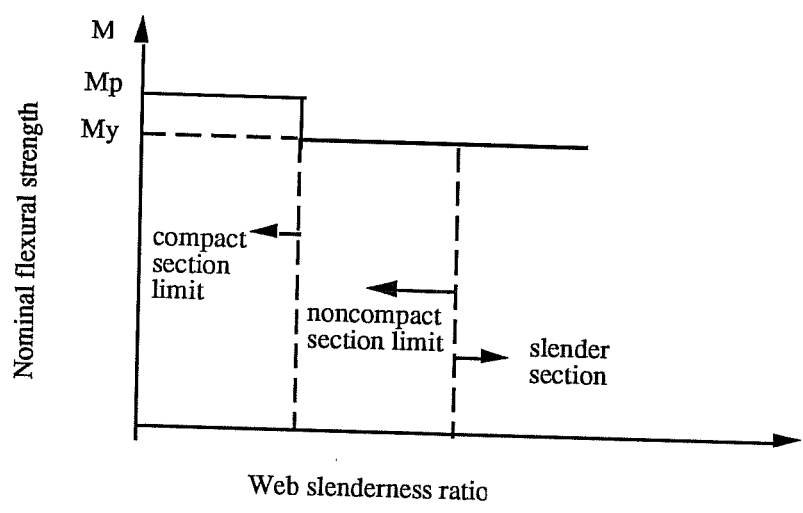
(b) Nominal flexural strength vs web slenderness ratio

Figure 3.7 Nominal moment strength in the 1990
AASHTO Specifications

exceeds the noncompact section limit, longitudinal stiffeners shall be required, or the nominal flexural strength is reduced by the reduction factor of Eq. 3.9 to account for the bend-buckling effect of the slender web.

3.5 The Q formula

To evaluate the nominal moment strength of composite and non-composite plate girders, Frank developed the Q formula in the proposed AASHTO LRFD Bridge Sspecifications based on Johnson's test data[20]. The factor Q, which is the ratio of the plate buckling stress to the yield stress of the compression flange, may be expressed as

$$Q = \frac{k\pi^2 E}{12(1 - \mu^2)(b/t)^2 F_y}$$

(3.14)

where the buckling coefficient, k, is given as a function of the web slenderness ratio to account for the restraining effect of the web,

$$k = \frac{4.92}{\sqrt{h/t}}$$

(3.15)

Substituting Eq. 3.15 into Eq. 3.14 gives

$$Q = \frac{1.29 * 10^8}{\lambda_w^{\frac{1}{2}} \lambda_f^2 F_{yf}}$$

(3.16)

where,

λ_w = web slenderness ratio = $2D_{cp}/t_w$

D_{cp} = web depth in compression at plastic moment

t_w = web thickness

λ_f = flange slenderness ratio = $b_f/2t_f$

b_f = total width of compression flange

t_f = thickness of compression flange

F_{yf} = yield stress of compression flange in psi

For a section to reach its plastic moment capacity, M_p, Q must exceed Q_p,

$$Q_p = 5.47f - 3.13 \qquad (3.17)$$

where,

f = shape factor for noncomposite section

= M_p/M_{yc} for composite section

M_{yc} = yield moment calculated considering sequence of loading

The nominal moment strength can be obtained in three categories:

(1) plastic moment is reached;

For $Q \geq Q_p$,

$$M_u = M_p \qquad (3.18)$$

(2) nominal strength occurs in the inelastic range;

For $Q_p > Q \geq 0.7$,

$$M_u = Mp - (M_p - 0.7M_y)[(Q_p - Q)/(Q_p - 0.7)] \qquad (3.19)$$

(3) nominal strength is equal to the elastic buckling strength;

For $Q < 0.7$,

$$M_u = QM_y \qquad (3.20)$$

The variation in the nominal moment strength with the Q value is shown in Fig. 3.8. The Q formula calculates the ultimate moment capacity only. When Q exceeds Q_p, the plastic moment can be reached. But it does not mean that the section can necessarily provide sufficient rotation capacity at the plastic moment.

The nominal moment strengths predicted by the Q formula were compared with the experimental strengths for 29 test specimens[13],[19],[26],[27]. The histogram of the ratio of the predicted strength to the experimental strength is shown in Fig. 3.9. The average was 0.97 and the standard deviation was 0.06.
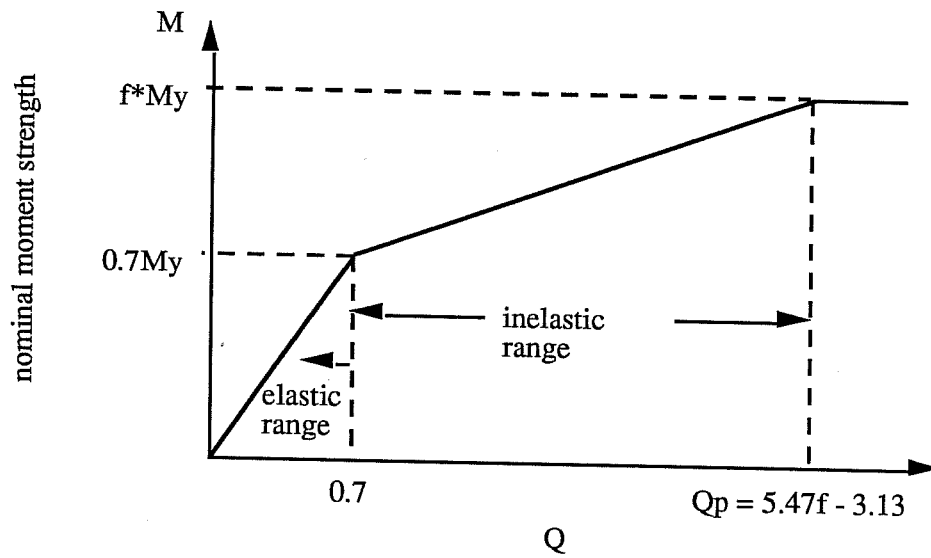
Figure 3.8 Nominal moment strength vs Q value of the Q formula
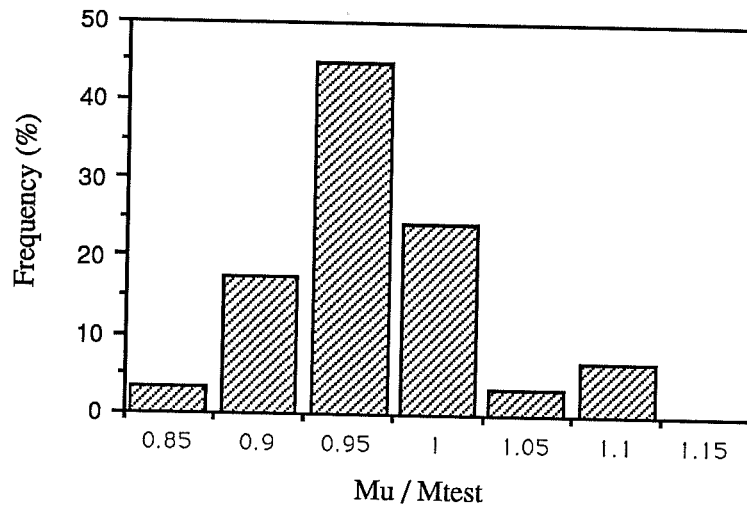
Figure 3.9 Histogram of the ratio of predicted strength to test strength

3.6 Modification of The Q formula

The value of Q (Eq. 3.16) increases greatly as the flange slenderness ratio is reduced. A section with an ultracompact compression flange may reach its plastic moment by the Q formula even if the web is very slender. Actually, however, Fig. 3.3 shows that the plate buckling strength is not affected significantly by b/t as the buckling strength approaches the yield stress. Therefore, the Q formula may give unconservative results for sections with very stocky compression flanges.

In the Q formula, the moment strength of an unsymmetrical section (in which the compression flange is smaller) is smaller than that of a symmetric section at the same Q value because the high shape factor of the unsymmetrical section increases the Q_p value (Eq. 3.17). A larger amount of plastic strain is necessary at the compression flange for an unsymmetric section to achieve the plastic moment. Fig. 3.10 shows the moment in terms of the strain at the compression flange for two sections with different shape factors. The unsymmetrical section with a shape factor of 1.4 started to yield at a low value of $0.71M_p$, but it could reach up to $0.97M_p$ and $0.99M_p$ at a flange strain of $3\varepsilon_y$ and $5\varepsilon_y$ respectively. Since a compact compression flange can achieve a plastic strain of $7\text{-}9\varepsilon_y$, an unsymmetrical section with a high shape factor may reach its plastic moment if λ_f and λ_w are equal to the compact section limits.

Based on the preceding discussions, the original Q formula can be modified as follows:

1. The flange compact section limit of Eq. 3.7 is used for λ_f in Eq. 3.16 when the flange slenderness ratio is less than the compact section limit.

2. When the compact section limits of Eq. 3.7 and Eq. 3.10 are used for λ_f and λ_w in Eq.3.16, the value of Q is 3. Therefore, M_p $(= fM_y)$ can be reached at $Q = 3.0$ for both symmetrical and unsymmetrical sections.

3. When the nominal flexural strength is less than the yield moment (or Q is less than 2.34), both unsymmetrical and symmetrical sections are assumed
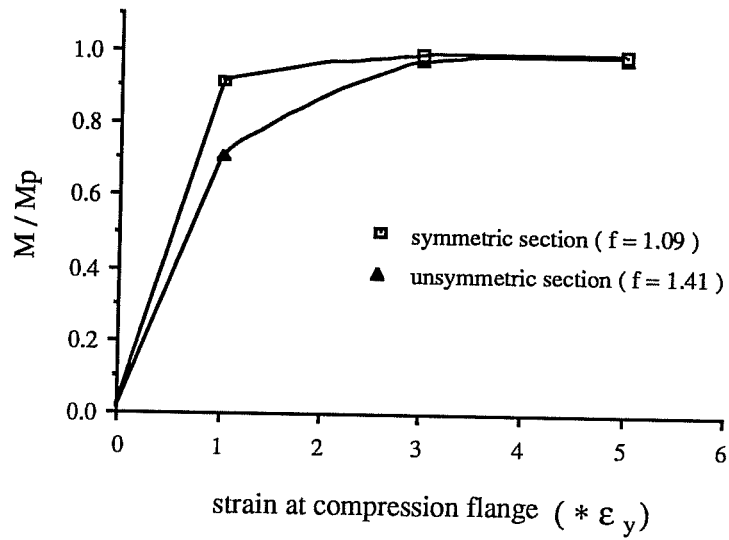
Figure 3.10 Moment vs strain at compression flange curve

to have the same nominal strength at the same Q value.

The nominal moment strength can be obtained in four categories:

(1) For $Q \geq 3.0$,

$$M_u = M_p \tag{3.21}$$

(2) For $3.0 > Q \geq 2.34$,

$$M_u = Mp - 1.52(M_p - M_y)(3.0 - Q) \tag{3.22}$$

(3) For $2.34 > Q \geq 0.7$,

$$M_u = M_y(0.58 + 0.18Q) \tag{3.23}$$

(4) For $Q < 0.7$,

$$M_u = QM_y \tag{3.24}$$
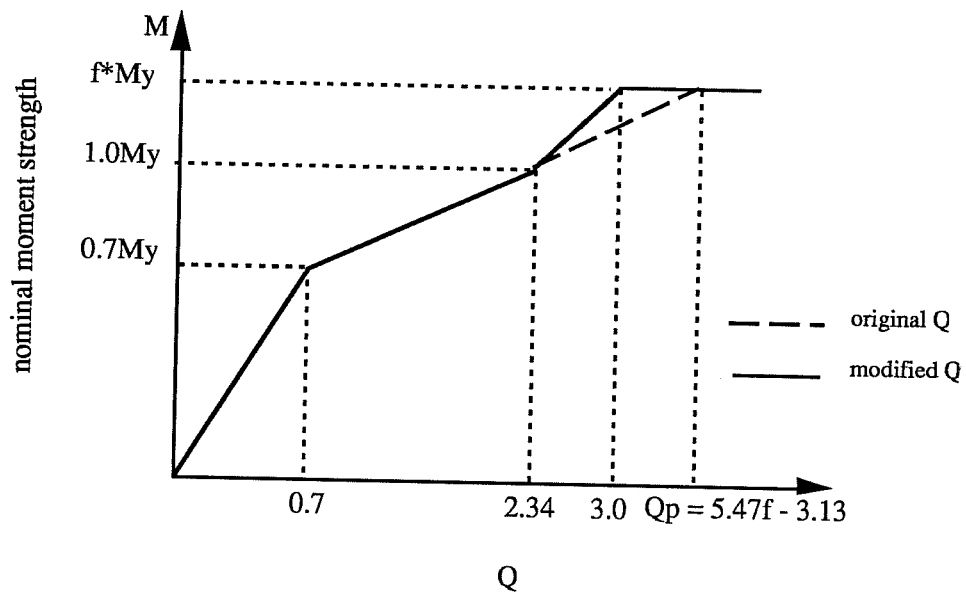
Figure 3.11 Nominal moment strength vs Q value of the modified Q formula

The nominal moment strength vs Q value curve for the modified Q formula is shown in Fig. 3.11.

The nominal moment strength obtained by the original and modified Q formulas are compared with experimental strengths for 8 test specimens in Table 3.2 and Fig. 3.12. Three specimens[13],[27] had ultracompact compression flanges and five specimens[19],[26] had high shape factors. As shown in Table 3.2, the original Q formula gave unconservative results for sections with ultracompact compression flanges (Girder D and 8) and conservative results for sections with high shape factors (Girder WS-2,3,4). The modified Q formula gave a better estimate as shown in Fig. 3.12. Both the original and modified Q formulas gave the same values for Girder UL and US despite high shape factors because the nominal moment strength was less than the yield moment.

Table 3.2 Comparision of the modified Q formula with the original Q formula

Ref. No	Test Girder	$b_f / 2t_f$	$2D_{cp} / t_w$	F_{yf}	Shape Factor	M_{test} / M_p	M_u / M_{test}	
							Original Q	Modified Q
27	M	6.60	117.3	58.93	1.11	1.02	0.98	0.96
	D	6.56	153.5	58.87	1.13	0.9	1.11	1.01
13	8	7.07	197.6	53.68	1.11	0.91	1.10	0.96
19	WS-2	9.67	99.9	46.79	1.21	1.01	0.91	0.98
	WS-3	9.67	119.9	46.84	1.23	0.93	0.94	0.98
	WS-4	9.67	140.0	46.82	1.24	0.89	0.93	0.96
26	US	9.03	159.5	59.37	1.47	0.65	1.00	1.00
	UL	9.15	158.3	58.32	1.26	0.79	0.96	0.96
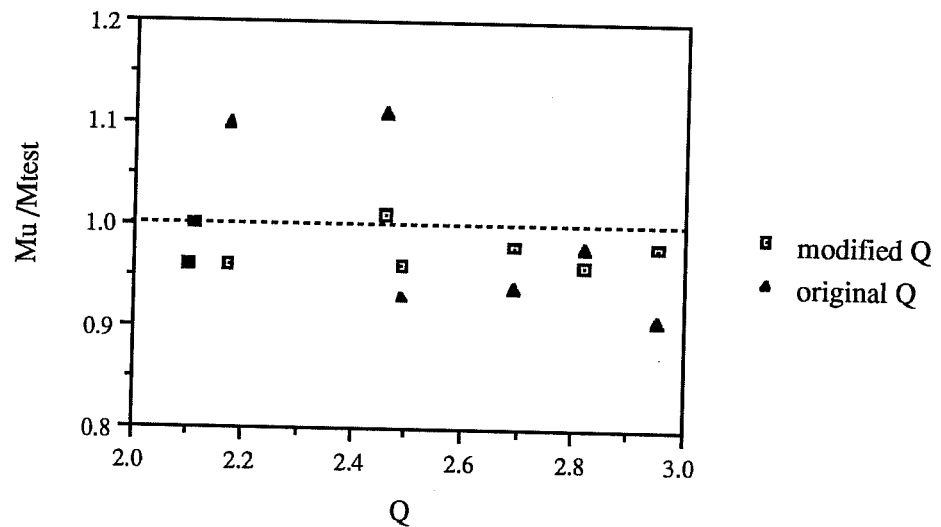
Figure 3.12 Comparison of the modified Q formula
with the original Q formula

CHAPTER FOUR

REVIEW OF DESIGN AND ANALYSIS METHODS OF COMPOSITE GIRDER BRIDGES

For the design of composite and noncomposite plate girder bridges, the AASHTO Specifications contain Working Stress Design (WSD) and Load Factor Design (LFD) procedures. The LFD procedure has been extended by including Autostress Design concepts[21] in the Guide Specifications for Alternate Load Factor Design (ALFD) Procedures for Steel Beam Bridges Using Braced Compact Sections[5].

4.1 Load Levels and Performance Requirements

The AASHTO Specifications specify three levels of loading, i.e., Service Load, Overload and Maximum Load. In the LFD and ALFD methods, a bridge is designed to assure satisfactory structural performances at these three load levels. These load levels and the corresponding performance conditions are listed in Table 4.1. Service Load includes nominal dead load plus live load of standard vehicles. Adequate fatigue life, acceptable live load deflection, and limited concrete cracking are performance requirements at this load level. Overload consists of nominal dead load plus live load of overload vehicles which weigh approximately 5/3 times the standard vehicles. The Overload check is intended to control permanent deflections that could create objectionable riding quality. Maximum load which is 1.3 times Overload consists of increased dead load plus exceptionally heavy vehicles. The bridge is required to have adequate strength to resist this Maximum Load. The design requirements of the LFD method are summarized in the third column of Table 4.1.

Table 4.1. Load levels and performance conditions (LFD method)

Loading	Performance Conditions	Design Requirements
Service Load DL + LL	fatigue life live load deflection	limit stress range L / 800
Over Load DL + 1.67 LL	objectionable permanent deformation	composite 0.95My noncomposite 0.80My
Maximum Load 1.3 (DL + 1.67 LL)	collapse	compact Mp noncompact My

4.2 Alternate Load Factor Design Method

Both the LFD and ALFD methods use the same design requirements at Service Load. At Overload, the LFD method limits the elastic maximum positive and negative moments to some fraction of the yield moments. For compact sections, the elastic maximum negative moment may be redistributed by a maximum of 10% before the comparison is made. The load distribution patterns which produce the maximum positive and negative moments are shown in Fig. 4.1. In contrast, the ALFD method places no limit on the negative moment by allowing a continuous-span bridge to adjust automatically the shake-down due to the local yielding and/or concrete cracking over the interior pier. Fig. 4.2 shows a set of self-equilibrating residual forces and automoments which are induced during the shake-down process and remain after the Overload is removed.

The automoments can be computed using a beam-line method based on the experimental moment-permanent rotation curve of the pier section as shown in Fig. 4.3. In this figure, Point A is the elastic Overload moment at the pier.

(a) Positive Moment Loading

(b) Negative Moment Loading
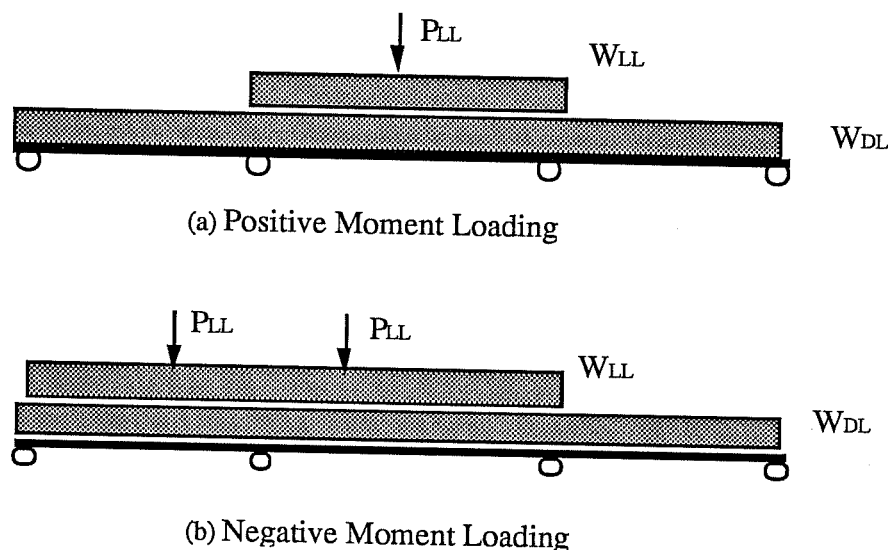
Fig. 4.1 Load distribution patterns

Point B is the slope change at the pier caused by the Overload assuming a free hinge at the pier. The line which connects Point A and B is the beam line. Point C is the intersection of the beam line and the experimental curve. This point represents the actual Overload moment and the permanent rotation at the pier. The difference between the elastic Overload moment (Point A) and the actual Overload moment (Point C) is the automoment at the pier. Under subsequent unloading and reloading of the Overload live load, the pier section remains elastic on the line CD as long as the load does not exceed the initial Overload. A typical moment-rotation curve obtained from test data[23] is used to determine the automoments for composite sections in the AASHTO Guide Specifications. The maximum positive moment plus any corresponding automoment is limited to the same design requirements as in the LFD method.

At Maximum Load, the LFD method limits the elastic maximum moment to the plastic moment for compact sections and to the yield moment for noncompact sections. For compact sections, 10% redistribution of the elastic maximum
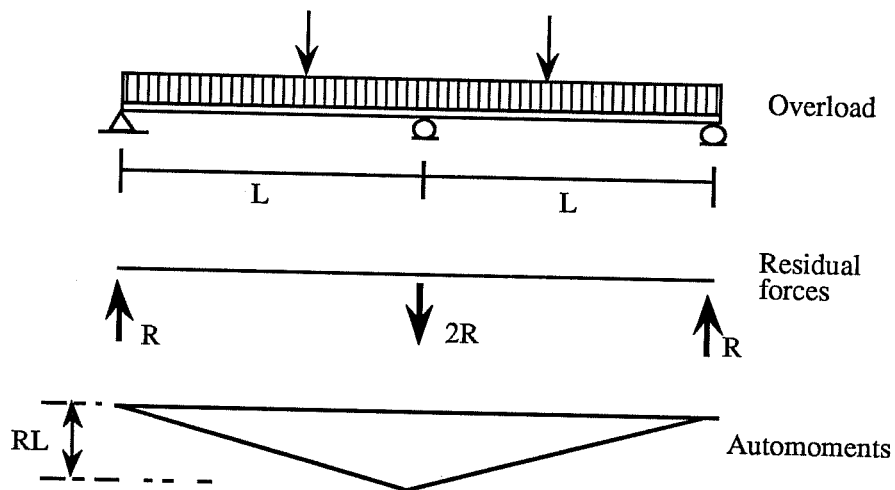
Fig. 4.2 Residual forces and automoments
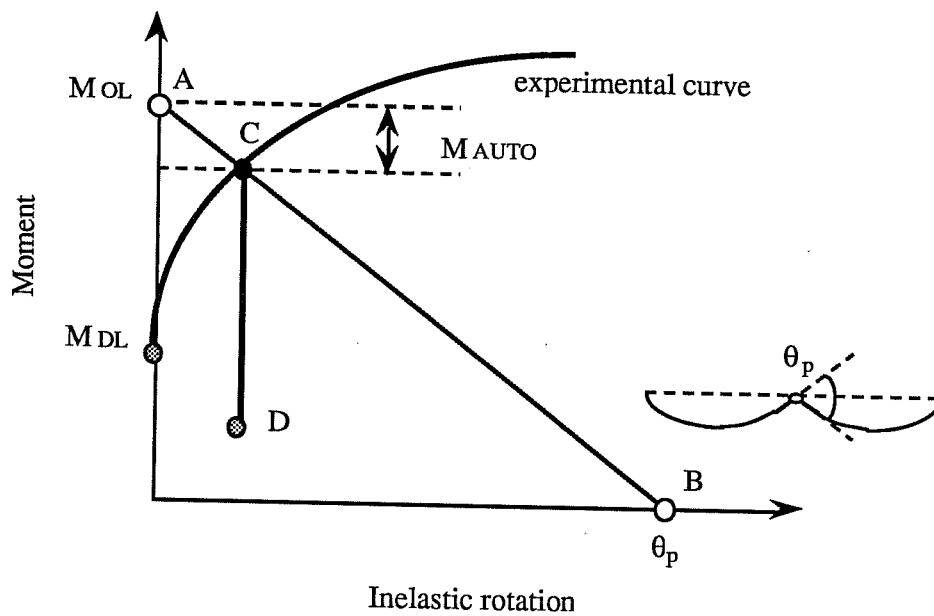
Fig. 4.3 Beam line method

negative moment is allowed. The ALFD method calculates the ultimate load capacity of a continuous bridge using the plastic mechanism method. For plastic design, a considerable amount of plastic rotation is required at the interior support, which can be provided by specifying the flange and web slenderness ratios and lateral bracing requirements. In the Guide Specifications, a compact section is defined as a section which can reach its plastic moment with a limited rotation capacity. Instead of using those sections with specified slenderness ratios for plastic design, the ALFD method determines an effective plastic moment, M_{pe}, at which enough plastic rotation is provided as shown in Fig. 4.4. In this method, the ultimate capacity is assumed to be reached when the positive bending section reaches the plastic moment. The moment diagram at the mechanism is shown in Fig. 4.5. The capacity calculated by the ALFD method is usually much larger than that by the LFD procedures.

The main advantage of the ALFD method is that it predicts the actual behavior of continuous-span bridges more accurately and provides much greater flexibility in selecting negative bending sections and more economical design than the present LFD procedure. Even with these benefits, however, the ALFD method needs further improvements in the design procedures for the following reasons:

1. Using the concept of an effective plastic moment at the Maximum Load check gives conservative results because the required rotation capacity at the pier is generally much smaller than the provided rotation capacity at the effective plastic moment[22].

2. The typical moment-rotation curve used to calculate the automoments for composite sections is based on a single component test for shored construction[23]. Most composite bridges are built without shores. And no experimental data are available on composite sections for unshored construction.

3. Presently, the ALFD method applies only to bridges with compact sec-
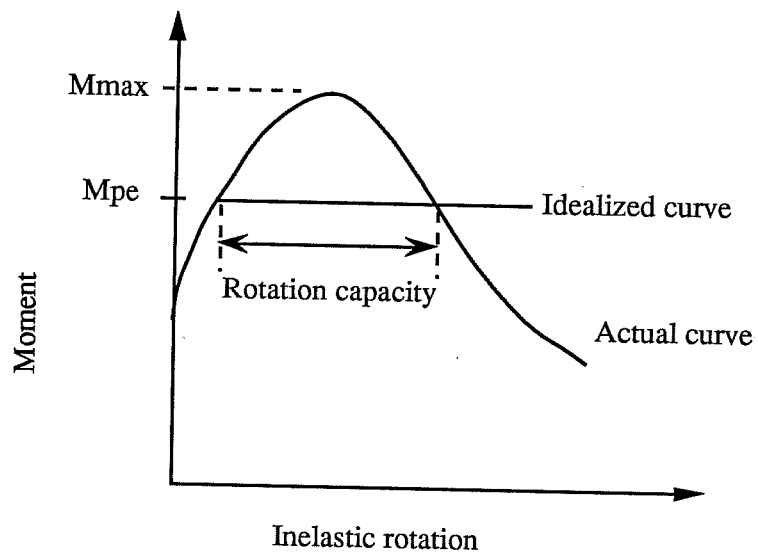
Fig. 4.4 Effective plastic moment
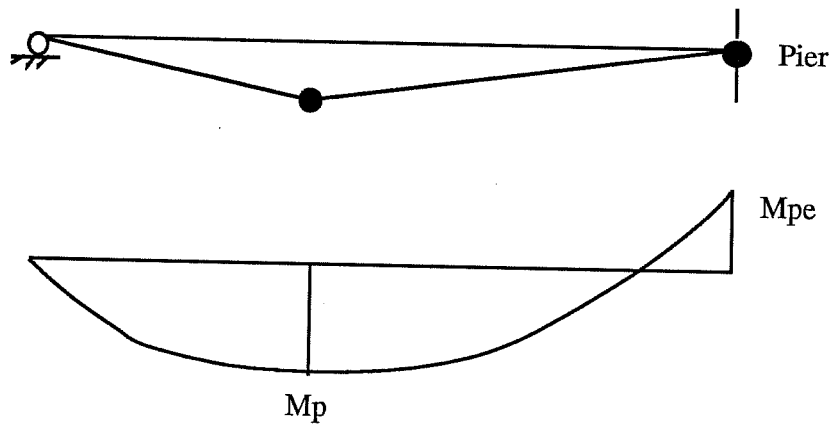
Fig. 4.5 Moment diagram at mechanism

tions. To extend this method to noncompact section bridges, more tests need to be performed for better understanding of the moment-rotation behavior of noncompact sections.

4.3 Compact Section Design Method

The results of research conducted at UT Austin[9] have shown that typical composite plate girders can reach their plastic moment capacities in the positive moment region due to the small web depth in compression. However, the use of the plastic moment capacity is limited to simple span bridge design because the moment-rotation behavior of negative moment sections is not well known. To use the plastic moment capacity of a positive moment section in the design of a continuous composite plate girder bridge, Vasseghi proposed a design method which uses a compact section in the negative bending region[24]. To satisfy the requirements for compact sections, the pier section is proportioned as an unsymmetrical cross section with a much larger compression flange which reduces the web depth in compression.

But unsymmetrical sections are susceptible to fatigue cracking due to high tensile stress at Service Load. This problem can be avoided by prestressing the concrete slab in the negative bending region to control the tensile stress. Vasseghi compared his method with the LFD and ASD methods by designing a continuous bridge using the three different design methods. The saving in the in-place costs was not significant but his method improved the structural performance greatly. In this method, the ultimate load capacity is easily calculated by the plastic mechanism method using the plastic moment capacities of the positive and negative bending sections.

4.4 Equilibrium Method

To design a continuous-span bridge using the plastic moment capacity of a positive moment section, Frank and Grubb proposed an Equilibrium Method which does not require the knowledge of the moment-rotation behaviors of a negative moment section[25]. In a design of a continuous-span bridge, different loading patterns are used to calculate the maximum positive and maximum negative moments as shown in Fig. 4.1. In the elastic range, the negative moment at the pier produced by the positive moment loading of Fig. 4.1(a) is less than that by the negative moment loading of Fig. 4.1(b). If the maximum positive moment by the positive moment loading exceeds the yield moment of the positive bending section, moment redistribution occurs increasing the negative moment at the pier. The amount of the increase in the pier moment depends on the inelastic stiffness of the positive bending section. The largest increase occurs when the inelastic stiffness of the positive section is zero after the yield moment.

In the Equilibrium Method, the pier section is designed to resist the elastic maximum negative moment by the negative moment loading and the positive bending section is designed to resist the elastic maximum positive moment by the positive moment loading using its plastic moment capacity. Fig. 4.6 shows the elastic moment diagram for the positive moment loading. The dashed curve is the moment diagram after the redistribution of moment when the inelastic stiffness of the positive section is zero. The pier moment by the positive moment loading, M_s, is increased by δM, which is the difference between the plastic moment, M_p, and the yield moment, M_y, of the positive section. As long as the increased pier moment, $M_s + \delta M$, is less than or equal to the moment capacity of the pier section, the design is satisfactory. The ultimate capacity of a continuous-span bridge calculated by this method is less than the actual capacity because no collapse mechanism is formed.
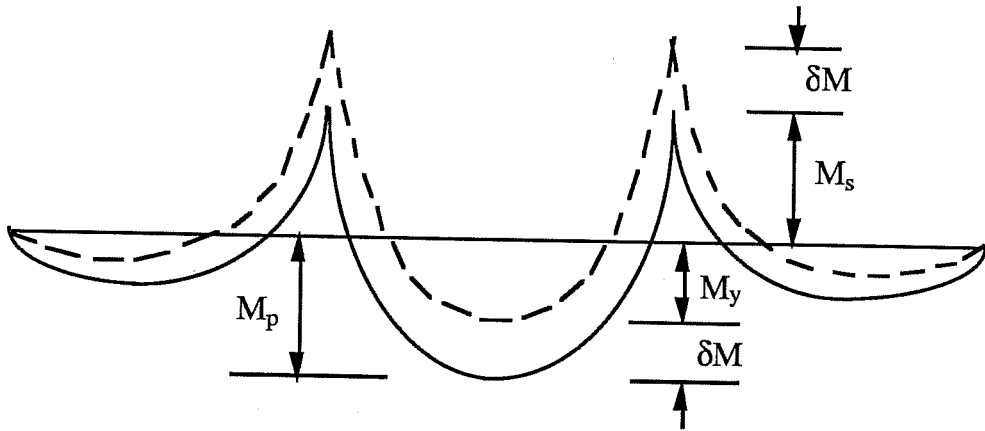
Fig. 4.6 Equilibrium method

Since Overload flange stress is limited to $0.95F_y$, maximum positive moment at Maximum Load can not exceed $1.23M_y$. A typical shape factor for a composite section in positive bending is about 1.4. Therefore, the capacity and the size of the positive bending section are controlled by the Overload limit state in most bridge designs.

CHAPTER FIVE

SUMMARY OF EXPERIMENTAL RESULTS

5.1 Ultimate Strength of Composite Plate Girders (AISIproject 320)

The AASHTO Specifications limit the moment capacity of a composite plate girder to the first yield moment based on the result of tests on symmetrical plate girders. But the behavior and strength of a composite plate girder in positive bending are different from those of a steel plate girder. To evaluate the ultimate strength of a composite plate girder, Vasseghi and Frank conducted ultimate load tests on three large-size composite plate girders[9].

In the experimental program, Girder 1 and 2 were designed to be simply supported to simulate a positive bending region, while Girder 3 simulated a two span continuous girder by extending an overhang beyond one of the supports. The negative bending section of Girder 3 was post-tensioned with low relaxation strands. For Girder 1 and 2 and the positive bending section of Girder 3, the ratio of web depth to thickness was about equal to the 1983 AASHTO limiting ratio for noncompact sections.

All three sections reached their plastic bending moments in the positive bending region and exhibited ductile behaviors despite slender webs because the concrete slab shifted the neutral axis close to the top flange. The moment-rotation curves showed that some permanent deformation occurred at loads well below the yield moment due to the slip caused by concrete crushing around the shear studs. But the permanent set does not affect the moment-curvature curves in Fig. 2.16 because the moment-curvature behaviors were measured at midspan where there was no slip.

The negative bending section of Girder 3 had an ultracompact compression

flange and a slender web whose overall depth-to-thickness ratio exceeded the compact section limit of the 1983 AASHTO Specifications. The plastic neutral axis was close to the compression flange due to the much larger compression flange than the tension flange. The negative bending section reached its plastic moment and exhibited ductile behaviors. In calculating the plastic moment, the concrete slab and the reinforcing bars were ignored and the nominal ultimate strength was used for the strands.

5.2 Interior-Support-Model Test (AISI project 188)

In the ALFD method, the moment-rotation behavior of the pier section of a continuous-span bridge affects the design requirements at Overload and Maximum Load. At Overload, the automoments are calculated using the loading portion of the moment-rotation curve. At Maximum Load, the concept of an effective plastic moment which depends on the descending portion of the moment-rotation curve is used. To study the moment-rotation behavior of the pier section of a continuous composite beam bridge, a half-scale component specimen with shored construction was tested[23].

The flange slenderness ratio was 8.0 which is about halfway between the compact section limit of the 1990 AASHTO Specifications and the ultracompact section limit (or the compact section limit of the 1983 AASHTO Specifications). The ratio of web depth to thickness was 58. The reinforcing bars in the concrete slab shifted the neutral axis above the mid depth of the web. The ratio of twice the web depth in compression to the web thickness was 96.6 at the plastic state. The limiting web slenderness ratio for compact sections of the 1990 AASHTO Specifications is 86.

Test results showed that inelastic rotation occurred well below the yield moment largely due to the concrete cracking. The ultimate moment capacity

was about 90% of the plastic moment. After the ultimate moment, the rotation continued to increase as the moment decreased. The test was stopped when the slab pulled away from the steel beam. The loading portion of the moment-permanent rotation curve obtained in this test is used in the AASHTO Guide Specifications to compute the automoments for composite beams with compact sections. In the Guide Specifications, this curve was adjusted vertically to reach the plastic moment because the specimen could not reach its plastic moment.

5.3 Moment-Rotation Tests of Steel Girders (AISI project 188)

The ALFD procedures in the current Guide Specifications apply specifically to compact sections. To extend these new limit state criteria to plate girders, three transversely stiffened plate girders, US, UL, and SL, were tested and the moment-rotation curves were developed[26]. For all three specimens, the equivalent flange and web slenderness ratios for 50 ksi steel were close to the AASHTO limiting values for noncompact sections, 9.8 and 163.2, respectively. Twice the web depth in compression at plastic moment was used to calculate the web slenderness ratio for unsymmetrical specimens US and UL. Using twice the web depth in compression at the yield moment reduces the web slenderness to 146 for US and 133.6 for UL. Lateral braces were provided at the ends and midspan of all specimens. The spacing of the lateral braces satisfied the requirements of the Guide Specifications for plastic analyses.

Test results showed that the ultimate moment was just below the yield moment for each specimen. The ratio of the slope of the descending curve to that of the elastic rising curve ranged from -0.1 to -0.16. Based on the moment-rotation curves, Schilling developed a lower bound curve for the descending portion. The effective plastic moments which depend on the web and flange slenderness ratios were calculated based on the procedure in AASHTO Guide

Specifications. The values were very low and varied from 35% to 45% of the yield moment. The plastic rotation at the effective plastic moment was 0.07, 0.068, and 0.037 radians for specimens US, UL, and SL respectively. The plastic rotation requirement at the effective plastic moment is 0.063 radians in the Guide Specifications.

To develop improved moment-rotation characteristics for steel girders with noncompact webs, three symmetrical plate girders with ultracompact compression flanges were tested[27]. One-sided transverse stiffeners were welded to the web and the compression flange at a distance equal to one-half the web depth on each side of midspan. The equivalent web slenderness ratios were about 87, 127, and 166 for specimens S, M, and D respectively. The spacing of the lateral braces satisfied the requirements of the Guide Specifications for plastic analyses.

All three specimens showed improved moment-rotation characteristics compared with the previous tests. The ratio of the slope of the descending curve to that of the elastic rising curve for specimen D was -0.083. The ultimate moments were 1.11Mp, 1.02Mp, and 0.90Mp (Mp = plastic moment) for specimens S, M, and D respectively. The effective plastic moments decreased from 0.89Mp to 0.75Mp as the web slenderness ratio increased. The ratio of the effective plastic moment to the ultimate moment was 0.835 and the plastic rotation at the effective plastic moment was 0.0345 radians for specimen D. The closely spaced stiffeners in the plastic hinge region reduced the wave length of the flange local buckling and improved the rotation capacity.

5.4 Component Test Report (AISI project 330)

To develop experimental moment-rotation curves for the pier section of a continuous composite girder bridge, a composite plate girder component specimen was tested at the laboratory of the Federal Highway Administra-

tion (FHWA)[28]. The specimen had an ultracompact compression flange and the concrete deck consisted of precast concrete panels. The height-to-thickness ratio of the web plate was 103.8. Using twice the web depth in compression at the plastic moment increased the ratio to 140.1 because of the prestressing strands in the concrete slab. The specimen was supported at the center and loaded down at a distance of 9 ft on each side of the center.

In the first phase, noncomposite dead load was applied to the steel girder to simulate the unshored construction. After that, the precast panels were erected and post-tensioned longitudinally using mechanical leveling and hold-down devices and then made composite with the steel plate girder by filling the shear stud block-outs in the precast panels with grout. After grouting had cured, the composite girder was tested at Overload by loading through the precast deck. In the final phase, the loading points were moved 3 ft toward the center support to simulate the actual moment-to-shear ratio and the complete moment rotation curve including the descending portion was obtained.

Test results showed that the specimen behaved elastically under the non-composite dead load, even though the maximum moment was above the first yield moment of the steel section. Deviation from the linear elastic moment rotation curve started at an early stage of composite action. A drastic change in slope at Service Load occurred due to concrete cracking. After that, compression flange yielding caused further inelastic rotation. After the moment reached its maximum value of $1.1M_y$ (or $0.85M_p$), it started to decrease as the rotation continued to increase. The ultimate moment capacity calculated using the modified Q formula in Chapter 3 is $0.86M_p$.

The moment vs permanent rotation curve of the specimen is compared with those from Schilling's tests in Fig. 5.1. The inelastic rotation capacity of the specimen was reduced considerably when the shear connectors pulled out of the precast panel. Nevertheless, the curve is still well above Schilling's lower bound curve. The web slenderness ratio of this specimen is between the ratios

for Schilling's specimens M and D. Closely spaced transverse stiffeners adjacent to midspan were not used in this component test. The curve for the component specimen fell below the curve for specimen D as shown in Fig. 5.1. The ratio of the average slope of the descending curve to the slope of the elastic rising curve was -0.069.

In calculating the effective plastic moment based on the procedure in the AASHTO Guide Specifications, only the web component of the plastic moment was reduced because an ultracompact section was used for the compression flange. Since the web component was less than 20% of the total plastic moment, the effective plastic moment of this specimen was about 94% of the maximum moment capacity despite the slender web.

5.5 Moment-rotation test of a composite plate girder in negative bending (AISI project 51)

5.5.1 Test specimen

To evaluate the moment-rotation characteristics of the pier section of a continuous composite plate girder bridge, a component test was performed on a 1/2 scale specimen at the Ferguson Structural Engineering Laboratory (FSEL). The prototype was a 200 ft two span continuous composite plate girder with 13.0 ft transverse girder spacing. An unsymmetrical steel section with a larger compression flange than the tension flange was used. The elevation of the girder, the actual dimensions of the cross section and the material properties are shown in Fig. 5.2. The maximum web bowing between flanges and the maximum compression flange bowing between supports were taken as the initial out-of-flatness. The initial out-of-flatness was 1/16 inch for the 24 inch web panel and 7/16 inch for the compression flange respectively. To prevent the splitting of the concrete slab off the steel plate girder, the composite section was extended 6 ft beyond the support at both ends. Continuous submerged arc welding was
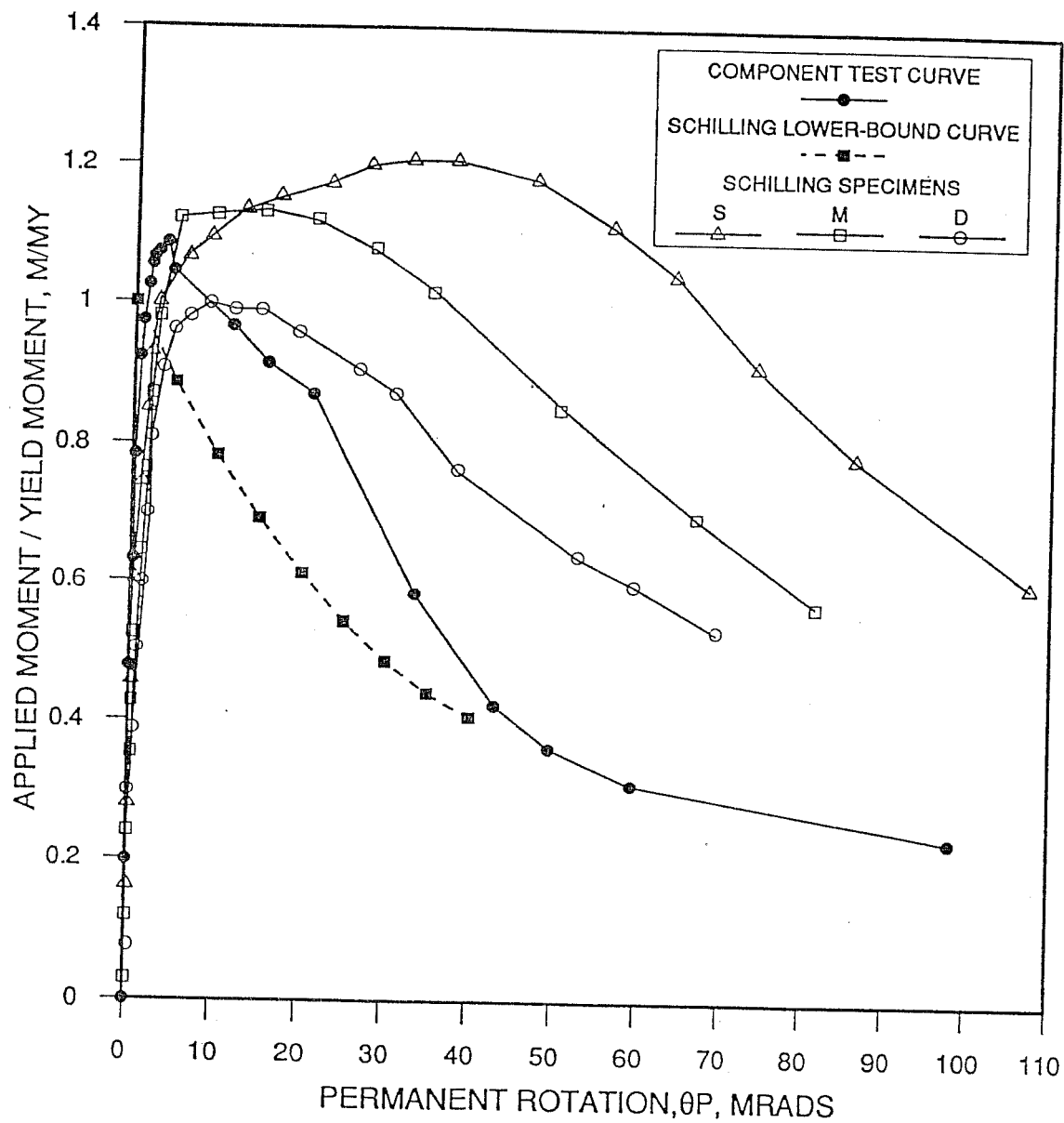
Fig. 5.1 Comparison of moment-permanent rotation curves
(reference [28])

used to fabricate the specimen.

To improve the rotation behavior, an ultracompact section with a slenderness ratio of 7.3 was used for the compression flange. The depth-to-thickness ratio of the web plate was 155.6. The elastic neutral axis of the steel section was below the mid height of the web due to the larger compression flange. When twice the elastic web depth in compression of the steel section was used, the slenderness ratio was 143. The calculated web slenderness ratio using twice the web depth in compression of the composite section at the plastic moment increased to 198.9 due to the reinforcing bars in the concrete slab.

5.5.2 Test set-up

To simulate the negative bending area between two inflection points of a continuous composite bridge, the specimen was tested as a simple beam restrained by steel rods at the reaction points and loaded upward by a hydraulic ram at midspan. To assure that the bending capacity of the specimen was not affected by lateral-torsional buckling, lateral bracing was provided for the compression flange at 12 ft spacing. The maximum spacing allowed by the AISC LRFD Specification for plastic analyses was 12.5 ft for this specimen. The tension flange was braced at supports. A considerable amount of inelastic deflection occurred during the ultimate load test. To avoid the restraint by the bracing system, a bracing design based on Watt's straight line mechanism[35] was used except at the supports and midspan. A manually adjusted brace was used at midspan. An overall view of the test setup is shown in Fig. 5.3.

5.5.3 Test procedure

For an unshored composite bridge, the initial dead load which consists of the weight of the concrete slab and the steel girder is carried by the steel girder alone. The additional dead load plus live load is carried by the composite sec-

81"

6'

3@69"

6@24"

3@69"

24'

24'

60'

9.31"

(a) Elevation

81"

6'

75.0"

4.0"

12'*0.761"

40"*0.257"

13"*0.893"

Stiffner (A36)
shear: 3/8" * 4" PL single sided
bearing: 1 1/4 " * 5 5/8 " PL double sided

Reinforcing Bar (Fy = 72.5 ksi)
longitudinal: top 18-#3, bottom 10-#3
transverse : top & bottom #3 @4.5"

Structural steel (A572 Grade 50)
flange: top Fy= 53.8 ksi, bottom Fy=48.9 ksi
web : Fy = 51.3 ksi

Concrete (f'c = 5100 psi)
Composite section
  My = 25780 k-in
  Mp = 31625 k-in
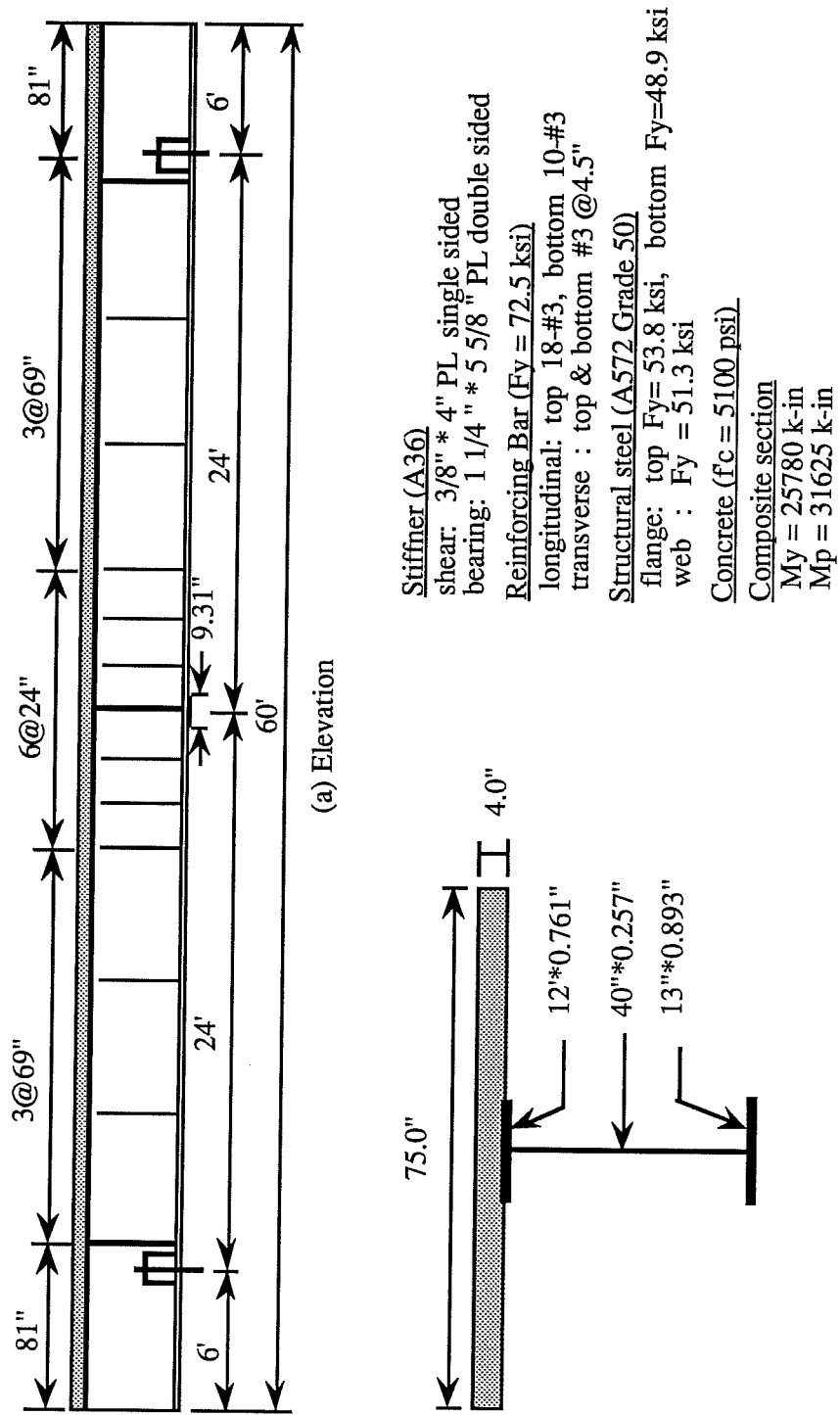
(b) Cross section and material properties

Fig. 5.2 Elevation and cross section and material properties of test specimen
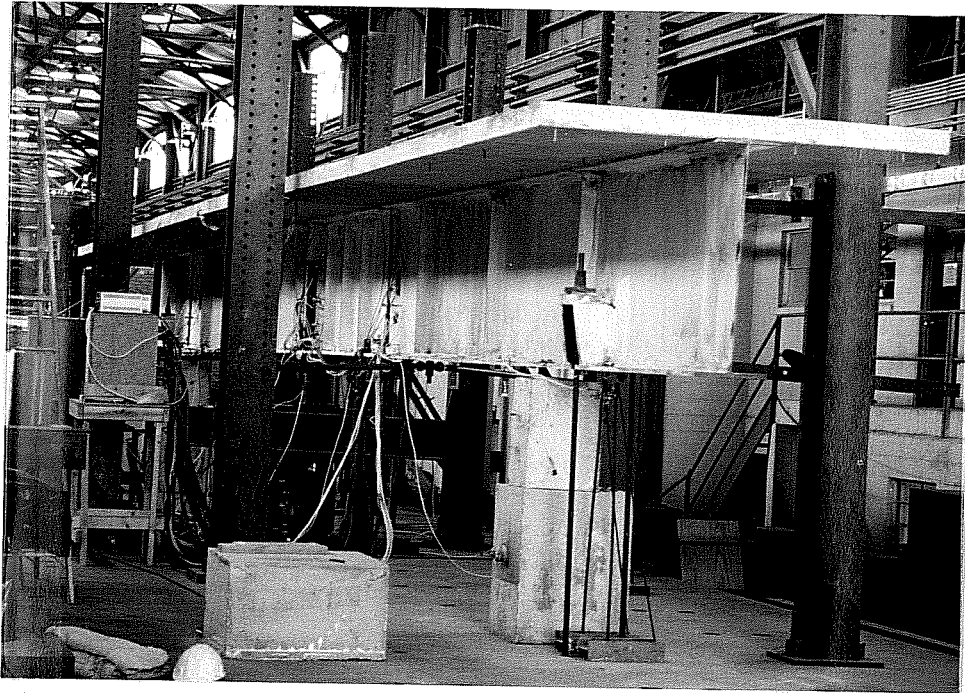
Figure. 5.3 Overall view of the test setup

tion. To investigate the behavior of a pier section under noncomposite dead load, the steel plate girder was loaded up to a load of 100 kips prior to casting the concrete slab. With the plate girder held at the simulated dead load, concrete was placed on the formwork which were supported by the shorings. After the concrete cured, the composite plate girder was loaded up to the design Overload. During the Overload test, the composite plate girder was unloaded and reloaded at several locations to investigate the behavior at Overload. Following the Overload test, the specimen was loaded up to its ultimate capacity. The descending portion of the moment-rotation curve was obtained by applying deflection increments after the ultimate strength was reached.

The significant features characterizing the cross sectional behavior are indicated on the load deflection curve in Fig. 5.4 and the loads at the characterizing features are summarized in Table 5.1.
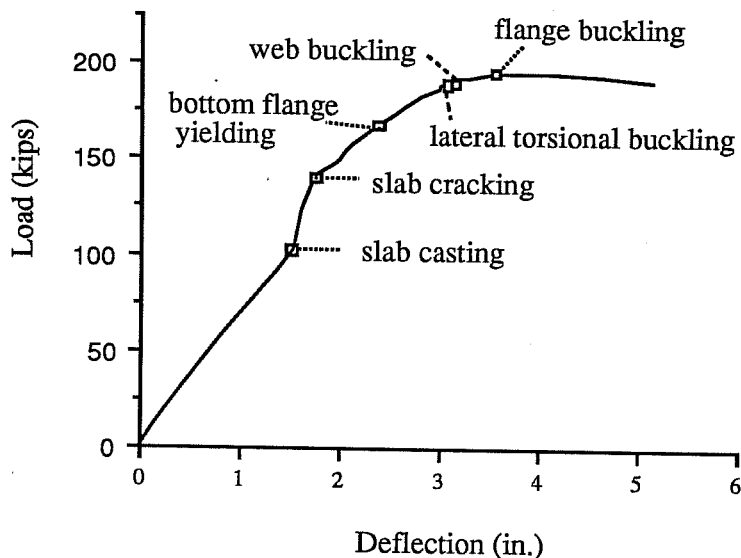
Figure. 5.4 Features characterizing the cross sectional behavior

Table 5.1 Loads at the characterizing features

Concrete casting	Concrete cracking	Bottom flange yielding	Lateral-torsional buckling	Web local buckling	Bottom flange buckling
100 kips	140 kips	167 kips	189 kips	191 kips	195 kips

5.5.4 Dead load test

The steel plate girder was loaded up to a simulated noncomposite dead load of 100 kips. The cross section was designed for the maximum stress to be smaller than the yield stress at the noncomposite dead load. Several yield lines were observed on the web at an early stage when the applied load was about 50 kips. These yield lines (whitewash flaking) started at the top of the web near

the stiffeners and gradually extended to near the center of the web as shown in Fig.5.5. Residual stresses induced from the welding of the stiffeners to the web are assumed to have caused the web yielding. Due to the web yielding, bending stresses were redistributed across the cross section. This yielding also induced some permanent deformation under the dead load test. As shown in Fig. 5.6 and Fig. 5.7, the specimen could not return to its original position when it was unloaded. During the dead load test, lateral bracing was provided at supports and halfway between the supports and the center. No lateral or local buckling was observed during this loading.
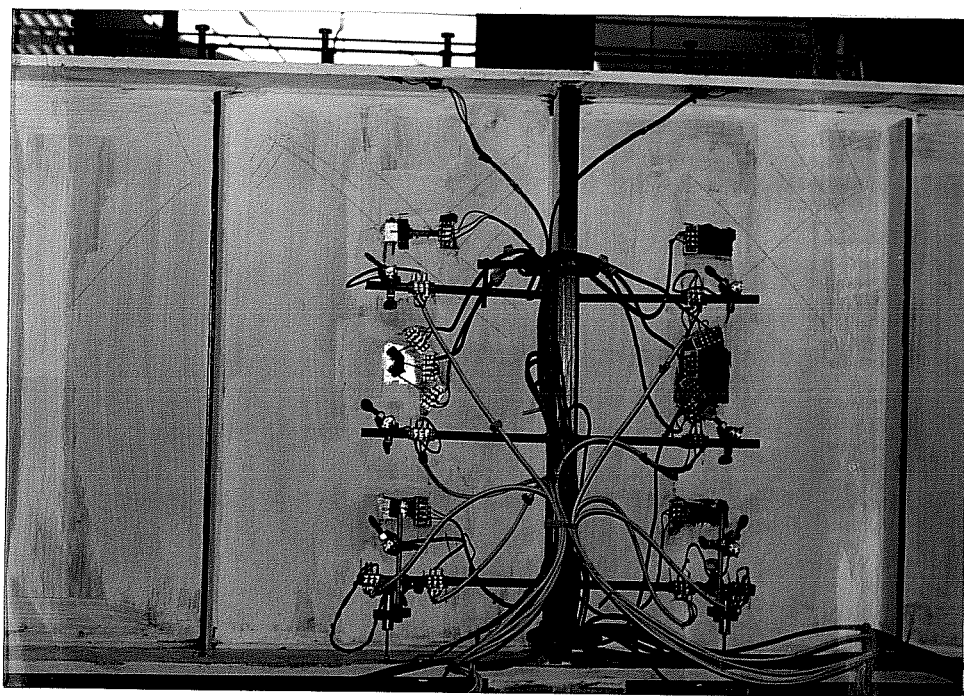

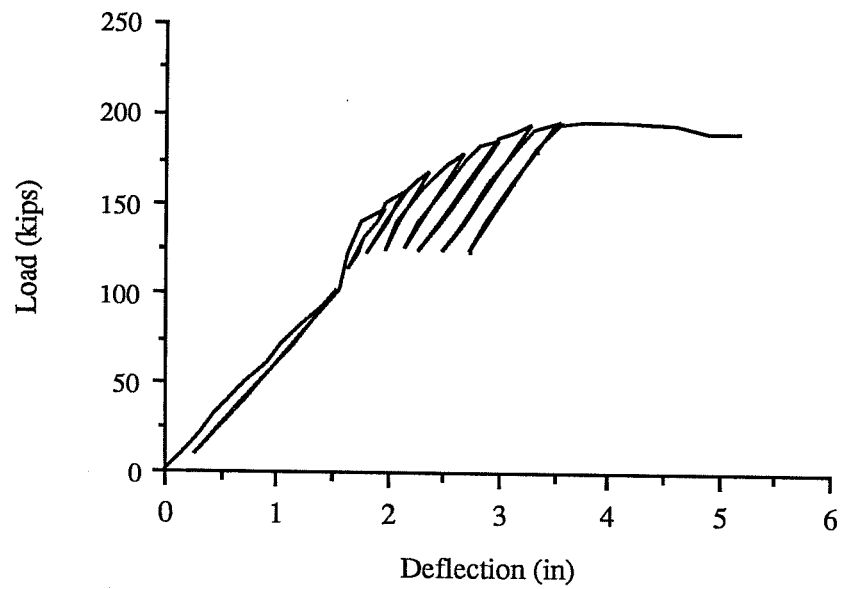Figure. 5.5 Web yielding under dead load test
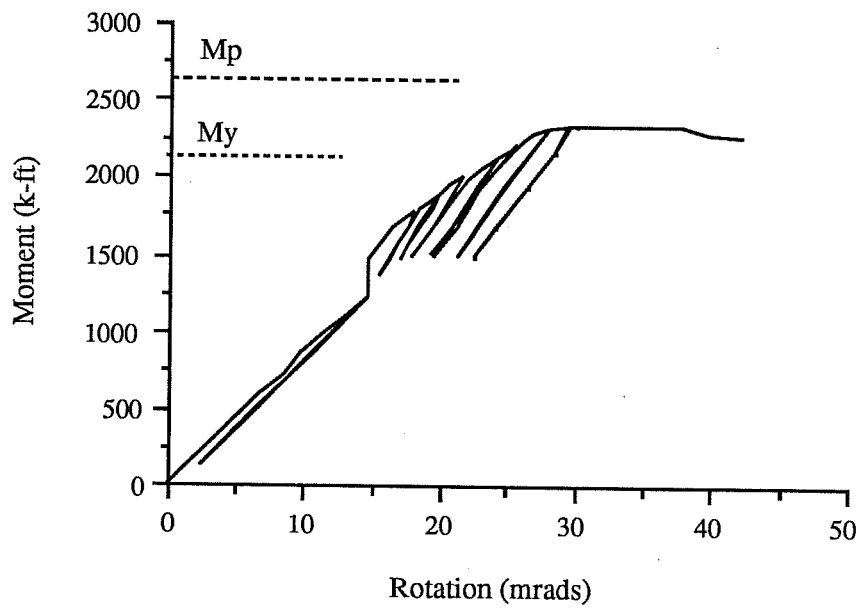
Figure. 5.6 Load vs deflection curve

Figure. 5.7 Moment vs rotation curve

5.5.5 Overload test

The load increased to 123 kips due to the weight and shrinkage of the concrete slab after the dead load test. The Overload test was performed on the composite plate girder. As shown in Fig. 5.6, the stiffness of the cross section increased greatly due to the concrete slab, but it was less than the theoretical stiffness of the composite section calculated using the actual slab width as the effective slab width. This could be the effects of shear lag, shrinkage of the concrete slab, the slip between the concrete slab and the steel girder, and the yielded web.

Rotations due to the weight of the concrete slab were not measured because electronic rotation gauges were removed from the specimen for protection during the casting of the slab. This is represented by the vertical line in the moment-rotation curve of Fig. 5.7 after the dead load test. The web yielding (whitewash flaking) did not progress as rapidly as in the dead load test because the concrete slab shifted the neutral axis upward. The concrete cracking reduced the flexural stiffness of the cross section considerably. The flexural stiffness after concrete cracking was smaller than the theoretical stiffness of the cracked section probably due to the yielded web.

At Overload, the ALFD method uses the automoment concept which is based on the assumption that the unloading occurs elastically with the same stiffness as the uncracked section. To examine the validity of this assumption, the specimen was unloaded to the Service Load level and reloaded again at various stages. The initial slopes of the unloading curves were nearly the same as that of the elastic loading curve of the composite section as shown in Fig. 5.6 and Fig. 5.7. The slopes became smaller as the specimen suffered yielding and permanent deformations, but the reduction was insignificant.

The yielding of the bottom flange started at a load of 167 kips which is about 90% of the design Overload and progressed up through the web increasing the web depth in compression. The theoretical yield load calculated considering the
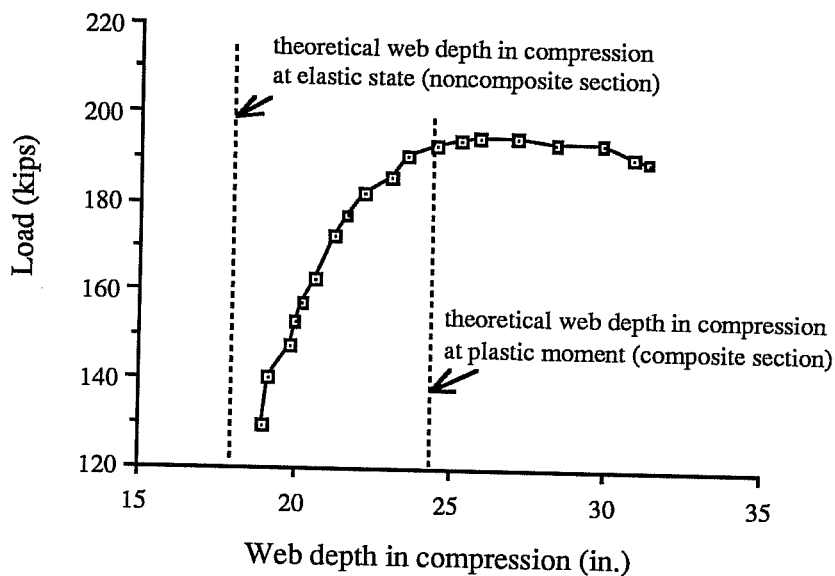
Fig. 5.8 Variation of the web depth in compression

sequence of loading was 179 kips. The change of the web depth in compression in the first 24″ panel from the center is shown in Fig. 5.8. The web depth in compression was calculated from the measured strains along the steel section.

5.5.6 Ultimate load test

After the Overload test, the specimen was loaded to failure. Due to the initial out-of-flatness, the out-of-plane deflections of the web and the compression flange occurred at the beginning of the loading and continued as the load increased. In the elastic range, the lateral and/or local instability is assumed to start at the point where the slope of the load vs out-of-plane deflection curve changes drastically. However, in the inelastic range, the slope can be reduced by the inelastic behavior of the specimen before the start of the instability.

To evaluate the onset of the instability in the inelastic range, the midspan
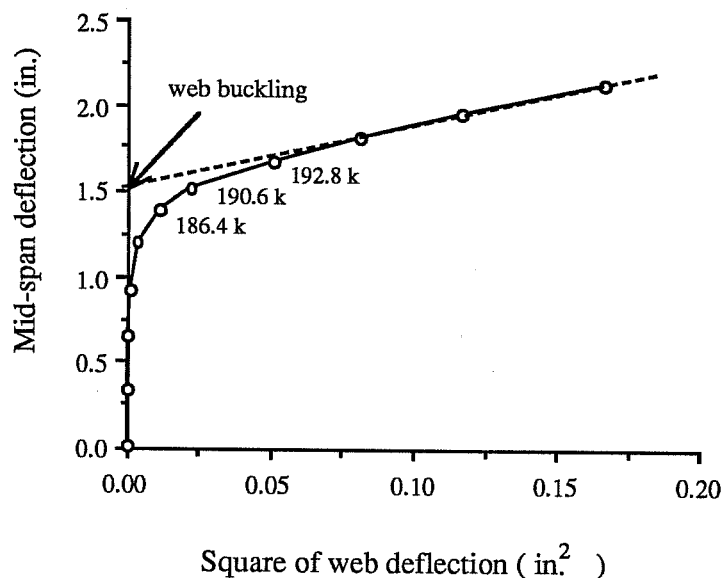
Figure. 5.9 Determination of web buckling

deflection vs lateral deflection curve was used for the lateral torsional buckling[32] and the midspan deflection vs square of the web deflection curve was used for the web bend-buckling[31].

The point of drastic change in the slope of the curve is determined as the onset of the instability as shown in Fig. 5.9 (191 kips) and Fig. 5.10 (189 kips). Fig. 5.11 shows the laterally buckled shape of the test specimen.

The load continued to increase after lateral torsional buckling occurred, until local buckling of the compression flange started at a load of 195 kips. The ultimate load calculated by the modified Q formula was 178 kips. The local flange buckling which triggered the descending curve occurred in the second panel from the center as shown in Fig. 5.12. This was because the bearing plate welded to the compression flange at the loading point provided large restraint to the compression flange in the first panel. The complete descending curve could not be obtained due to the failure of the bracing system.
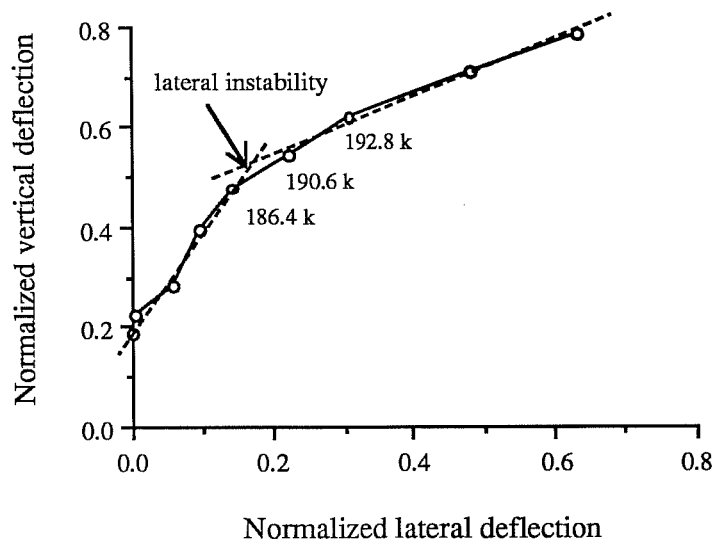
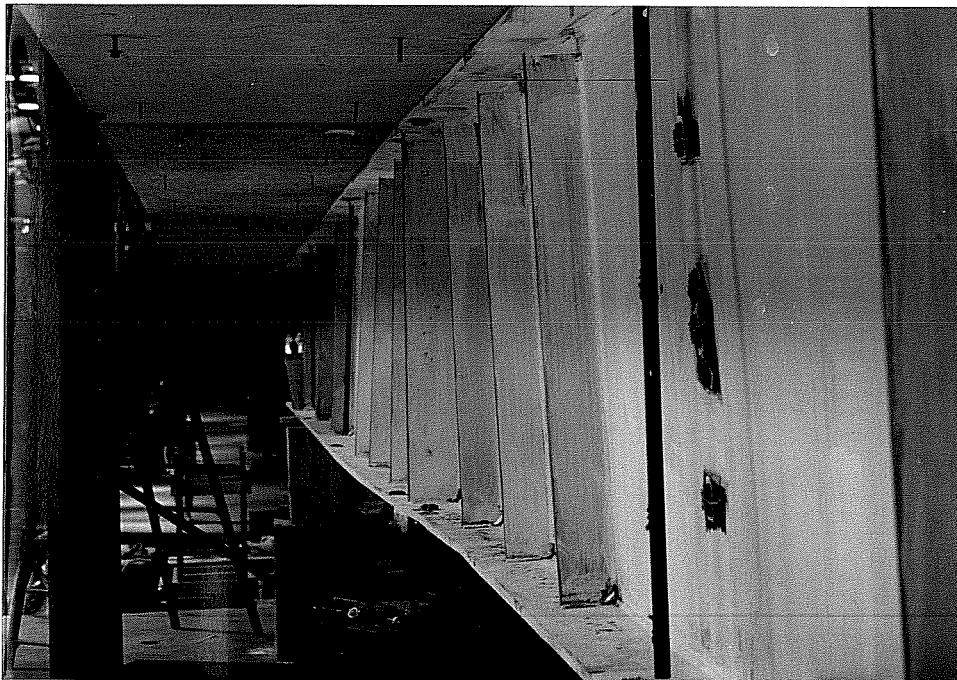Figure. 5.10 Determination of lateral torsional buckling

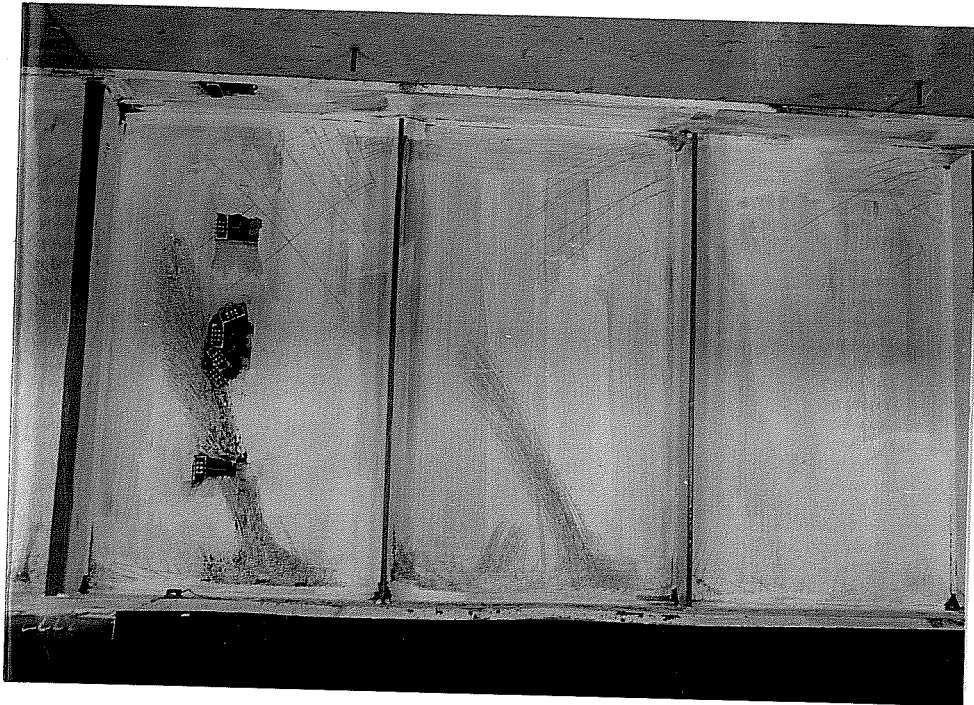
Figure. 5.11 Laterally buckled shape

Figure. 5.12 Local buckling of compression flange

5.5.7 Comparison with other test results

The rising portions of the moment vs permanent rotation curves for the test specimens with slender webs and ultracompact compression flanges were compared with the design curves of the AASHTO Guide Specifications in Fig. 5.13 and Fig. 5.14. The permanent rotation was calculated by subtracting the theoretical elastic rotation of the uncracked section from the measured total rotation. In Fig. 5.13, the moment was normalized with respect to the plastic moment. The AASHTO design curves, which apply to compact sections, were above the experimental curves.

In Fig. 5.14, the moment was normalized with respect to the yield moment. In this figure, the AASHTO design curves were adjusted to reach the yield moment because the web slenderness ratios of the test specimens exceeded the limit for compact sections. For unshored composite sections, the theoretical
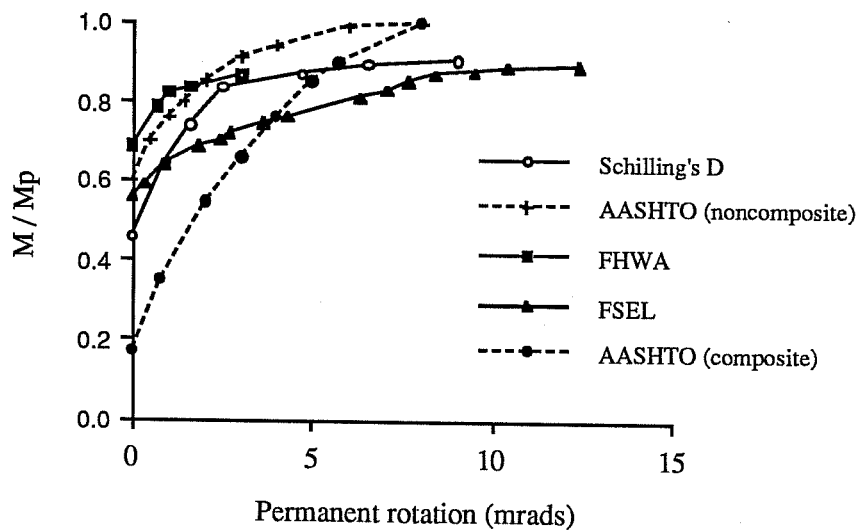
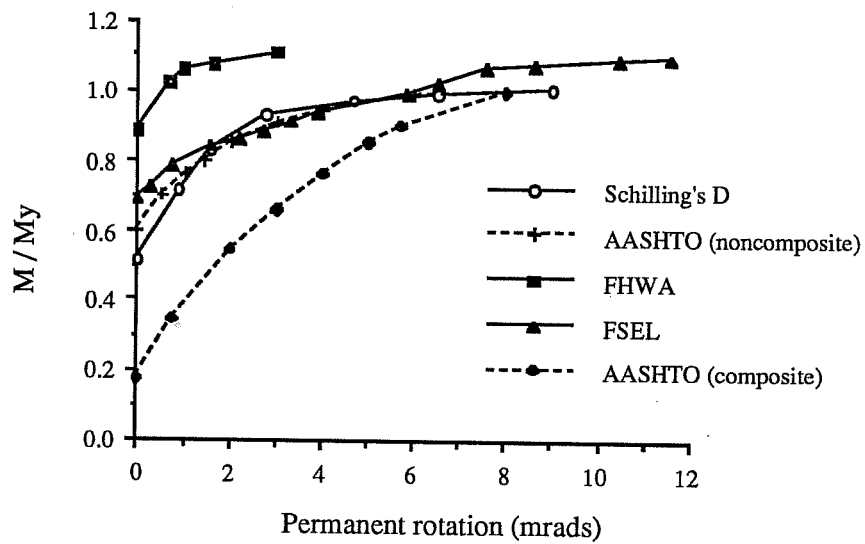**Figure. 5.13 M/Mp vs permanent rotation curve**

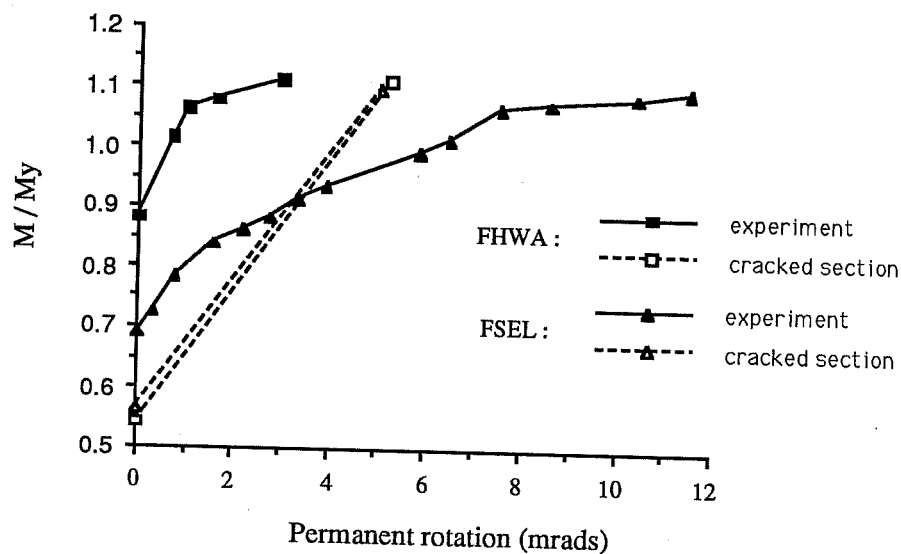**Figure. 5.14 M/My vs permanent rotation curve**

Figure. 5.15 Lower bound curves

yield moment was calculated considering the load sequence. As shown in Fig. 5.14, the curve of Schilling's specimen D agreed very well with the AASHTO design curve for noncomposite sections. But the AASHTO curve for composite sections was well below the curves for the FHWA and FSEL specimens. This is because the AASHTO curve for composite sections was developed based on a component test for shored construction in which the concrete cracking occurs at an early stage. In addition, the ultimate moment capacities of the FHWA and FSEL specimens were greater than their yield moments. Therefore, a new design curve needs to be developed for composite girders with noncompact sections.

Since the experimental moment-permanent rotation curves for the FHWA and FSEL specimens did not have sufficiently similar behavior for the development of one typical curve, a lower bound curve must be developed for each specimen. The dashed lines in Fig. 5.15 were developed to represent the lower bounds for the moment-permanent rotation curves of the specimens. The per-
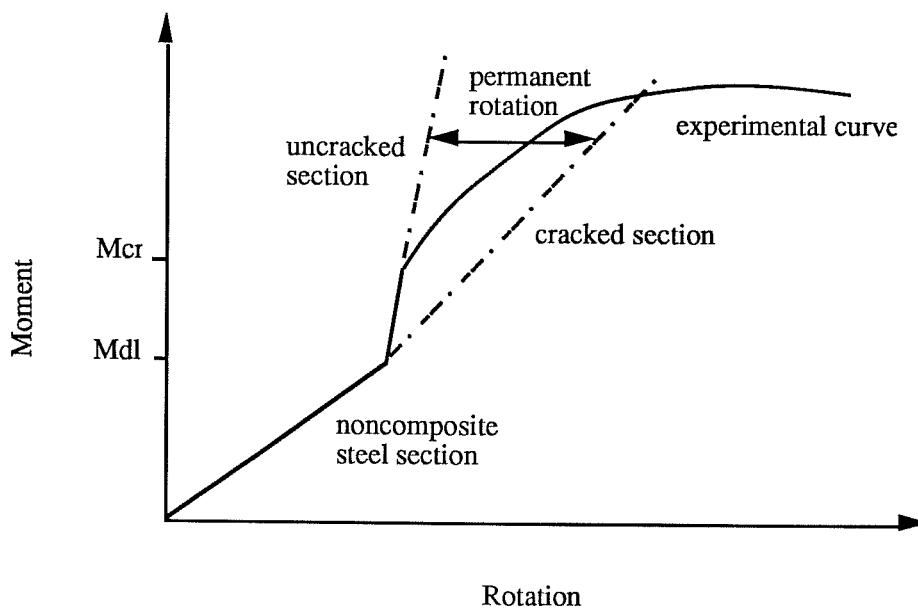
Figure. 5.16 Development of lower bound curve

manent rotation of the dashed lines was determined by subtracting the theoretical elastic rotation of the uncracked section from the theoretical elastic rotation of the cracked section as shown in Fig. 5.16. The dashed lines started at the noncomposite dead load moment instead of the cracking moment to give a conservative fit to the experimental curves. If the dashed lines provide the lower bounds, the automoments at Overload can be calculated conservatively as the difference between the moments obtained using the uncracked section and the cracked section for the negative bending area as shown in Fig. 5.17.

As shown in Fig. 5.15, the cracked section curve of the FHWA specimen was below the experimental curve. For the FSEL specimen, the cracked section curve was below the experimental one at first, but went above it later. Fig. 5.18 shows the beam line developed based on the prototype design in which the elastic Overload moment at the pier was close to the yield moment. The cracked section curve gives a smaller automoment than the experimental curve,
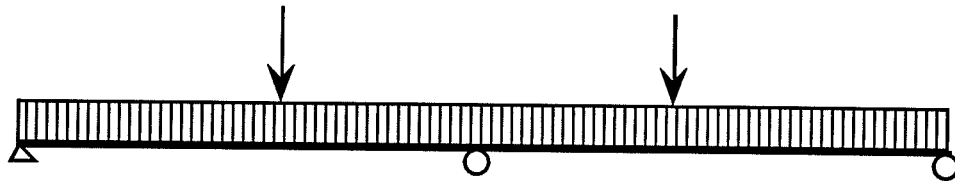
(a) Overload (negative bending loading)

uncracked section for negative bending region

Mauto

cracked section for negative bending region
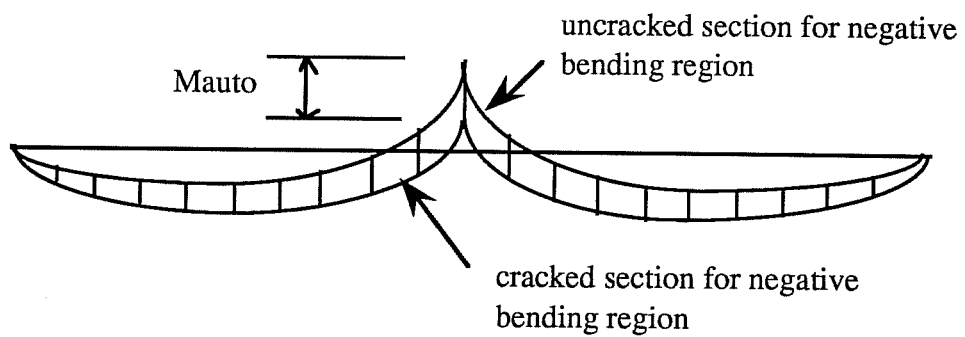
(b) moment distribution curves

Mauto
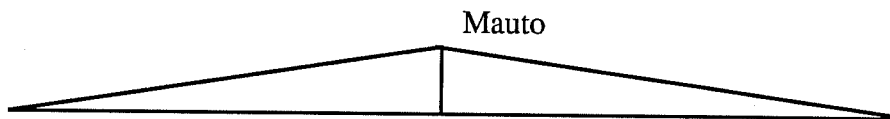
(c) automoment diagram

Figure. 5.17 Calculation of automoments

**Figure. 5.18 Automoments by beam line method
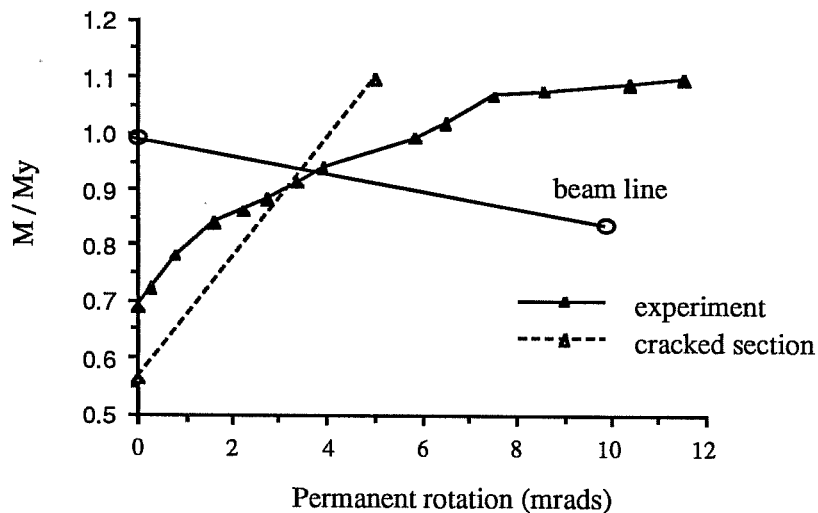(FSEL specimen)**

but the difference is insignificant. Therefore, the cracked section curve can be assumed to provide a lower bound and the automoments at Overload can be calculated as shown in Fig. 5.17 as long as the elastic Overload moment at the pier is less than the yield moment.

In most composite plate girder bridges, the shape factor (Mp/My) of the pier section is less than 1.3 and the ultimate bending strength of the pier section is less than its plastic moment. Therefore, as long as the elastic Maximum Load moment at the pier is limited to its ultimate bending strength, the elastic Overload moment at the pier can not exceed the yield moment.

5.6 Overall Summary

1. Most composite plate girders with slender webs can reach the plastic moment capacity and have sufficient ductility under positive bending.

2. The ratio of the slope of the descending curve to that of the initial rising curve ranged from -0.1 to -0.16 for the plate girders with slender webs and compression flanges. When an ultracompact section was used for the compression flange, the slope was improved to -0.083 for Schilling's specimen D and -0.069 for the FHWA specimen.

3. The effective plastic moment calculated based on the procedure in the AASHTO Guide Specifications was too high for composite plate girders with ultracompact compression flanges. The ratio of the effective plastic moment to the ultimate moment was 0.94 for FHWA specimen and 0.88 for FSEL specimen.

4. The ultimate moment capacity by the modified Q formula was close to the experimental strength for the FHWA specimen but smaller than the experimental strength by about 9% for the FSEL specimen.

5. The AASHTO design curves adjusted to reach the yield moment for plate girders agreed well with the test curve for a noncomposite section, but gave conservative results for composite sections under unshored construction.

6. The automoments at Overload can be calculated as the difference between the moments obtained using the uncracked section and the cracked section for the negative bending area as long as the elastic Overload moment at the pier is less than the yield moment.

CHAPTER SIX

# DEVELOPMENT OF A COMPUTER PROGRAM

6.1 Introduction

The redistribution of moment and the ultimate strength of a continuous beam can be obtained easily if the cross section has elastic-perfectly plastic moment curvature relationship. The structure behaves elastically until the plastic moment is reached at the pier section. For the additional loading, moment redistribution occurs with the pier section rotating at the plastic moment. When the positive section reaches the plastic moment, a mechanism is formed and the ultimate load is obtained.

However, in most continuous composite plate girder bridges, the maximum moment capacity of the pier section is less than the plastic moment and the moment-rotation curve has a descending portion beyond its maximum moment as shown in Fig.5.1. Therefore, the ultimate load capacity can not be calculated by the plastic mechanism method. In order to predict the inelastic behavior and the ultimate capacity of continuous composite plate girder bridges, the redistribution of the pier moment to the span region must be considered. This moment redistribution occurs through the interaction of the descending curve of the pier section and the rising inelastic curve of the midspan section as shown in Fig. 6.1.

To study the redistribution of moment, an one-dimensional nonlinear computer program, NACB, is developed. In this program, a bridge is modeled using a finite element idealization and a combined stiffness method is used to solve the resulting nonlinear equations. The basis of this program is described in this chapter.

76
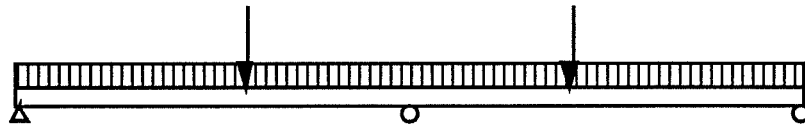
(a) the loading
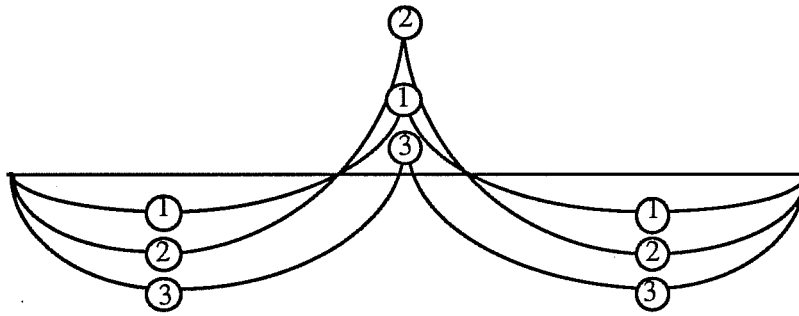
(b) the moment diagram
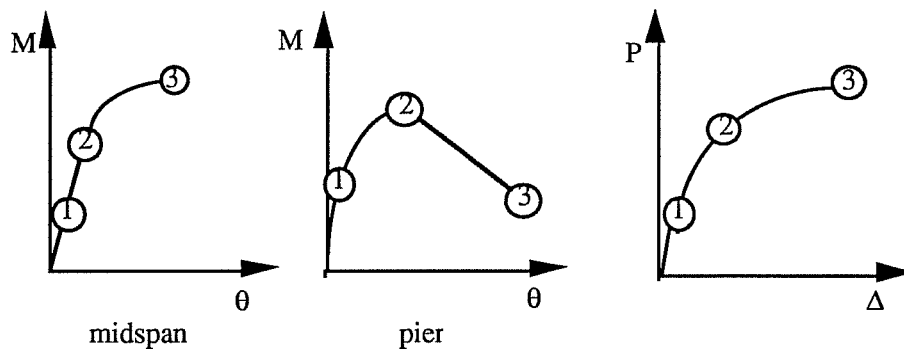
(c) moment-curvature curve

(d) load-deflection curve

Figure 6.1 Redistribution of moment in a continuous bridge

6.2 Assumptions

Several assumptions which were made to simplify the nonlinear program are listed below:

1. Small deflection theory is adopted and geometrical nonlinearity is not considered.

2. Inelastic behavior is considered for flexural stiffness only and shear rigidity is assumed to remain elastic.

3. Nonlinear effect due to the local buckling of the pier section is assumed to occur over a length equal to the depth of the steel section[36]. Hence, the steel section depth is used as the element length for the first element on each side of the pier.

4. The effect of lateral-torsional buckling is accounted for in the moment-curvature curve.

5. The stiffness of the unloading curve is assumed to be the same as the elastic stiffness.

6. Actual moment-curvature curve is approximated using several straight lines.

7. Ultimate load carrying capacity is assumed to be reached when the solution convergence is not obtained.

6.3 Moment-Curvature Relationship

In the computer program, moment-curvature characteristics are used as input data instead of moment-rotation characteristics. The descending portion of the moment-curvature curve of the pier section can be obtained from the moment-rotation curve as shown in Fig. 6.2. The rotation, θ, is defined as shown in Fig. 6.2(a). After the pier section reaches the ultimate moment, the rotation continues to increase while the moment decreases. In Fig. 6.2(b),

θ_p is the total rotation and θ_e the elastic rotation at a moment of Ma. The curvature diagram in Fig. 6.2(c) has two regions. Region 1 represents the elastic behavior. Region 2 represents the inelastic behavior and the curvature is assumed to be constant over a length equal to the depth of the steel section. The area of region 1 is equal to θ_e and the area of region 2 is equal to the inelastic rotation, $(\theta_p - \theta_e)$. From this curvature-area theorem, the total curvature, ϕ_p, on the moment-curvature curve in Fig. 6.2(d) can be determined. When the slope of the descending curve, u, is -1/60 in the moment-curvature curve, it is approximately equivalent to the value of m = - 1/10 in the moment-rotation curve.
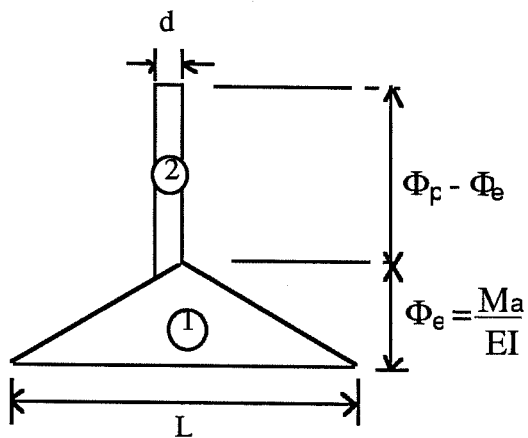
6.4 Combined Stiffness Method

In the nonlinear program, the coefficients of the stiffness matrix depend on the deformations. Therefore, a direct solution can not be obtained and an incremental and iterative method must be used to solve the nonlinear equation. Two generally available methods for structural application are initial stiffness method and tangential stiffness method. Tangential stiffness method results in faster convergence. But the descending portion of the moment curvature curve of the pier section exhibits negative stiffness. To consider the descending portion and fast convergence, the initial stiffness method which is unconditionally convergent is combined with the tangential stiffness method[29]. In this combined stiffness method, a new stiffness matrix is evaluated at selective incremental intervals when the flexural stiffness of an element is changed. Several iterations are made using the same stiffness matrix until the convergence is obtained. The solution algorithm of this method is shown schematically in Fig. 6.3.
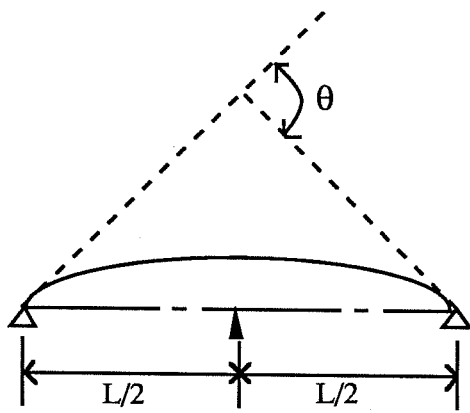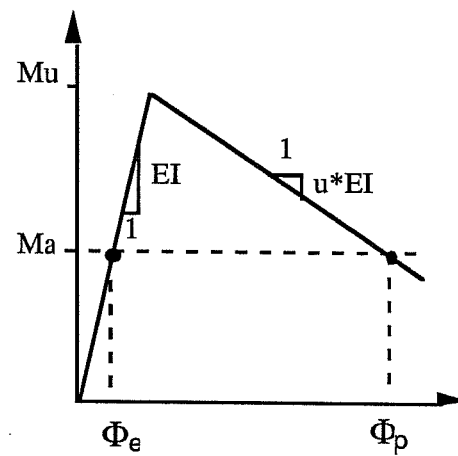
a) Rotation
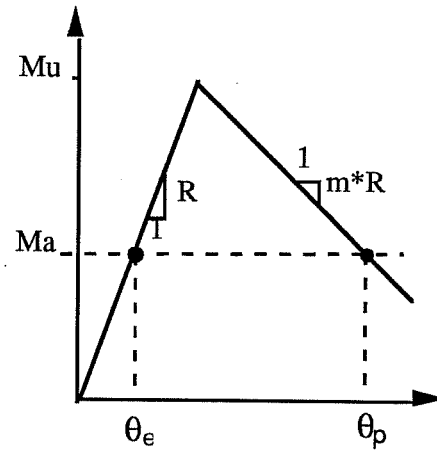
b) Moment-rotation curve

c) Curvature diagram

d) Moment-curvature curve

Figure 6.2 Prediction of the descending part
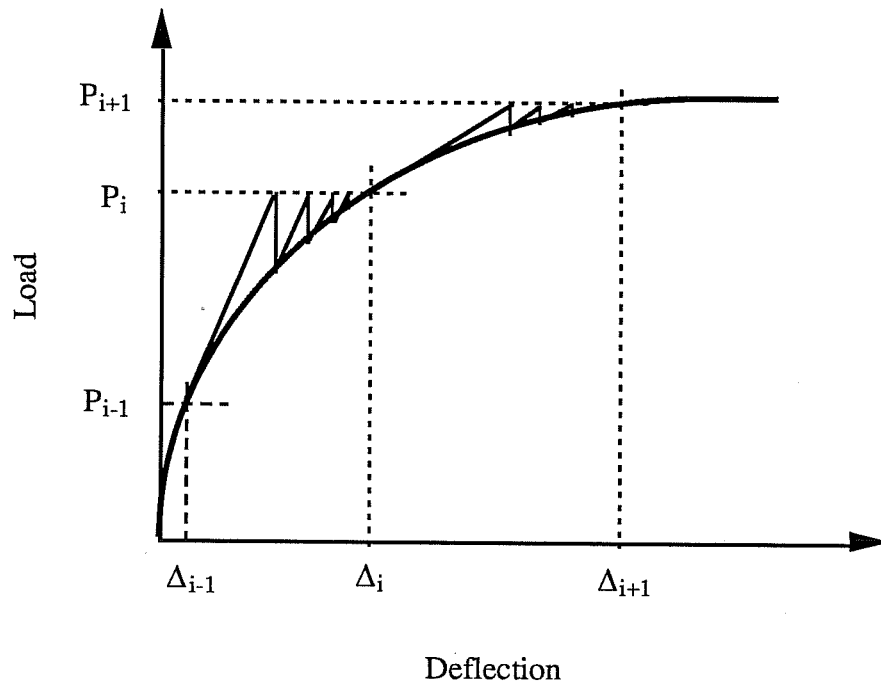of the moment-curvature curve

Figure 6.3 Combined stiffness method

6.5 Program Organization

In addition to the basic subroutines which are used for elastic analyses, this nonlinear finite element program includes two more subroutines. One is used to evaluate the unbalanced forces and the other is to check the convergence. Two primary loops are necessary. The inner loop controls the iteration of the solution and the outer loop controls the load increment.

The flow chart of this program is shown in Fig 6.4. The solution procedure which consists of seven major steps is described below:

1. Load increments are applied.

2. New tangential stiffness matrix corresponding to the deformation is evaluated if necessary.

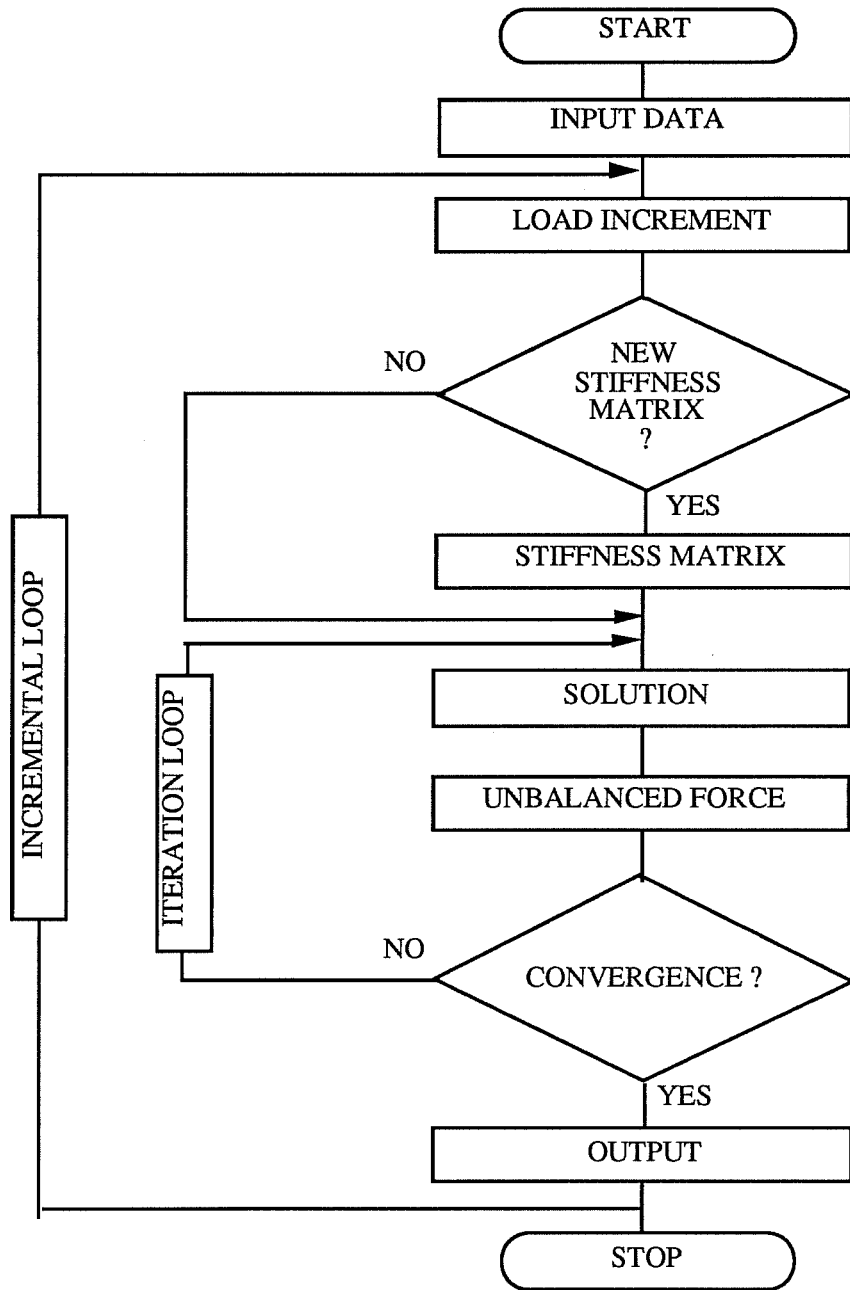3. Solution is implemented using finite element analysis procedure to get the

Figure 6.4 Flow chart

nodal displacements.

4. Unbalanced forces are calculated as the difference between the total applied loads and the equivalent nodal forces for each nodal point.

5. Convergence is checked. To satisfy the convergence criteria, the norm of the unbalanced forces must become less than the tolerance factor times the norm of the total applied forces This criteria is represented by an equation,

$$\frac{\sqrt{\sum_{i=1}^{N}(\varphi_i)^2}}{\sqrt{\sum_{i=1}^{N}(f_i)^2}} \leq tolerance\, factor \qquad (6.1)$$

where N is the total number of nodal points, φ is the unbalanced forces, and f is the total applied force.

6. If solution has not converged, go to step 3 and carry out the next iteration using the unbalanced forces as applied loads.

7. Otherwise output results and go to step 1.

CHAPTER SEVEN

ULTIMATE CAPACITY OF CONTINUOUS COMPOSITE PLATE GIRDERS

7.1 Introduction

When a continuous beam is loaded beyond its elastic limit, moment redistribution occurs. If the cross section has an elastic-perfectly plastic moment-curvature relationship, the load-deflection curve can be obtained easily in two steps as shown in Fig. 7.1[30]. First plastic hinge forms at the pier section when the elastic pier moment reaches the plastic moment, Mp. This is represented by the number 1 in the figure. Upon further loading, the moment is redistributed with the pier section rotating at the plastic moment, Mp. Due to the plastic hinge action of the pier section, the structure behaves as if it is simply supported during subsequent loading. When the positive bending section reaches its plastic moment, a mechanism is formed and the ultimate load capacity is obtained. This is represented by the number 2. After that, the beam continues to deform as a mechanism under constant load until one of the plastic hinges reaches its deformation capacity (number 3).

The ultimate load can be calculated by a plastic mechanism method. When the same plastic moment value is used for the positive bending section and the pier section, the load at which first plastic hinge occurs at the pier is about 67% of the plastic collapse load for uniformly distributed load and about 82% of the plastic collapse load for concentrated load at midspan.

In actual continuous composite plate girders, the positive and negative bending sections will exhibit inelastic behaviors before the plastic moment is reached due to steel yielding and/or concrete cracking. Moreover, the moment-

84
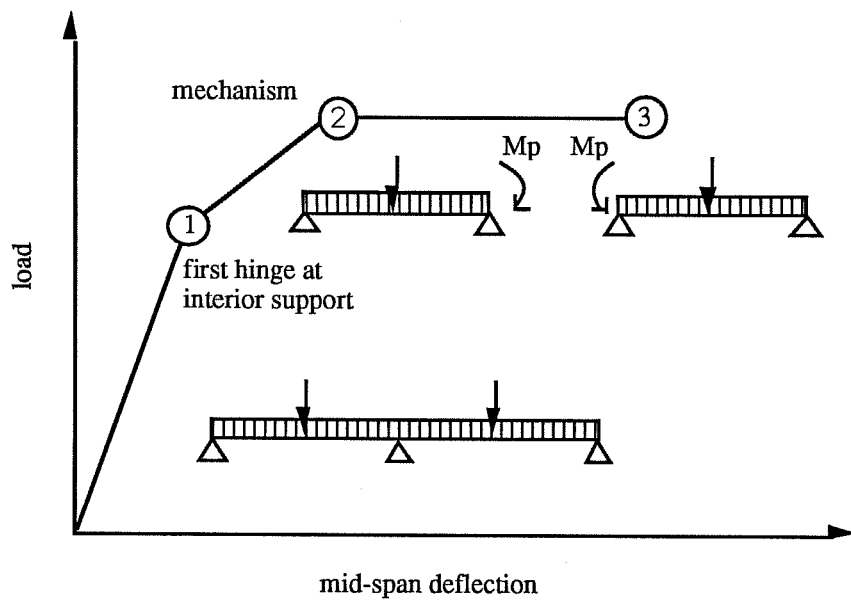
(a) Theoretical load-deflection curve
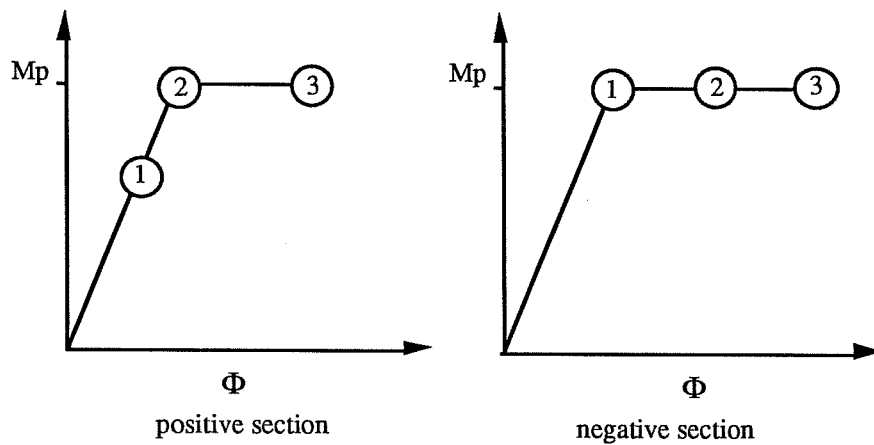
(b) Moment curvature actions at hinge locations

Figure 7.1 Moment redistribution in a continuous beam with an elastic-plastic section

rotation curve of the negative bending section has a descending curve beyond the maximum moment capacity due to the local buckling. The rotation capacity is not sufficient for simple plastic design. The interaction of the descending curve with the inelastic rising portion of the positive bending section makes the redistribution of moment more complicated and the ultimate load can not be calculated by the plastic mechanism method.

As a simple way to compute the ultimate load capacity of a continuous bridge with limited rotation capacity at the interior support, the concept of an effective plastic moment is given in the AASHTO Guide Specifications. The effective plastic moment is obtained by reducing the flange and/or web components of the full plastic moment to account for local instabilities. In this method, the ultimate load capacity can be calculated by the simple plastic design method assuming the pier moment to remain at the effective plastic moment during the plastic hinge action. This method gives conservative results because the actual pier moment remains above the effective plastic moment when the ultimate load is reached.

In this chapter, the inelastic behavior and the ultimate capacity of continuous composite plate girders are investigated using the nonlinear computer program, NACB, developed in chapter 6.

7.2 Historical Review

In order to evaluate the ultimate load capacity of continuous composite plate girders, Kubo and Galambos performed a plastic analysis of two-span continuous composite plate girders[31]. In the analysis, the moment-rotation curve of the negative bending section was idealized by two straight lines (elastic part and descending part) based on experimental data. The ultimate capacity was assumed to be reached when the first hinge formed in the positive bending region. The moment-curvature curve of the positive bending section was

assumed to be elastic-perfectly plastic.

The results of the analysis showed that the ultimate load capacity was affected considerably by the ratio of the ultimate bending strengths of the positive and negative bending sections. The effect of the slope of the descending curve on the ultimate capacity was relatively small. In this study, using the concept of an effective plastic moment was found to give conservative results for plate girders with noncompact compression flanges and webs.

In Eurocode 4, the sections that can reach the yield moment with limited rotation capacity are categorized as semi-compact sections. A composite beam with a semi-compact section can reach its yield moment in negative bending. In positive bending, however, it can reach the plastic moment which is much greater than the yield moment in negative bending. Moreover, the elastic maximum pier moment is usually greater than the elastic maximum midspan moment. Therefore, limiting the elastic maximum pier moment to the yield moment gives an overly conservative estimation of the ultimate load capacity of continuous composite beams with semi-compact sections.

In the design of continuous composite beams with semi-compact sections, the Eurocode 4 method allows a redistribution of up to 20% of the elastic pier moment to the midspan region. Johnson and Fan examined the safety of this method by analyzing two-span continuous composite beams using iteration calculations[32]. The falling branch of the moment-rotation curve of the pier section was predicted from the results of double-cantilever tests.

Based on 43 design examples, the Eurocode 4 design method was found to be safe and economical for the design of continuous composite beams with semi-compact sections. The effects of the slope of the descending curve of the pier section, residual stresses, and the construction methods on the ultimate capacity were negligible.

7.3 Numerical Example

To investigate the inelastic behavior and the ultimate capacity of continuous composite plate girder bridges using the nonlinear program, NACB, a 200 ft two-span unshored composite bridge with 13 ft transverse girder spacing was considered as a numerical example. Material properties and girder dimensions for the positive bending section and the pier section are shown in Fig. 7.2.

7.3.1 Cross sectional properties

Moment-curvature curves of the positive and negative bending sections are approximated by several straight lines as shown in Fig. 7.3. Inelastic behaviors of the cross sections are initiated by yielding of the bottom flange in the positive bending section and by concrete cracking in the negative bending section. Basic cross sectional properties used in this numerical example are listed below.

For composite section:

M_{pc} = plastic moment of positive section = 20,000 $kip - ft$

M_y = yield moment of positive section = 15,000 $kip - ft$

M_{pn} = plastic moment of pier section = 23,000 $kip - ft$

M_u = ultimate moment of pier section = 20,000 $kip - ft$

M_{cr} = cracking moment of pier section = 15,000 $kip - ft$

EI_c = elastic flexural stiffness of positive section = $6.0*10^7$ $kip - ft^2$

$k_s * EI_c$ = inelastic flexural stiffness of positive section = $1.2*10^7$ $kip - ft^2$

EI_n = elastic flexural stiffness of pier section = $6.0*10^7$ $kip - ft^2$

$k_n * EI_n$ = inelastic flexural stiffness of pier section = $2.4*10^7$ $kip - ft^2$

$u * EI_n$ = negative flexural stiffness of pier section = $-2.0*10^6$ $kip - ft^2$

155.0

8.5

25 * 1.75

81. * 0.563

27. * 1.875

Negative section

Concrete:
f'c = 4000 psi

Reinforcing bar
As = 13.19 in
Fy = 60,000 psi

Structural steel:
Fy = 50,000 psi
Fu = 70,000 psi
Es = 29,000 ksi

155.0

8.5

15 * 0.875

81. * 0.563

19. * 1.875
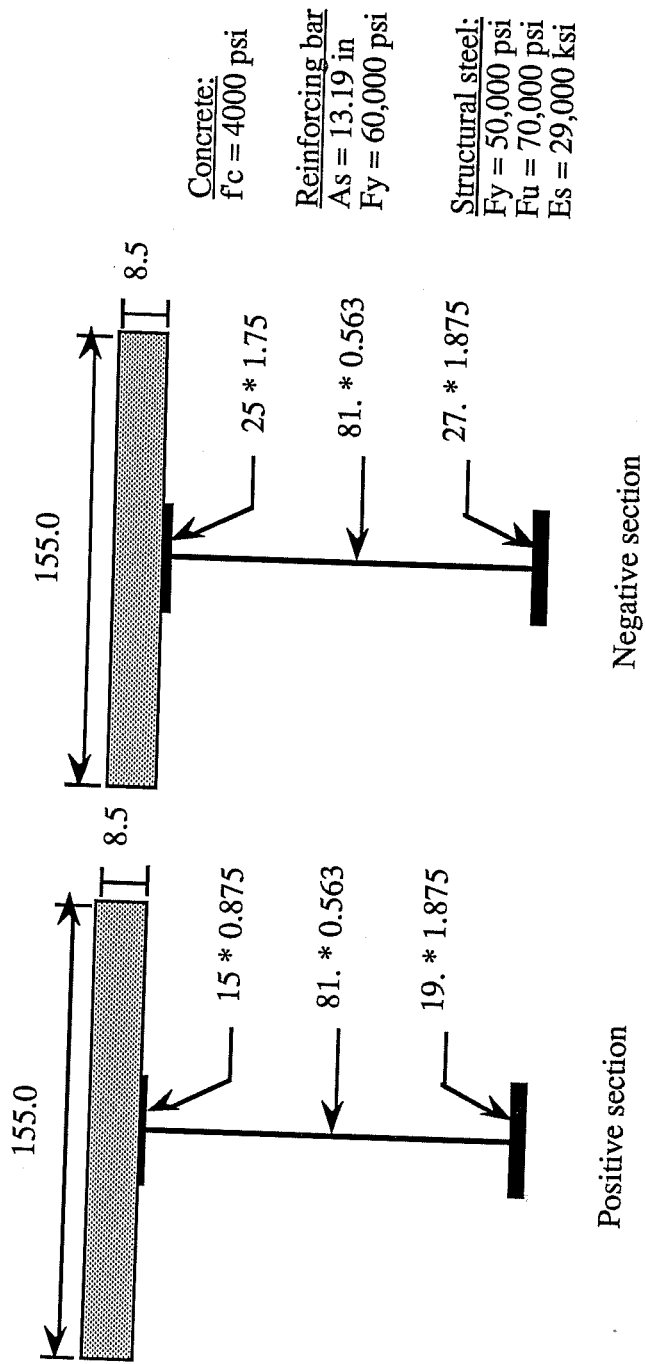
Positive section

Fig. 7.2 Cross sections and material properties of the numerical example
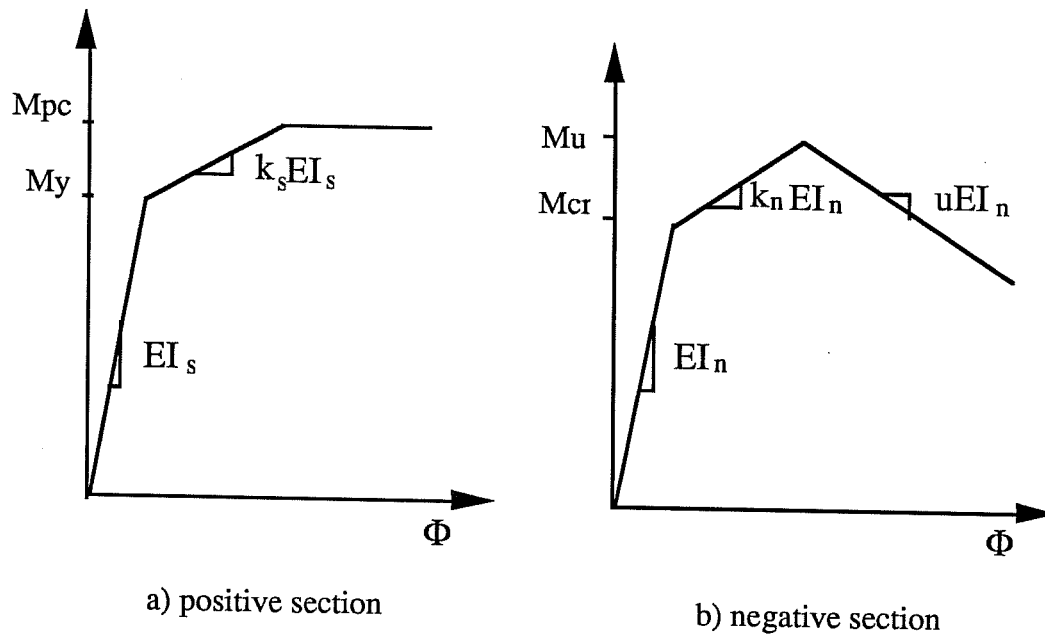
a) positive section

b) negative section

Figure 7.3 Idealized moment-curvature curves

For steel section:

M_{ys} = yield moment of positive section = 9045 $kip - ft$

M_{yn} = yield moment of pier section = 17506 $kip - ft$

EI_s = elastic flexural stiffness of positive section = $2.16*10^7$ $kip - ft^2$

EI'_s = elastic flexural stiffness of pier section = $3.75*10^7$ $kip - ft^2$

The yield moment, M_y, and the cracking moment, M_{cr}, of the composite section were calculated considering the loading sequence in unshored construction. The inelastic stiffness of the positive section was predicted based on the cross sectional analyses given in chapter 2. Instead of using the theoretical values, the cross sectional properties of the pier section were developed based on the results of the FSEL test in chapter 5. Due to local instabilities, a composite

plate girder in negative bending can not reach its plastic moment, M_{pn}. The maximum moment capacity of the pier section, M_u, was assumed to be $0.87M_{pn}$ based on the test results. The elastic stiffness of the pier section was selected to be about mid-way between the theoretical uncracked section stiffness and cracked section stiffness. The slope of the descending branch was assumed to be -1/30 of the elastic flexural stiffness based on Schilling's and FHWA test results. This value is approximately equivalent to a slope ratio of -0.2 in the moment-rotation curve.

7.3.2 Loading

In unshored construction, the noncomposite dead load composed of the weight of the concrete slab and the steel girder is supported by the steel girder only. After the concrete hardens, superimposed dead load such as parapets and future wearing surface is supported by the composite section. In this example, the noncomposite dead load was 1.68 k/ft and the superimposed dead load was 0.514 k/ft. Dead load was increased by a factor of 1.3 for the maximum design load.

For a 200 ft span bridge, lane loading governs. Therefore, AASHTO HS20 lane loading was used for live load. The governing positive and negative bending loadings are shown in Fig. 7.4. The concentrated load was placed at midspan for both the positive and negative bending loadings to compare the two loading cases. The concentrated load position in the AASHTO Specifications was a little different. But calculations for both cases showed that the effect on the ultimate load capacity was insignificant. The impact factor of 0.154 and the distribution factor of 1.82 were applied to the loading in the figure. Live load was increased by a factor of 2.17 for the maximum design load.
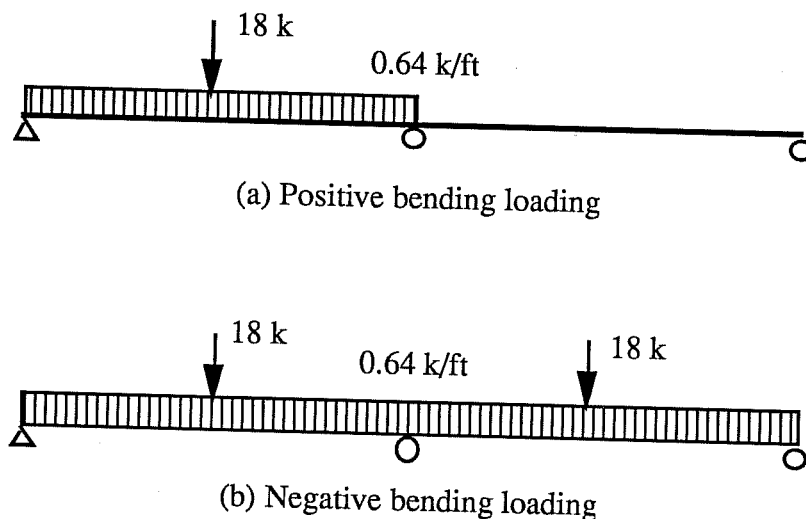
(a) Positive bending loading

(b) Negative bending loading

Figure 7.4 AASHTO HS 20 loading

7.3.3 Results

The load vs deflection curve is shown in Fig. 7.5. Load number 1 and Load number 2 represent the noncomposite dead load and the superimposed dead load respectively. The ratio of the applied live load to the maximum design live load at failure is 1.525 under the negative bending loading (Load number 6) and 1.60 under the positive bending loading (Load number 7) respectively. Therefore, the negative bending loading governs for this girder. The dashed line represents the load-deflection curve when the slope of the descending curve of the pier section is zero. In this case, the ratio of the applied live load to the maximum design live load is 1.76 regardless of the loading patterns.

The cross sectional behaviors are shown in Fig. 7.6 and Fig. 7.7. The negative bending loading causes higher pier moment at the same load level. The maximum moment capacity of the pier section, Mu, is reached at Load
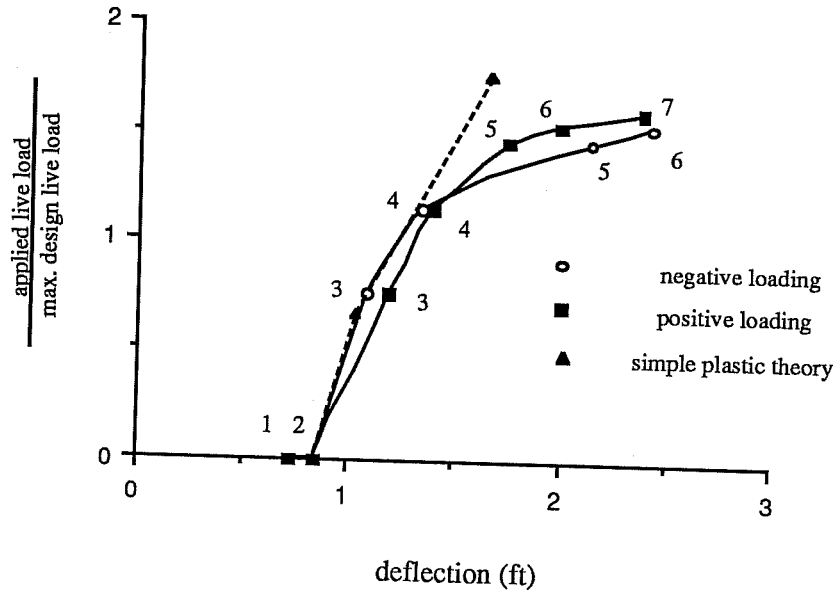
Figure 7.5 Load deflection curve

number 3 under negative loading(Fig. 7.6(b)), but at Load number 5 under positive loading(Fig. 7.7(b)). After the pier section reaches its maximum moment capacity, the redistribution of moment occurs through the interaction of the rising portion of the positive section and the descending curve of the pier section. Even under positive bending loading, first hinge occurs at the pier due to the high dead load pier moment. The ultimate loading capacity is obtained when the positive section reaches its plastic moment at Load number 6 under negative loading(Fig. 7.6(a)) and at Load number 7 under positive loading(Fig. 7.7(a)).

When the ultimate load capacity is reached, the pier section moment is further down on the descending curve under the negative loading (Load number 6 in Fig. 7.6(b)) than under the positive loading (Load number 7 in Fig. 7.7(b)). This is why the capacity under the positive bending loading is a little higher than the capacity under the negative bending loading as shown in Fig. 7.5.
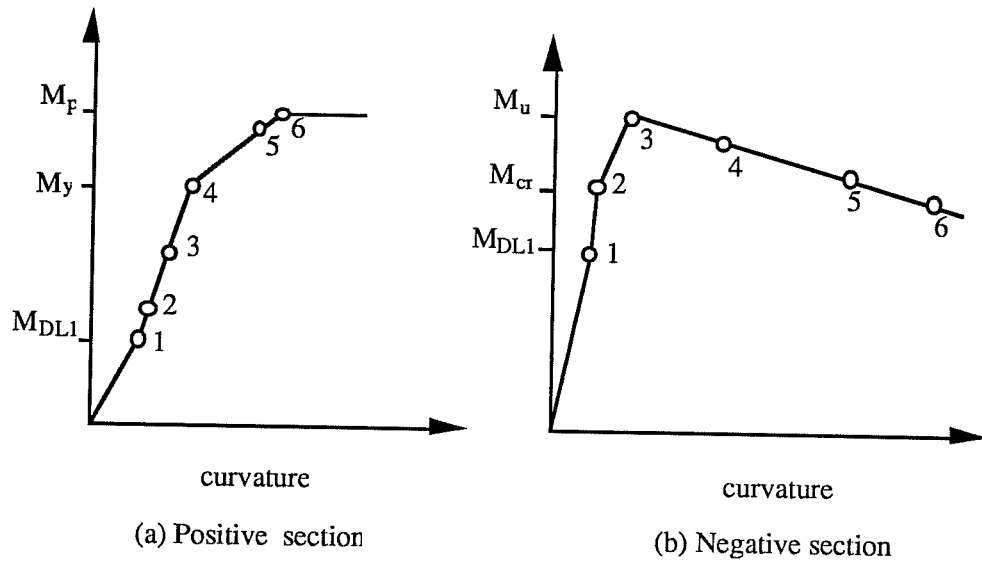
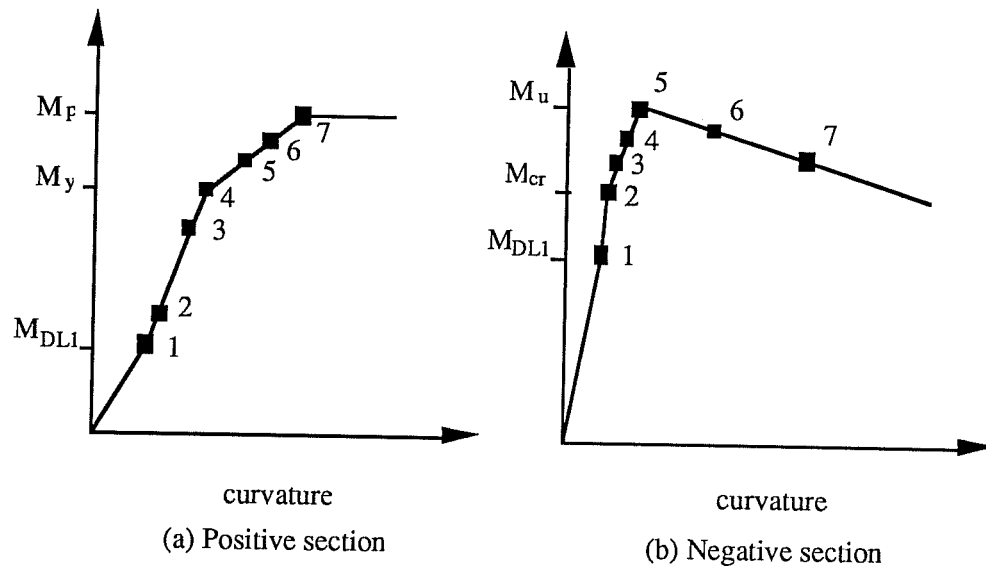Figure 7.6 Cross sectional behavior under negative bending loading

Figure 7.7 Cross sectional behavior under positive bending loading

7.3.4 Effective plastic moment

The effective plastic moment of the pier section computed based on the procedure in the AASHTO Guide Specifications is $0.845 M_{pn}$ or $0.98 M_u$. The ultimate load capacity calculated using this effective plastic moment is about 10% higher than the capacity under the negative bending loading obtained in the numerical example. This shows that using the equations in the Guide Specifications for a composite plate girder with an ultracompact compression flange may give unconservative results. To get the same ultimate load capacity as in the example, an effective plastic moment of $0.74 M_{pn}$ or $0.85 M_u$ must be used.

7.4 Parametric Study of Ultimate Load Capacity

The ultimate load capacity of a continuous girder bridge depends on the moment-curvature characteristics of the positive and negative bending sections. The main parameters which characterize the moment-curvature curves are k_s and M_y/M_{pc} for the positive section and k_n, M_{cr}/M_u, and u for the pier section as shown in Fig. 7.3. The parameters k_s and k_n are the ratios of the inelastic flexural stiffness to the elastic flexural stiffness for the positive section and the negative section respectively. The parameter u is the ratio of the negative stiffness (of the falling branch) to the elastic flexural stiffness of the negative bending section. Four different values of -1/15, -1/20, -1/30, and -1/60 were used for the parameter u in this study. When u is -1/15, the descending curve drops four times as fast as that with $u = -1/60$.

In this parametric study, the composite plate girder bridge used in the numerical example of the previous section is used as the analytical model. The effects of variations in the above-mentioned parameters on the ultimate load capacity are investigated. The noncomposite section behavior is not considered

to simplify the analyses. The ultimate load capacities obtained from the analyses are represented in a nondimensional form. The ultimate load is represented by w_u for uniformly distributed load and by P_u for concentrated load. The load at which the solution convergence can not be obtained is taken as the ultimate load. w_p and P_p are the simple plastic collapse loads. These values are calculated assuming that u is 0.0 (or the pier section has enough rotation capacity at the maximum moment capacity, M_u).

7.4.1 Inelastic stiffness of positive section

In order to evaluate the effects of the inelastic flexural stiffness of the positive section on the ultimate loading capacity, k_s was changed from 0.05 to 1.0 while keeping the other properties the same as those in the numerical example. Fig. 7.8 and Fig. 7.9 show the positive section moment and the pier section moment when the ultimate capacity was reached. When u is -1/60, the positive section could reach its plastic moment, M_{pc}, even with very small inelastic stiffness ($k_s = 0.05$) as shown in Fig. 7.8(a). As the inelastic stiffness of the positive section decreased, more moment was redistributed to the pier section. Therefore, the pier section moment went further down on the descending curve at the ultimate load as shown in Fig. 7.8(b). When u is -1/15, the positive section moment at the ultimate load decreased as the inelastic stiffness, k_s, was reduced as shown in Fig. 7.9(a). As the descending curve dropped more rapidly, the interaction of the inelastic stiffness of the positive section and the negative stiffness of the descending curve of the pier section made the solution diverge earlier. For $k_s = 0.1$ or less, the ultimate load capacity was reached when the positive section reached the yield moment as shown in Fig. 7.9(a).

Fig. 7.10 and Fig. 7.11 show the ultimate load in terms of k_s for uniformly distributed load and concentrated load respectively. As can be seen in these figures, an increase in the inelastic stiffness of the positive section increased
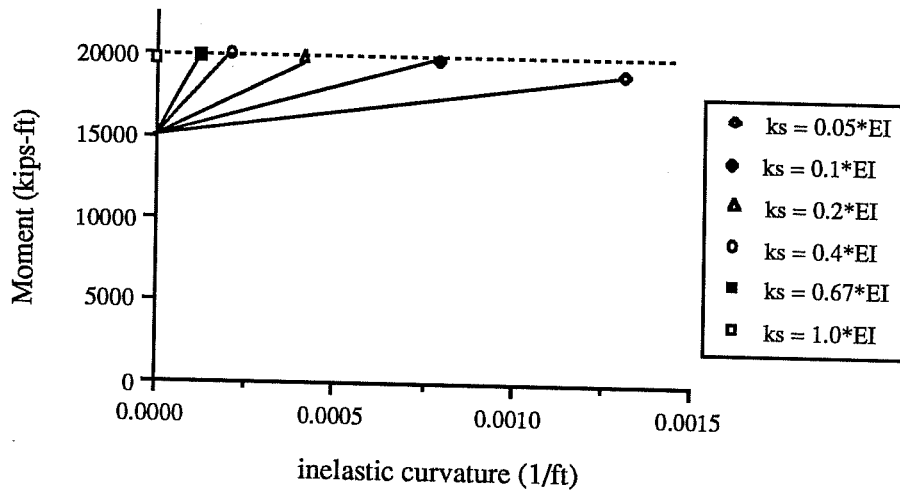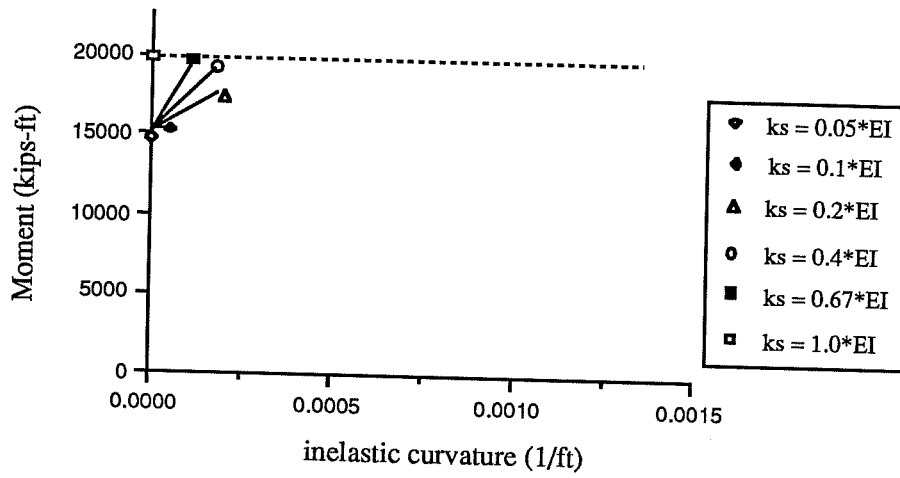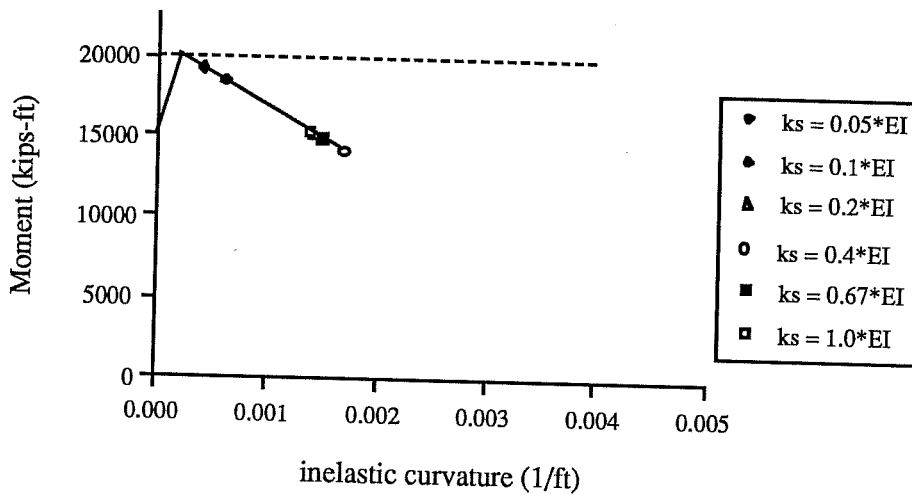
(a) Positive section
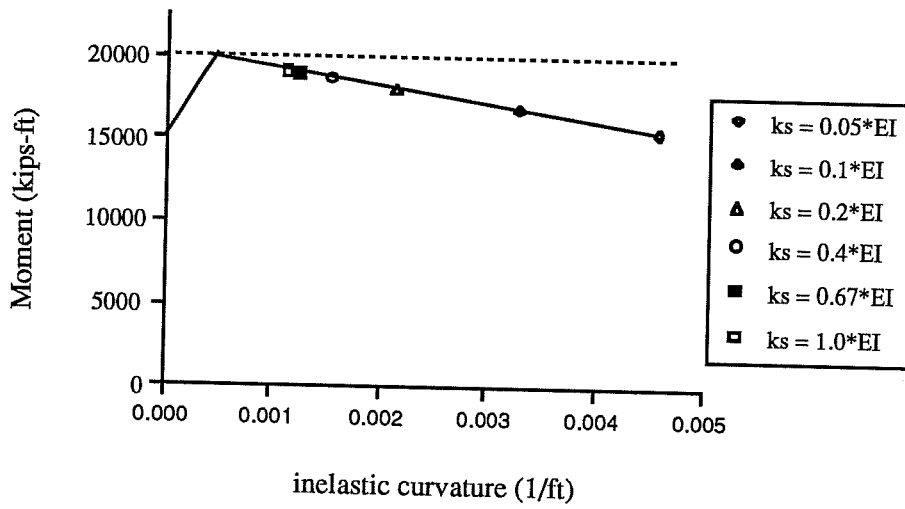
(b) Negative section

Figure 7.8 Moments at ultimate load for ks and u = -1/60

(a) Positive section

(b) Negative section

Figure 7.9 Moments at ultimate load for ks and u = -1/15

the ultimate loading capacity. The ultimate load was not affected much by k_s when k_s was greater than 0.4. At $k_s = 0.05$, the ultimate loads, w_u and P_u, were reduced to about $0.9w_p$ and $0.96P_p$ for $u = -1/60$, and $0.8w_p$ and $0.87P_p$ for $u = -1/15$ respectively. The dotted line represents the first hinge load at which the elastic maximum positive moment reaches the plastic moment, M_{pc}, or the elastic maximum pier moment reaches the maximum moment capacity of the pier section, M_u. Fig. 7.12 shows the loading and moment diagrams corresponding to the first hinge load for uniformly distributed load. The ultimate loads were well above the first hinge load.

7.4.2 Inelastic stiffness of pier section

To investigate the effects of the inelastic flexural stiffness of the negative section on the ultimate loading capacity, k_n was changed from 0.05 to 1.0 while keeping the other properties the same as those in the numerical example. Fig. 7.13 and Fig. 7.14 show the positive section moment and the pier section moment when the ultimate load was reached. As k_n was reduced, more moment was redistributed to the positive section and the positive section moment was closer to its plastic moment, M_{pc}, when the negative section reached its maximum moment capacity, M_u. Therefore, at the ultimate load, the pier section moment stayed higher on the descending curve for smaller k_n value as shown in Fig. 7.13(b) and Fig. 7.14(b). When k_n was about 0.05, the pier section moment was just below its maximum moment capacity, M_u, at the ultimate load and the positive section moment was close to the plastic moment, M_{pc}.

Fig. 7.15 and Fig. 7.16 show the effects of the inelastic stiffness of the pier section on the ultimate loading capacity. In contrast with the positive section, a reduction in the inelastic stiffness of the pier section increased the ultimate load as shown in these figures. The reduction in the inelastic stiffness of the pier section had the same effect as increasing the rotation capacity of the pier
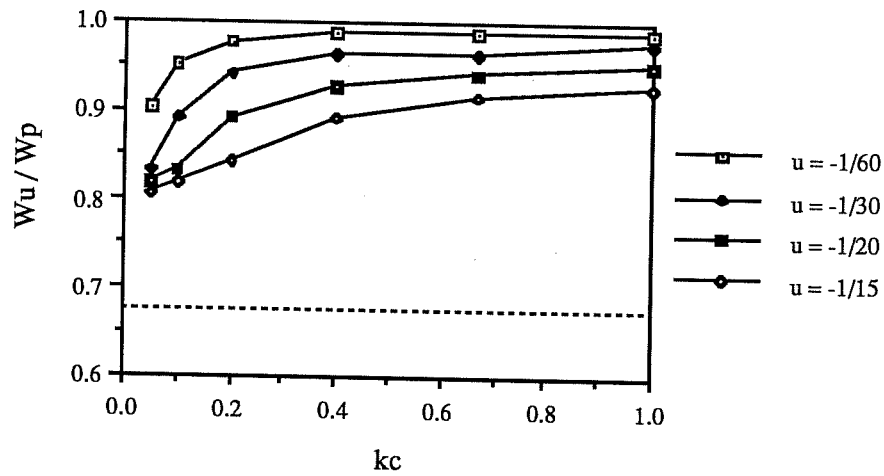
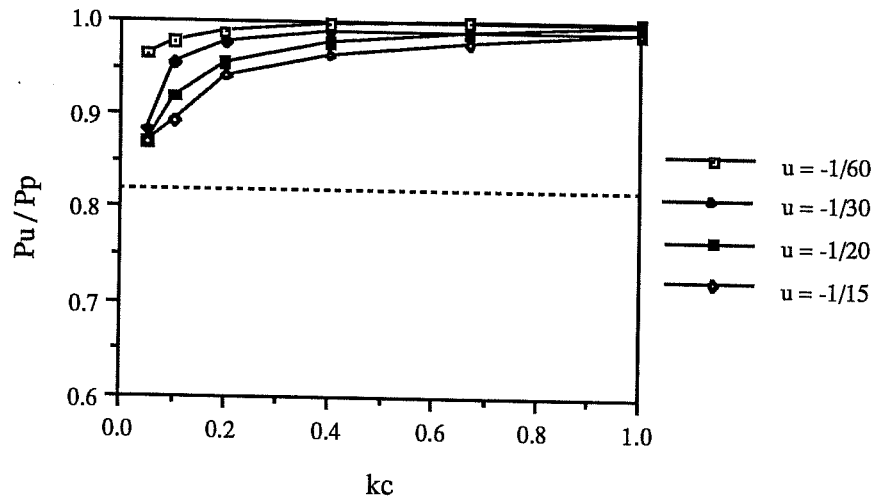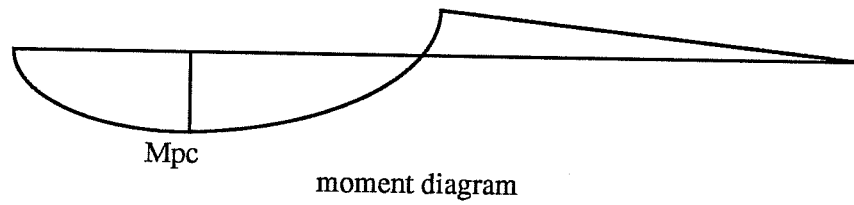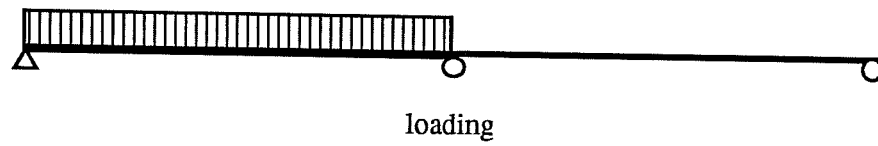Figure 7.10 Ultimate load vs ks for uniformly
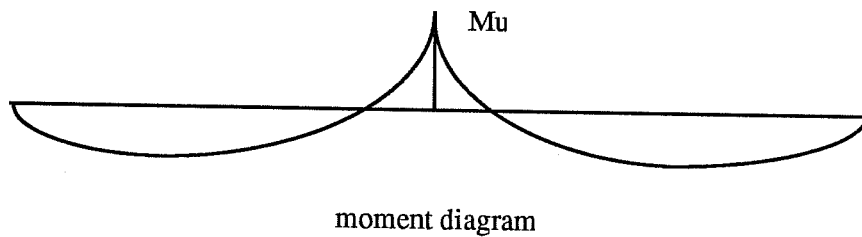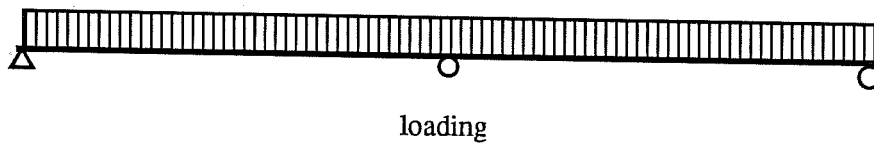distributed load

Figure 7.11 Ultimate load vs ks for concentrated load
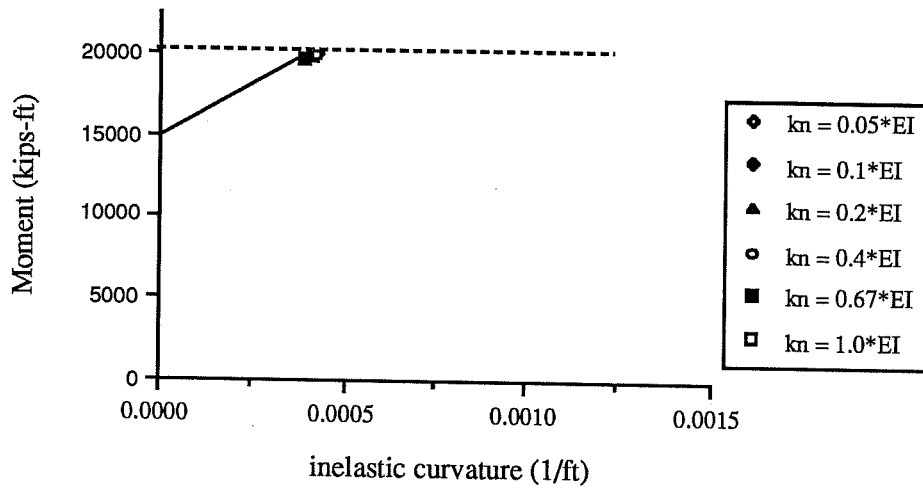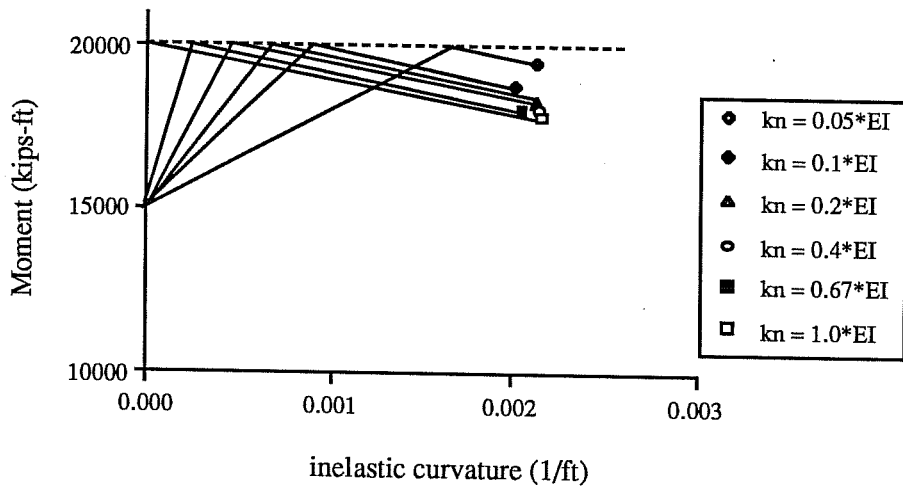
a) Positive moment loading

b) Negative moment loading

Figure 7.12 Determination of a first hinge load

(a) Positive section

(b) Negative section
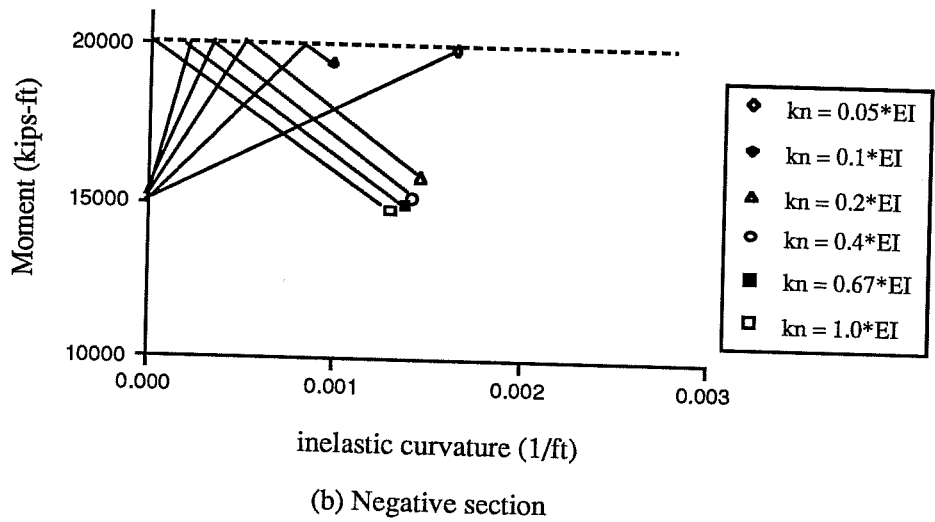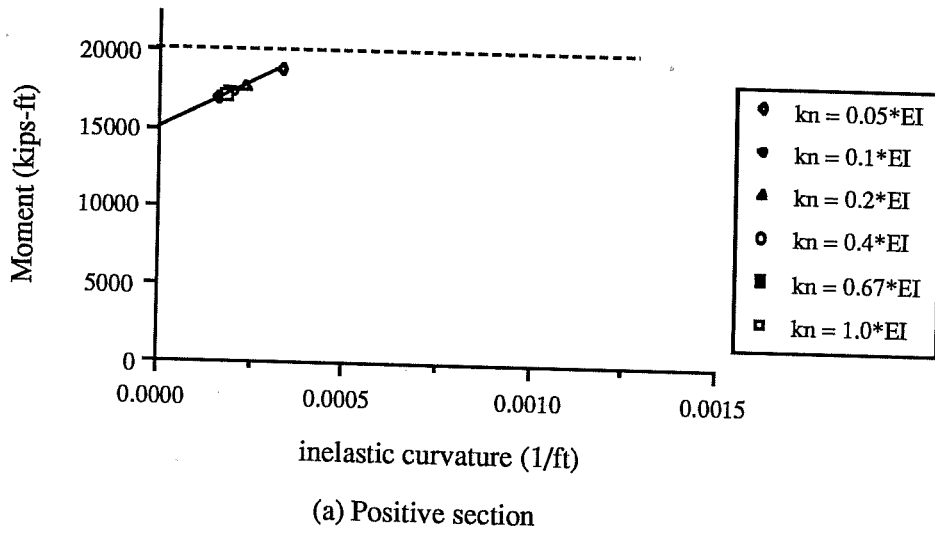
Figure 7.13 Moments at ultimate load for kn and u = -1/60

(a) Positive section

(b) Negative section

Figure 7.14 Moments at ultimate load for kn and u = -1/15

section at the maximum moment capacity, M_u. At $k_n = 0.05$, the ultimate loads, w_u and P_u, were increased close to the simple plastic collapse loads, w_p and P_p, even for $u = -1/15$. The ultimate loads were not sensitive to the value of k_n when k_n is greater than 0.2. The ultimate loads were well above the first hinge load represented by the dotted line.

7.4.3 Yield moment of positive section

To evaluate the effects of the yield moment value of the positive section on the ultimate load, the yield moment, M_y, was changed from $0.3M_{pc}$ to $1.0M_{pc}$ while keeping the other properties the same as those in the numerical example. Fig. 7.17 and Fig. 7.18 show the positive section moment and the pier section moment when the ultimate load capacity was reached. More moment was redistributed to the pier section as the ratio of M_y/M_{pc} decreased. Therefore, for $u = -1/60$, the pier section moment went further down on the descending curve at the ultimate load as can be seen in Fig. 7.17(b). For $u = -1/15$, the positive section moment at the ultimate load decreased as M_y/M_{pc} decreased as shown in Fig. 7.18(a).

Fig. 7.19 and Fig. 7.20 show the ultimate load in terms of M_y/M_{pc}. The ultimate load was reduced considerably as M_y/M_{pc} decreased. The reduction got bigger especially when the descending curve dropped more rapidly ($u = -1/15$) as shown in the figure. At $M_y/M_{pc} = 0.3$, the ultimate loads, w_u and P_u, were decreased to $0.92w_p$ and $0.94P_p$ for $u = -1/60$, and $0.8w_p$ and $0.87P_p$ for $u = -1/30$ respectively. For $u = -1/15$, the ultimate load was reduced below the first hinge load represented by the dotted line. But most composite plate girders have u value between -1/60 and -1/30. Therefore, the first hinge load still provides the lower bound to the ultimate load capacity.

Figure 7.15 Ultimate load vs kn for uniformly distributed load

Figure 7.16 Ultimate load vs kn for concentrated load

(a) Positive section

(b) Negative section

Figure 7.17 Moments at ultimate load for My/Mpc and u = -1/60

(a) Positive section

(b) Negative section

Figure 7.18 Moments at ultimate load for My/Mpc and u = -1/15
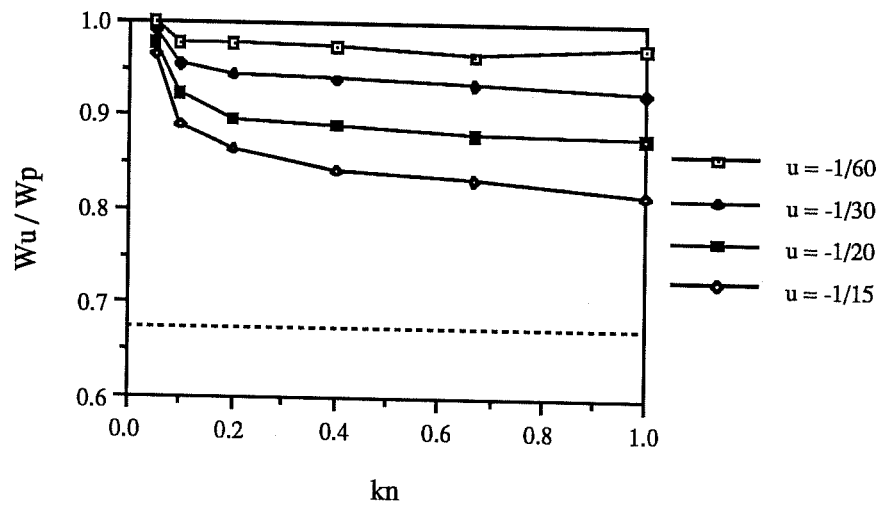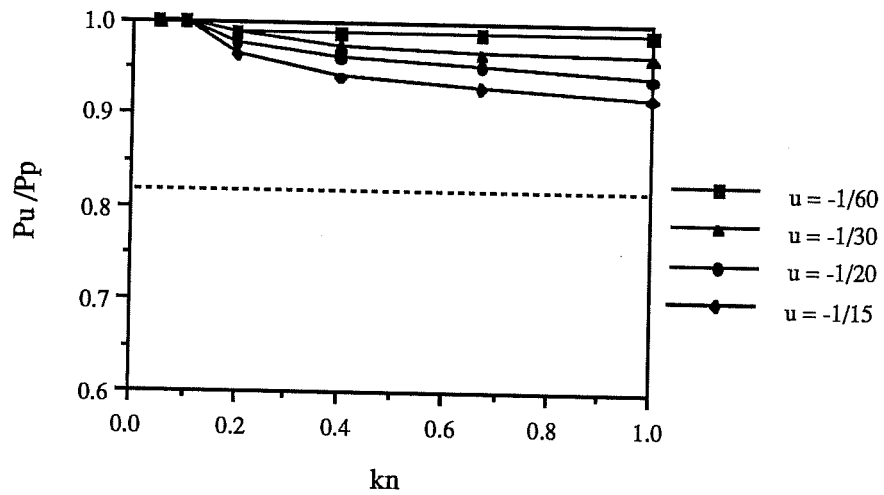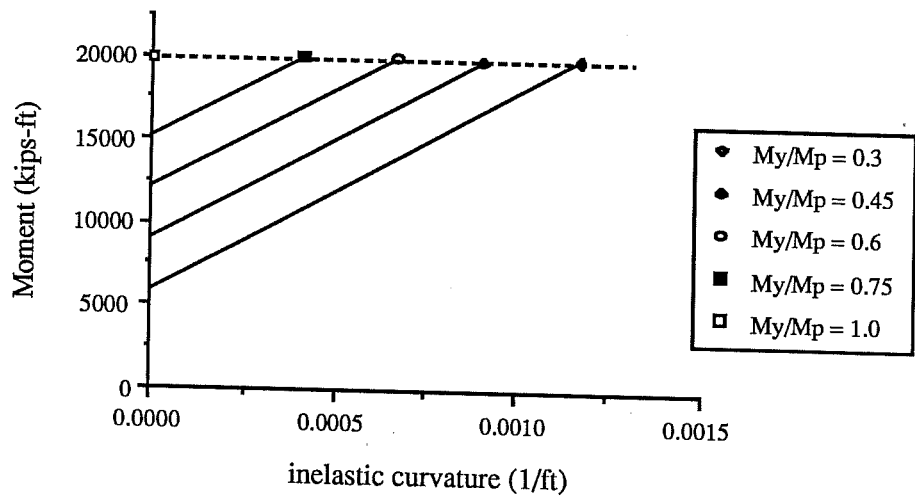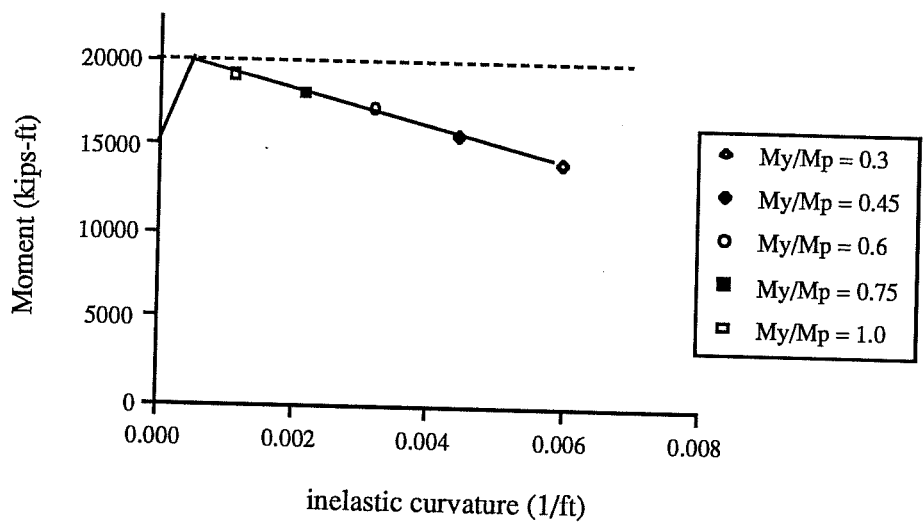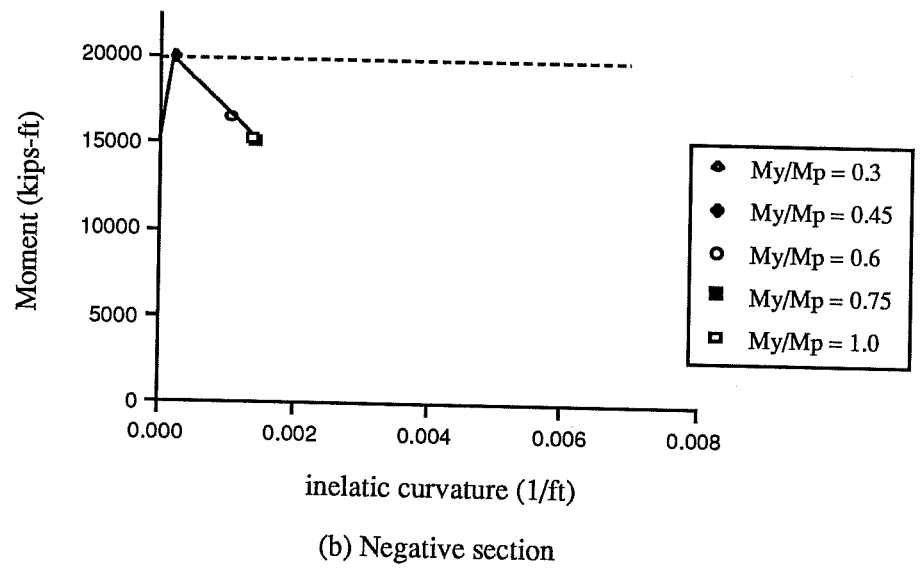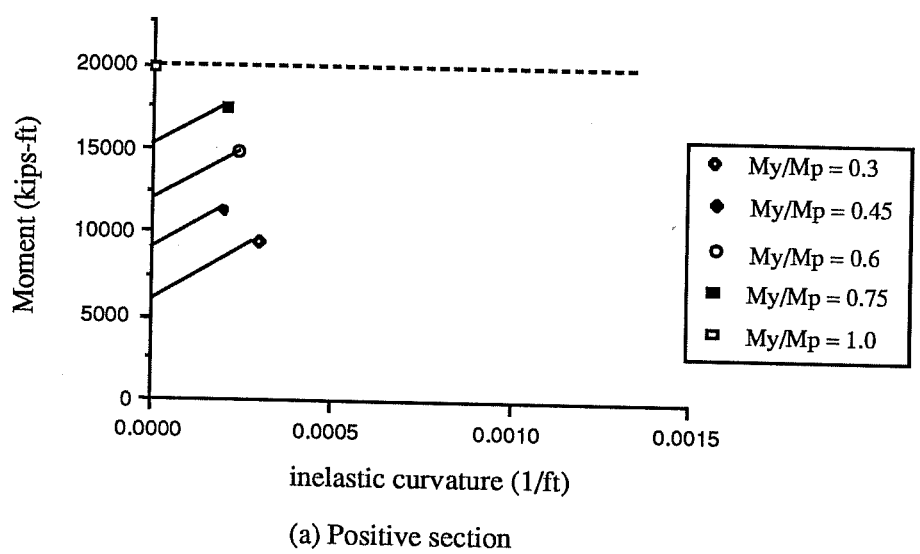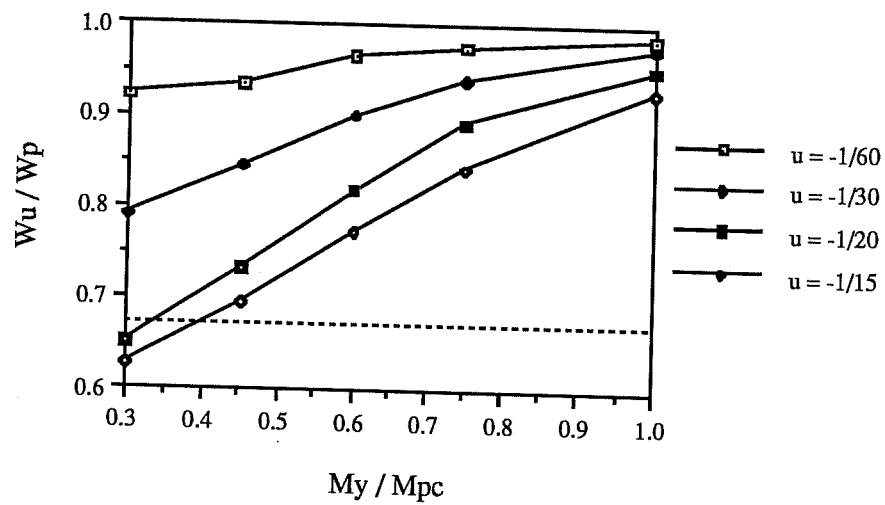
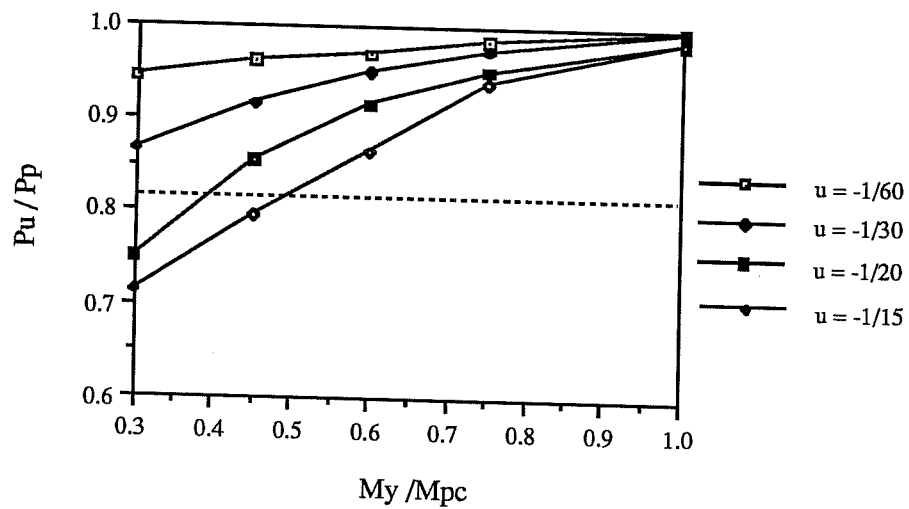Figure 7.19 Ultimate load vs My/Mpc for uniformly distributed load

Figure 7.20 Ultimate load vs My/Mpc for concentrated load

7.4.4 Cracking moment of pier section

To evaluate the effects of the cracking moment value of the pier section on the ultimate load, the cracking moment, M_{cr}, was changed from $0.3M_u$ to $1.0M_u$ while keeping the other properties the same as those in the numerical example. Fig. 7.21 and Fig. 7.22 show the positive section moment and the pier section moment at the ultimate load. More moment was redistributed to the positive section as the the ratio of M_{cr}/M_u decreased, but the effect was insignificant. For $u = -1/60$, the ultimate load capacity was obtained when the positive section reached the plastic moment (Fig. 7.21(a)) and the pier section moment at the ultimate load was not affected much by the variation in the ratio of M_{cr}/M_u (Fig. 7.21(b)). For $u = -1/15$, the positive section moment was a little below its plastic moment at the ultimate load (Fig. 7.22(a)) and the negative moment went further down on the descending curve as M_{cr}/M_u was increased (Fig. 7.22(b)).

Fig. 7.23 and Fig. 7.24 show the ultimate load in terms of M_{cr}/M_u. The ultimate load was reduced as M_{cr}/M_u was increased. For $u = -1/60$, the reduction was negligible. For $u = -1/15$, The ultimate load was reduced to $0.85w_p$ and $0.92P_p$ at $M_{cr}/M_u = 1.0$. The ultimate loads were well above the first hinge load represented by the dotted line.

7.4.5 The ratio of the maximum positive moment capacity to the maximum pier moment capacity

In the previous parametric study, the ratio of the maximum positive moment capacity to the maximum pier moment capacity, M_{pc}/M_u, was 1.0. Since composite plate girders in negative bending could not reach the plastic moment, M_{pn}, the maximum pier moment capacity, M_u, was used in the ratio. In order to evaluate the effects of the ratio, the value of M_{pc}/M_u was changed from 0.65 to 1.54. All the cross sectional properties of the pier section were adjusted at the

(a) Positive section

(b) Negative section
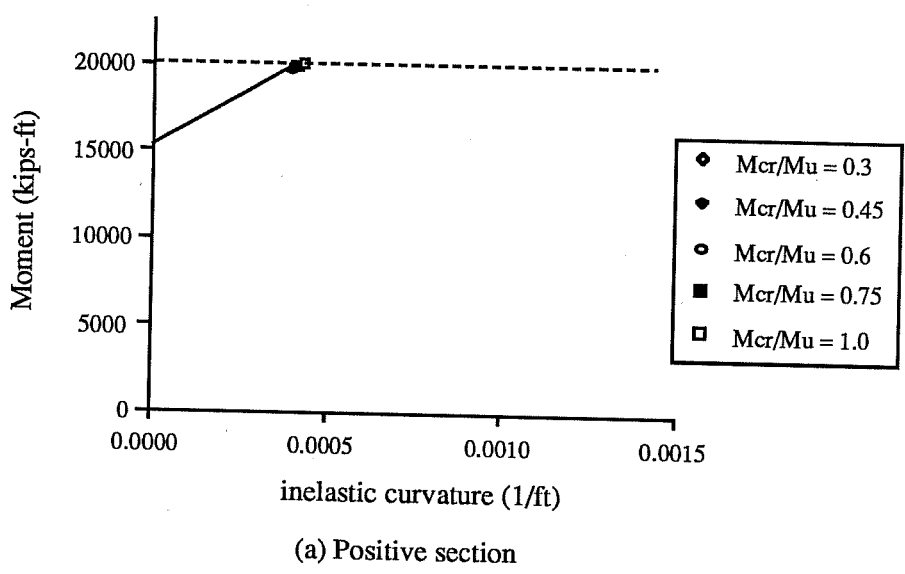
Figure 7.21 Moments at ultimate load for Mcr/Mu and u = -1/60

(a) Positive section

(b) Negative section
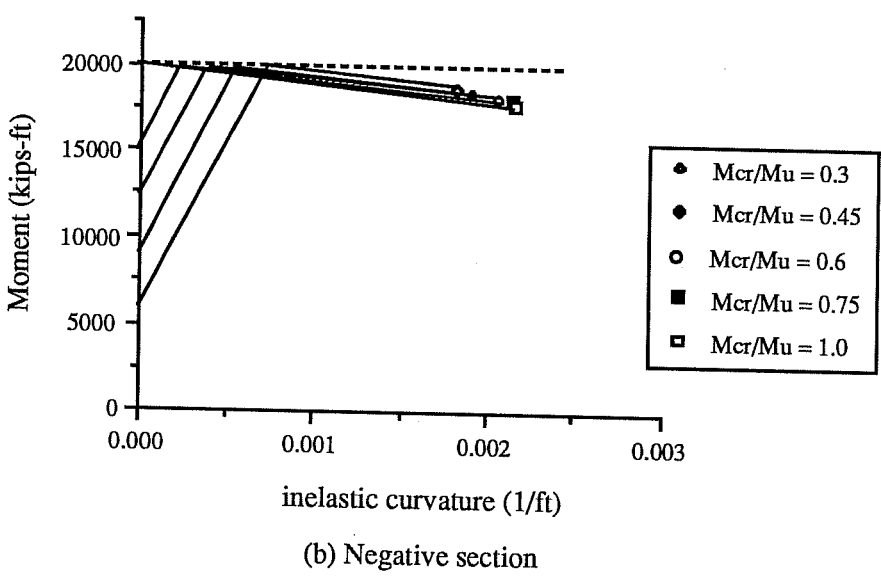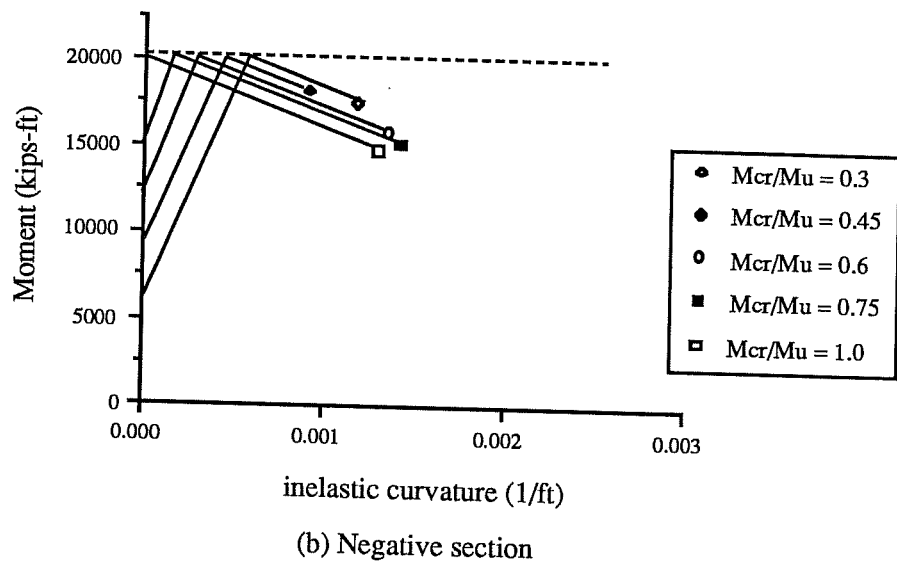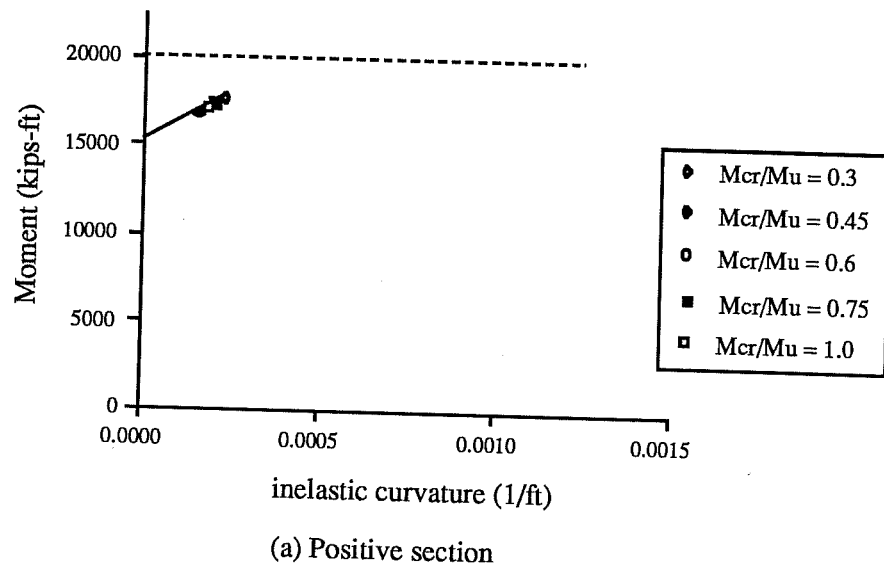
Figure 7.22 Moments at ultimate load for Mcr/Mu and u = -1/15
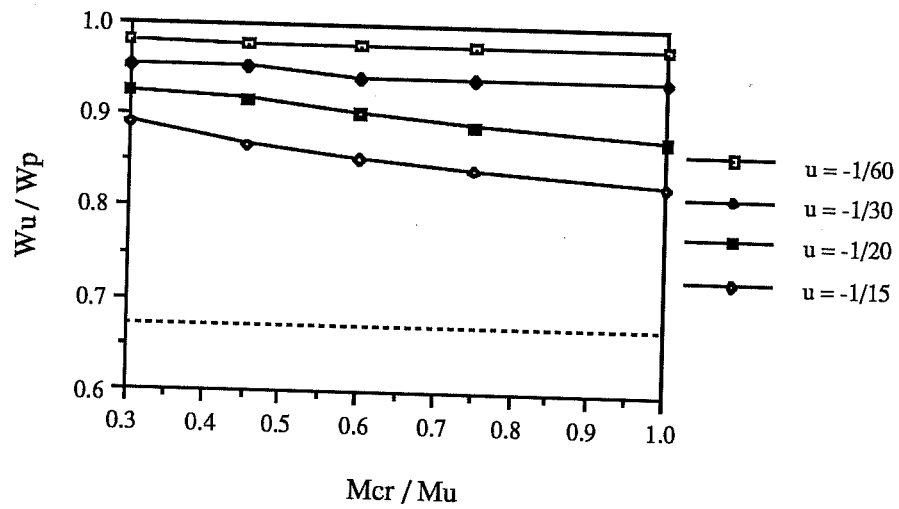
Figure 7.23 Ultimate load vs Mcr/Mu for uniformly distributed load
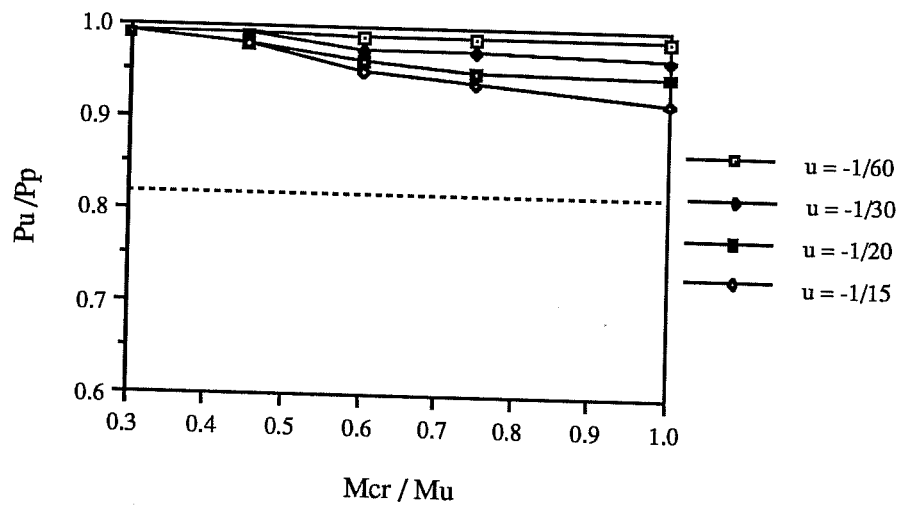
Figure 7.24 Ultimate load vs Mcr/Mu for concentrated load

same rate while keeping the cross sectional properties of the positive section the same as in the numerical example. Fig. 7.25 shows the ultimate load in terms of M_{pc}/M_u for uniformly distributed load which causes more reduction of the ultimate load than concentrated load. As the ratio of M_{pc}/M_u was increased, w_u/w_p was reduced, but the reduction was insignificant.

7.4.6 First hinge load as a lower bound estimate

The first hinge load at which the elastic maximum positive or negative moment reached its maximum moment capacity (Fig. 7.12) provided a lower bound to the ultimate load capacity of continuous composite plate girders for the case of M_{pc}/M_u =1.0. But the first hinge load changes as a function of the ratio, M_{pc}/M_u, as shown in Fig. 7.26. The maximum value of the first hinge load is $0.84P_p$ for concentrated load when M_{pc}/M_u is 1.08. This value is close to $0.82P_p$ which was used as the first hinge load for concentrated load in the ultimate load curves in section 7.4.1 through 7.4.4. The maximum value of the first hinge load is $0.79w_p$ for uniformly distributed load when M_{pc}/M_u is 0.76. This value is higher than $0.67w_p$ which was used as the first hinge load for uniformly distributed load in the ultimate load curves in section 7.4.1 through 7.4.4. However, the value of $0.79w_p$ still provides a lower bound for most cases. Moreover, the actual loading is a combination of the uniformly distributed load and the concentrated load. Therefore, a parametric study for the case of $M_{pc}/M_u = 0.76$ is not needed and the first hinge load can be used as a lower bound estimate of the ultimate load capacity of continuous composite plate girder bridges.

7.4.7 Ultimate load capacity by the Eurocode 4 method

To investigate the validity of the Eurocode 4 method for the design of
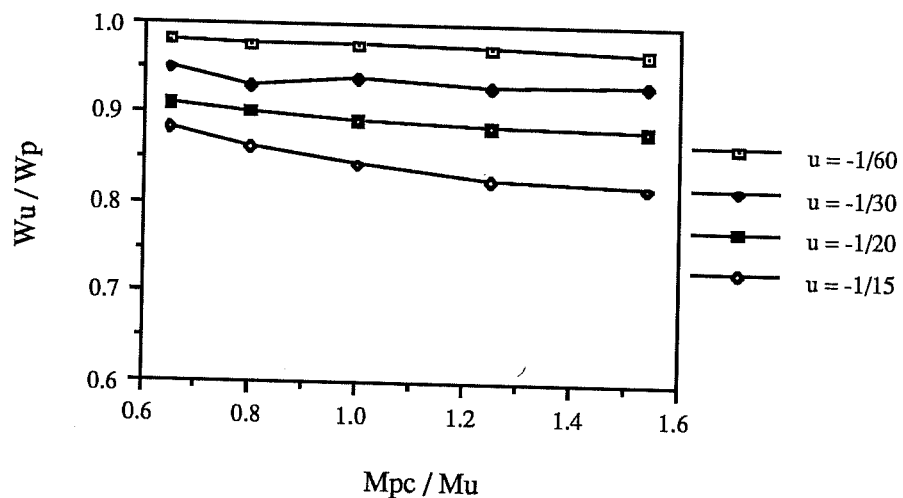
Figure 7.25 Ultimate load vs Mpc/Mu for uniformly distributed load
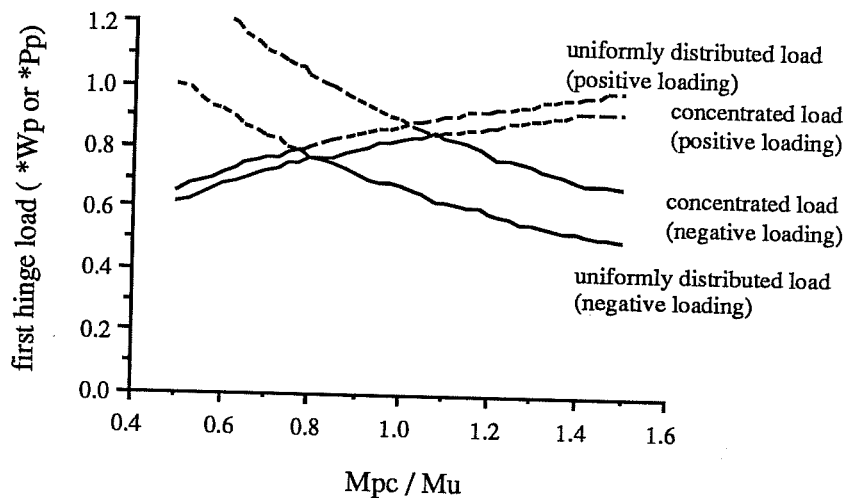
Figure 7.26 First hinge load vs Mpc/Mu

continuous composite plate girders, the ultimate load capacity of the girder used in the numerical example was calculated by this method. In the calculation, the maximum positive moment was limited to the plastic moment, M_{pc}, and the maximum pier moment was limited to the ultimate moment of the pier section, M_u. The Eurocode 4 method allows 20% of the maximum pier moment by elastic analysis to be redistributed before the sections are designed. The ultimate load capacity by the Eurocode 4 method was $0.86w_p$ for uniformly distributed load and $0.89 P_p$ for concentrated load. Fig. 7.19 and Fig. 7.20 show that the ultimate load can be reduced below $0.86w_p$ and $0.89P_p$ (the ultimate load capacity by the Eurocode 4 method) when the descending curve of the pier section drops very rapidly. The study by Johnson and Fan indicated that the ultimate load capacity was insensitive to the slope of the descending curve for continuous composite beams with semi-compact sections. Since the descending curve of a plate girder section may drop much faster than that of a semi-compact section, the Eurocode 4 method may give unconservative results for the design of continuous composite plate girders.

CHAPTER EIGHT

PROPOSED DESIGN METHOD OF CONTINUOUS COMPOSITE PLATE GIRDER BRIDGES

8.1 Introduction

In the AASHTO LFD method, continuous composite plate girder bridges are designed based on elastic analyses. The ALFD method in the AASHTO Guide Specifications, which is an extension of the LFD method, considers the effect of local yielding at Overload using a beam-line method and determines the maximum load capacity using a concept of an effective plastic moment. The ALFD procedures are based on the experimental moment-rotation behaviors of component specimens with compact sections and apply specifically to bridges with compact sections. Research has been underway to extend the ALFD method to noncompact beams and plate girders. However, currently available experimental moment-rotation curves of composite plate girders do not have sufficiently similar behaviors for the use of one typical curve for a beam-line method and the concept of an effective plastic moment may give unconservative results for plate girders with ultracompact compression flanges. Based on the test results for component specimens and a parametric study of the ultimate load capacity of continuous composite plate girder bridges, a new design method is developed.

8.2 Proposed Design Method

The proposed design method uses the same design requirements as the LFD method at Service Load. At Overload, the LFD method limits the flange stresses to $0.95F_y$ for composite sections in positive and negative bending. The

116

proposed design method uses an automoment procedure similar to that in the Guide Specifications. The flange stress due to elastic positive moment plus any corresponding automoment is limited to $0.95F_y$. However, the proposed design method does not use a beam-line method to calculate the automoments. In the proposed design method, the automoments are calculated as the difference between the moments obtained using the uncracked section stiffness and the cracked section stiffness for the negative bending area (Fig. 5.16). The elastic maximum negative moment at Overload is limited to the yield moment, M_y.

At maximum load, the LFD method limits the elastic maximum moment at any section in a continuous bridge to the yield moment for noncompact sections. However, test results indicated that composite plate girders could reach the plastic moment in positive bending and higher moment than the yield moment in negative bending. The results of a parametric study in chapter 7 showed that the first hinge load at which the maximum positive or negative moment capacity was reached (Fig. 7.12) provided a lower bound estimate of the ultimate load capacity of continuous composite plate girder bridges. Therefore, in the proposed design method, the elastic maximum positive moment is limited to the plastic moment, M_p, and the elastic maximum negative moment is limited to the maximum moment capacity of the pier section, M_u. In calculating the elastic maximum moment, uncracked section stiffness is used for the negative bending area. The design requirements of the proposed design method are summarized in Table 8.1.

8.3 Design Example

To compare the proposed design method with the LFD method, a 180 ft two-span continuous composite plate girder bridge was designed by the two design methods. General design criteria and the design by the LFD method are available in the literature[37]. The designs by the two methods are compared in

Table 8.1 Design requirements of the proposed design method

| Load | Design Requirements | |
	Positive section	Negative section
Service Load	same as LFD	same as LFD
Overload	$\dfrac{M_{dl}}{S_s} + \dfrac{M_{ol} + M_{auto}}{S_c} \leq 0.95 F_y$	$M \leq M_y$
Maximum Load	$M \leq M_F$	$M \leq M_u$

M_{dl} = noncomposite dead load moment

M_{ol} = superimposed dead load moment plus factored live load moment

M_{auto} = automoment at the maximum positive moment location

S_s = section modulus of steel section

S_c = section modulus of composite section calculated using the modular ratio n
     for live load moment and 3n for dead load moment and automoment

Table 8.2. Fig. 8.1 shows the cross sections of the bridge by the two methods. In the LFD method, the elastic maximum flange stress is limited to $0.95 F_y$ at Overload and the elastic maximum moment to $1.0 M_y$ at Maximum Load. Since the Maximum Load is 1.3 times the Overload, the Maximum Load check always governs the design of composite plate girder bridges in the LFD method. In the design example by the proposed design method, the Overload check controlled the design of the positive section due to the high shape factor of the composite section (M_p/M_y =1.5). The automoment at the location of the maximum positive moment was about 5% of the maximum positive moment at Overload. The top flange and the web were the same but the bottom flange by

Table 8.2 Comparison of the designs by the two design methods

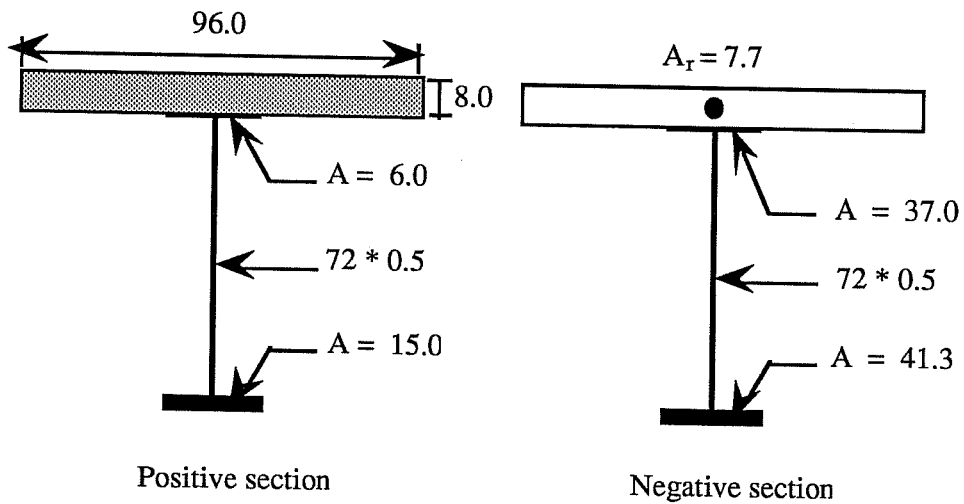|	LFD method		Proposed design method	
	positive section	negative section	positive section	negative section
Overload	$M_{dl} = 1880$ k-ft $M_{ol} = 4210$ k-ft $f_b = 37.08$ ksi $0.95F_y = 47.5$ ksi	$M_{dl} = 4950$ k-ft $M_{ol} = 5980$ k-ft $f_b = 38.55$ ksi $0.95F_y = 47.5$ ksi	$M_{dl} = 1850$ k-ft $M_{ol} = 4180$ k-ft $M_{auto} = 310$ k-ft $f_b = 44.46$ ksi	$M_{dl} = 5030$ k-ft $M_{ol} = 6160$ k-ft $M = 11190$ k-ft $M_y = 14230$ k-ft
	$f_b \leq 0.95F_y$ o.k.	$f_b \leq 0.95F_y$ o.k.	$f_b \leq 0.95F_y$ o.k. controls	$M \leq M_y$ o.k.
Maximum Load	$M = 7920$ k-ft $M_y = 8500$ k-ft	$M = 14210$ k-ft $M_y = 14230$ k-ft	$M = 7840$ k-ft $M_p = 10940$ k-ft	$M = 14550$ k-ft $M_u = 14610$ k-ft
	$M \leq M_y$ o.k. controls	$M \leq M_y$ o.k. controls	$M \leq M_p$ o.k.	$M \leq M_u$ o.k. controls

the proposed design method was substantially smaller than that by the LFD method. For the pier section, the ultimate moment capacity, M_u $(= 1.02M_y)$, by the modified Q formula was close to the yield moment, M_y. Therefore, the design of the pier section by the proposed design method was governed by the Maximum Load check. The reduction in the flexural stiffness of the positive section increased the elastic maximum negative moment, but the increase was less than 3%. The same cross section as that by the LFD method was used for the pier section. Total weight of the girder by the proposed design method was 4.5% smaller than that by the LFD method.
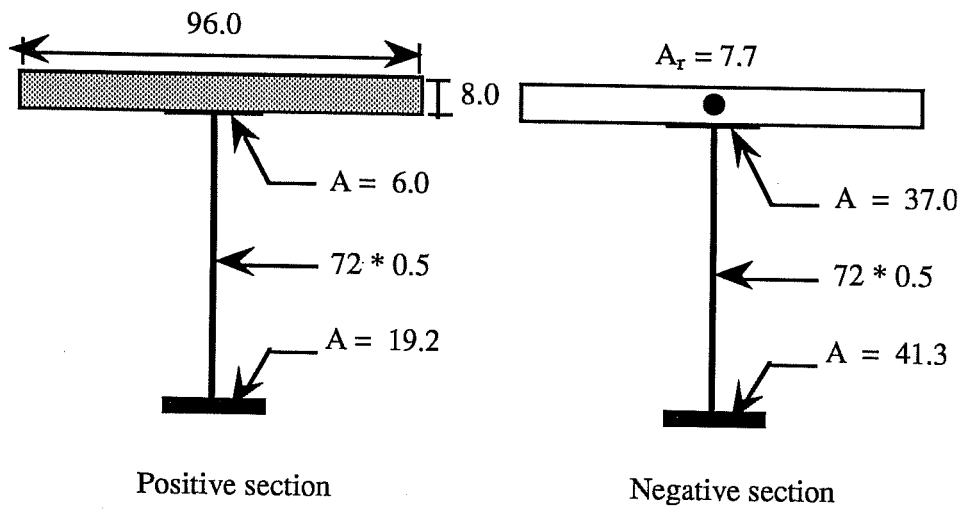
(a) LFD method

(b) Proposed design method

Figure 8.1 Comparison of designed cross sections

CHAPTER NINE

SUMMARY AND CONCLUSIONS

The primary objective of this study was to evaluate the ultimate load capacity of laterally braced continuous composite plate girder bridges and to develop a simple and safe design method.

The ultimate capacity of a continuous beam can be determined by the simple plastic mechanism method if the pier section has a sufficient rotation capacity for a mechanism to form. However, most plate girders have slenderness sections whose ultimate bending strengths and rotation capacities are affected by local instabilities.

In the LFD method of the AASHTO Specifications, continuous composite plate girder bridges are designed based on elastic analyses and the elastic Maximum Load moment at any section is limited to the yield moment. Test results have shown that typical composite plate girders in positive bending can reach their plastic moment capacities due to the small web depth in compression. When the maximum positive moment exceeds the yield moment of the positive bending section, moment redistribution occurs increasing the negative moment at the pier. Since the moment-rotation behaviors of negative bending sections are not well known, the use of the plastic moment capacity of positive bending sections is limited to simple span bridge design.

The ALFD method of the AASHTO Guide Specifications calculates the ultimate load capacity of continuous-span bridges using the plastic mechanism method. Though the ALFD method predicts the actual behavior more accurately and provides more economical design than the LFD method, the ALFD method applies only to bridges with compact sections.

The ultimate load capacity of continuous composite plate girder bridges

121

depends on the moment-curvature characteristics of the positive and negative bending sections. In this study, the moment-curvature behaviors of positive bending sections were investigated using a numerical analysis method. To evaluate the moment-rotation characteristics of a composite plate girder in negative bending, an ultimate load test was performed on a 1/2 scale component specimen. Based on the analytical and experimental work, a parametric study was made to evaluate the ultimate load capacity of continuous composite plate girders using a nonlinear computer program.

The most important conclusions from this study are as follows:

1. The load at which the maximum positive moment reaches the plastic moment or the maximum negative moment reaches the maximum bending capacity of the pier section (whichever is smaller) provides a lower bound estimate of the ultimate load capacity of continuous composite plate girders. The moments are calculated from elastic analyses using an uncracked section at the pier.

2. The proposed design method, in which the elastic maximum positive moment at Maximum Load is limited to the plastic moment, improves the limit state criteria and provides a more economical design of continuous composite plate girder bridges than the LFD method.

3. Experimental results show that the nominal moment strength of composite plate girders in negative bending can be greater than the first yield moment calculated considering the sequence of loading.

4. In evaluating the nominal moment strength of noncomposite sections and composite sections in negative bending, the Q formula in the proposed AASHTO LRFD Specification may give unconservative results for sections with very stocky compression flanges and conservative results for unsymmetrical sections with high shape factors. The modified Q formula developed in this study gives a better estimate.

5. The concept of an effective plastic moment in the AASHTO Guide Specifications may give unconservative results for plate girders with ultracompact compression flanges.

6. The typical moment-rotation curve used to calculate the automoments for composite sections in the AASHTO Guide Specifications gives conservative results for composite sections constructed without shorings.

REFERENCES

[1] "Specifications for Structural Steel Buildings-Allowable Stress Design and Plastic Design", Chicago, IL: American Institute of Steel Construction, 1989.

[2] "Load and Resistance Factor Design Specifications for Structural Steel Buildings", Chicago, IL: American Institute of Steel Construction, September 1986.

[3] "Specifications for the Design Fabrication and Erection of Structural Steel for Buildings", New York, American Institute of Steel Construction, 1978.

[4] "Interim Specifications - Bridges - 1990", American Association of State Highway Transportation Officials, Washington, D.C., 1990.

[5] "Guide Specification for Alternate Load Factor Design Procedures for Steel Beam Bridges Using Braced Compact Sections", American Association of State Highway Transportation Officials, Washington, D.C., 1985.

[6] "Standard Specification for Highway Bridges", 13th Ed., American Association of State Highway Transportation Officials, Washington, D.C., 1983.

[7] E. Hognestad. A study of Combined Bending and Axial Load in Reinforced Concrete Members. Urbana: University of Illinois Engineering Experiment Station, November 1951.

[8] Lambert Tall. Structural Steel Design(2nd Ed.). New York: Wiley & Sons, 1974 (Chap. 9).

[9] Vasseghi, A. and Frank, K. H., "Static Shear and Bending Strength of Composite Plate Girders", PMFSEL Report No. 87-4, The University of Texas at Austin, June 1987.

[10] Joseph A. Yura, Theodore V. Galambos, and Mayasandra K. Ravindra. "The Bending Resistance of Steel I-beams", Journal of Structural Division, ASCE, 104, ST9 (September 1978), 1355-1370.

124

[11] B. G. Johnston. "Guide to Stability Design Criteria for Metal Structures", Structural Stability Research Council, 4th Ed., New York: John Wiley, Inc. (Chap. 4).

[12] Charles G. Salmon and John E. Johnson. Steel Structures: Design and Behavior. New York: HarperCollins Publishers, 1990.

[13] D. L. Johnson. "An investigation into the interaction of Flanges and Webs in Wide-flange Shapes", 1985 Proceedings SSRC Annual Technical Session.

[14] Joseph A. Yura. "Interaction of flange and web buckling", Notes, The Univ. of Texas at Austin, 1991.

[15] A. F. Lukey, R. J. Smith, M. U. Hosain and P. F. Adams. "Experiments on Wide-Flange Beams Under Moment Gradient", WRC Bulletin No.142, July 1969.

[16] K. Basler and B. Thurlimann. "Strength of Plate Girders in Bending", Trans. ASCE, Vol. 128, Part II, 1963 (pp. 655-682).

[17] A. F. Della Croce. "The Strength of Continuous Welded Girders with Unstiffened Webs", thesis, The University of Texas at Austin, 1970.

[18] M. A. Grubb and P. S. Carskaddan "Autostress Design of Highway Bridges, Phase 3: Moment-Rotation Requirements", American Iron and Steel Institute, Project 188, Washington, D. C., July 1981.

[19] N. M. Holtz and G. L. Kulak. "Web Slenderness Limits for Compact Beams", Structural Engineering Report No. 43, University of Alberta, March 1973.

[20] K. H. Frank. "Proposed LRFD Bridge Specifications For Composite and Non- composite Steel Plate Girders", Proposal to AASHTO Specifications, 1990.

[21] G. Haaijer, P. S. Carskaddan, and M. A. Grubb. "Autostress Design of Steel Bridges", ASCE Journal of Structural Engineering, Vol.109, No. ST1, January 1983 (pp. 188-199).

[22] P. S. Carskaddan. "Autostress Design fo Highway Bridges, Phase 1: De-

sign Procedure and Example Design", Research Laboratory Report, United States Steel Corp., Monroeville, PA., March 1976.

[23] P. S. Carskaddan. "Autostress Design fo Highway Bridges, Phase 3: Interior-Support-Model Test", American Iron and Steel Institute, Project 188, Washington, D. C., Feb. 1980.

[24] A. Vasseghi. "Strength and Behavior of Composite Plate Girders Under Shear and Bending Moment", dissertation, The University of Texas at Austin, May 1989.

[25] K. H. Frank and M. A. Grubb. "Commentary on Changes to AASHTO Specifications for Design of Compact Composite Plate Girders in Positive Bending", 1989.

[26] C. G. Schilling. "Moment-Rotation Tests of Steel Plate Girders", AISI Project 188, Washington, D. C., April 1985.

[27] C. G. Schilling. and S. S. Marcos. "Moment-Rotation Tests of Steel Girders with Ultracompact Flanges", AISI Project 188, Washington, D. C., July 1988.

[28] "Component Test Report", Federal Highway Administration, Publication No. FHWA-RD-90-066, August 1990.

[29] E. Hinton and D. R. J. Owen., Finite Element in Plasticity, Academic Press, London, 1980.

[30] Lynn S. Beedle. Plastic Design of Steel Frames. New York: John Wiley & Sons, Inc., 1958 (Chap. 2).

[31] M. Kubo. and Theodore V. Galambos. "Plastic Collapse Load of Continuous Composite Plate Girders", 1988.

[32] R. P. Johnson and C. K. R. Fan. "Strength of Continuous Composite Beams Designed to Eurocode 4", IABSE Proceedings P-125/88, May 1988.

[33] Y. Ueda. "Elastic, Elastic- Plastic and Plastic Buckling of Plates with Residual Stresses", dissertation presented to Lehigh Univ., at Bethlehem, PA., 1962.

[34] J. P. Bansal. "The Lateral Instability of Continuous Steel Beam", dissertation presented to the University of Texas at Austin, TX., 1971.

[35] E. Yarimici, J. A. Yura. and L. W. Lu. "Techniques for Testing Structures Permitted to sway", Fritz Laboratory Report No. 273.40, Lehigh University, Bethlehem, Pennsylvania, May, 1966.

[36] J. J. Climenhaga and R. P. Johnson. "Local Buckling in Continuous Composite Beams", The Structural Engineer, Vol. 50, No. 9, September 1972.

[37] C. G. Schilling. "Exploratory Autostress Girder Designs", AISI Project 188, Washington, D. C., July 1986.

VITA

Chong One Bak was born in Milyang, Korea on December 6, 1957, the son of Young Sun Cho and Tae Gyu Bak. After completing his work at Chung Dong High School, Seoul, Korea in 1976, he entered Seoul National University in Seoul, Korea. In 1978, he enlisted and served three years in the army. He received the degree of Bachelor of Science in March 1983 and the degree of Master of Science in March 1985 in Architectural Engineering from Seoul National University. During the following two years, he was employed as a structural engineer at Chang Jo Company, Seoul, Korea.

Permanent address: 1474-20 , Sinlim 11 dong, Kuan-ak gu, Seoul, Korea

This dissertation was typed by the author.